Hydrogen Permeation Through Nickel And Nickel Alloys: Surface Reactions And Trapping

Thesis

Hydrogen Permeation Through Nickel and Nickel Alloys: Surface Reactions and Trapping

Thesis submitted by
Abdulkadir Altunoglu
BSc, MSc
for the degree of
Doctor of Philosophy
April 1994

Oxford Research Unit
Materials Discipline
The Open University

Dedicated to **Irfan Arpaz**, *who sadly could not see it completed*

DECLARATION

Parts of the data in this thesis have been published in two papers.

1. "Permeation of hydrogen through nickel foils: surface reaction rates at low temperatures", by A.K. Altunoglu, D.A. Blackburn, N.St.J. Braithwaite and D.M. Grant, Journal of Less Common Metals, 172-174 (1991).

2. " A study of hydrogen trapping in cold-worked pure nickel and nickel thoria by pressure modulation technique." by A.K. Altunoglu, N.St.J. Braithwaite and D.M. Grant." Physicalische Chemie, 1993"

Contents

List of Figures

List of Tables

Acknowledgements

I wish to express my thanks to the Open University for providing finance for myself and my equipment.
Thanks are also due to;
Prof. David Blackburn, for his ideas, thoughts and his hospitality,
Dr. N.St.J Braithwaite, for his friendship, supervision and his constant guidence after the departure of David Blackburn.
Dr. David Grant, for his friendship, and for his great help at the beginning of this project and throughout
Dr. Derek Cummings for the theoretical help.
Prof. Gerald Elliot, for his encouragement during this work.
Ted, David, Alan, John for their technical help
John Short, for his help in the student workshop of the materials departmant of Oxford University.
Naomi and Richard, for their help to get TEM pictures.
Colin Gagg, for technical help and frendship.
Invaluable moral support and friendship by the whole ORU.
Yalim, Ebru, Turkan, Kadriye, Haluk for their friendship. My Parents, for their encouragement and moral support
My wife, Nilgun, for her patience.

Abstract

The frequency variations of attenuation and phase lag of the modulated gas flow through thin metal foils have characteristic features whether permeation is diffusion controlled, is influenced by surface reactions or affected by internal trapping.

Analysis of data obtained for hydrogen permeation through nickel show that hydrogen is dissociatively chemisorbed in nickel.

The permeation parameters diffusivity, permeability and surface reaction rate obtained for nickel are:

$$D/(m^2 s^{-1}) = 7.12 \times 10^{-7} \exp\left[-40.64 \times 10^3/RT/(K)\right]$$

$$P_m/(molH_2 m^{-1} s^{-1} Pa^{-1/2}) = 3.35 \times 10^{-7} \exp\left[-54.25 \times 10^3/RT/(K)\right]$$

$$K_{sm}/(molH_2 m^{-3} Pa^{-1/2}) = 0.47 \exp\left[-13.6 \times 10^3/RT/(K)\right]$$

$$k_1/(molH_2 m^{-2} s^{-1} Pa^{-1}) = 1.44 \times 10^{-6} \exp\left[-29.68 \times 10^3/RT/(K)\right]$$

Where $R = 8.314 Jmol^{-1}$.

The experiments conducted on cold-worked nickel have revealed that hydrogen is trapped within the bulk during the permeation in this material.

A series of experiments conducted on cold worked nickel+2% thoria has also revealed that hydrogen is trapped within the bulk during the perme-

ation. Analysis of data obtained for cold worked nickel+2% thoria suggest that hydrogen is trapped at the dislocation networks around thoria particles.

Frequency variation of attenuation and phase lag of the modulated flow show that hydrogen trapping in both cold-worked nickel and nickel+2% thoria is in dynamic equilibrium. A trap depth of 40 kJ/mol has been obtained for nickel+2% thoria.

Nomenclature

Symbols	Descriptions	Dimensions
c, c	free diffusant concentration	$mol\,m^{-3}$
z, z	trapped diffusant concentratiom	$mol\,m^{3}$
J, J	flux	$mol\,m^{-2}s^{-1}$
p, p	pressure	Pa
x	position	m
t	time	s
ω	angular frequency	s^{-1}
D	diffusivity	m^2s^{-1}
K_{sm}	solubility	$mol\,m^{-3}Pa^{-1/2}$
P_m	permeability	$mol\,m^{-1}s^{-1}Pa^{-1/2}$
l	thickness	m
γ	cross sectional area	m^2
σ	γRT	m^4s^{-2}
V	output chamber volume	m^3
S	pump speed	m^3s^{-1}
n	permeation pressure law exponent	
Q_{og}	outgassing load	$mol\,m^2s^{-3}$
k_A	rate constant: trapping	s^{-1}
k_B	rate constant: detrapping	s^{-1}
k_1, k_1	rate constant: absorption	$mol\,m^2s^{-1}Pa^{-1}$
k_2, k_2	rate constant: desorption	$m^4s^{-1}mol^{-1}$
e, f, g, h	abbreviating parameters	
y, y', y, y'	principal experimental variables	
ϕ	phase lag	radian
Λ	relative modulation amplitude ratio	
ϵ	equipment response lag	
ζ	dimensionless frequency parameter	
μ	dimensionless surface symmetry parameter	
A	dimensionless trapping parameter	
B	dimensionless detrapping parameter	

F, G	boundary condition parameters	$mol\,m^{-3}$
a, b	complex wave numbers	m^{-1}
ξ, χ	$\Re(bl)$, $\Im(b)$	
R	entry:exit modulation amplitude ratio	
P	condition vector 1 × 2	
T, $T^{\dagger}$	translation matrix, 2 × 2	
S, S′	phase boundary matrices at entry, exit surfaces, 2 × 2	
E, E′	entry, exit matrices, 2 × 2	
g	(superscript) gas phase input side	
g'	(superscript) gas phase output side	
s	(subscript) steady state term	
o	(subscript) modulation term	
′	primed quantities indicate output variables	
$\Re$, $\Im$	indicate real and imaginary part of complex variables	
*	star indicates complex conjugate	
θ_m	adsorbed molecular surface concentration	$mol\,m^{-2}$
θ_a	adsorbed atoms surface concentration	$mol\,m^{-2}$
k_1	reaction rate: molecular adsorption	$mol\,m^{-2}s^{-1}Pa^{-1}$
k_2	reaction rate: molecular desorption	s^{-1}
k_3	reaction rate: atomic adsorption rate	s^{-1}
k_4	reaction rate: atomic desorption rate	$m^2s^{-1}mol^{-1}$
k_{4p}	reaction rate: atomic desorption rate	s^{-1}
k_5	reaction rate: atomic absorption rate	s^{-1}
k_6	reaction rate: atomic desorption rate	$m\,s^{-1}$

Chapter 1

Introduction

1.1 Introduction

This thesis is about the permeation of hydrogen through thin metal foils
Solids are normally considered impervious to gases but a hot solid that is held at a temperature about half way to its melting point may allow the entry of gas and that gas may move freely within the solid. The most mobile of these gases is unquestionably hydrogen, and the study of hydrogen movement in solids has received a great deal of attention both for its physical curiosity and for its technological importance.
It has long been known that the ability of hydrogen to enter and move in iron can cause the failure of mechanical components, a phenomenon known as hydrogen embrittlement.
More usefully the highly selective permeability of palladium to hydrogen has led to its use for the purification of hydrogen.

There are contrasting modern technological interests in hydrogen permeation. Safety requirements for thermonuclear fusion reactors call for walls that allow minimal permeation and minimal internal accumulation of tritium, a hydrogen isotope. For fuel and storage cells the need is for materials with a high storage capacity and a structure which allows it to move freely. Hydrogen moves interstitally between relatively immobile atoms of the host solid but its motion is readily interrupted by imperfections of crystal struc-

ture. Within a solid hydrogen may be trapped at grain boundaries, phase boundaries, micropores, dislocations or particular constituent atoms of the solid: it may even be trapped by vacant lattice sites. However, the nature of the gas /solid surface interaction is equally important as molecules adsorb, dissociate and enter the solid solution. The multiplicity of the processes involved has made the experimental analysis of hydrogen permeation difficult and there is long standing conflict between experimental data based on measurement of atomic motion and that based on macroscopic flow.

Diffusion of hydrogen in solids has been studied extensively and a large body of experimental data has been accumulated, for example [1] [2] [3] [4]. Data on some materials, such as nickel, are consistent while data on other materials, such as steels are dispersed. One reason for this disparity is that the conventional permeation techniques are not capable of isolating the surface processes from the bulk transport and identifying the trapping process in the presence of which permeation takes place.

This thesis details an experimental study and an extension to the modelling of permeation of hydrogen through nickel and nickel thoria foils using a modulated gas flow technique with the objective of investigating and separating those surface effects which are responsible for the reduction of diffusion flux and trapping effects which are responsible for the reduction of diffusion rate through bulk material.

After a brief discussion of the general measurement techniques employed in this field and a consideration of the evidence for trapping and surface effects, the remaining chapters of this thesis are outlined.

1.2 The Experimental Methods to Measure Hydrogen Diffusion

Diffusion is a thermally activated process in which material flow acts so as to reduce gradients of chemical potential. More specifically, a solid solution which has an inhomogeneity in the concentration of one or more of its components will tend to homogenise until it reaches an equilibrium in which there are no chemical potential gradients. The study of diffusion can be divided into two distinct type of experiment; those which use microscopic techniques by measuring the jump mechanism involved in diffusion and those which use macroscopic techniques and measure bulk effects.

1.2.1 Microscopic Techniques

The microscopic techniques used to study diffusion are: nuclear magnetic resonance (NMR), [5] [6] [7] [8]; quasi-elastic neutron scattering (QNS), [9]; internal friction [10] and the Mössbauer effect [11] [12].

(i) Nuclear Magnetic Resonance

The NMR technique is a well established method for studying atomic motion in solids. Data usually consist of measurements of the longitudinal spin-lattice relaxation time or the transverse spin-spin relaxation time. From the absolute values, or from the frequency and temperature dependency of these quantities, the rate of atomic motion can be calculated. The analysis also yields the activation energy.

(ii) Quasi-Elastic Neutron Scattering

The Quasi-Elastic Neutron Scattering technique uses a mono-energetic neutron beam which passes through the metal specimen. Incoherent scattering by the protons in the metal broadens the energy spectrum of the emergent beam, from which it is possible to deduce the rate of diffusion. Different scattering angles contain different information. Small scattering angles correspond to small momentum transfer and almost elastic scattering. From the half-width of the energy spectrum the diffusion coefficient is determined. From the line width at larger scattering angles, details such as the mean

jump rate or mean jump distance can be obtained.

(iii) Internal Friction

Internal friction is an effect which may be observed when any body is set in vibration. The amplitude of the oscillations decreases with time indicating that the motion of the crystal lattice is not perfectly elastic. The energy is dissipated, the process of dissipation being called internal friction. In these experiments, the energy loss of the oscillating system is measured at fixed frequency over a range of temperatures. Internal friction peaks are observed when it is plotted against reciprocal temperature and the form of these peaks suggests that they are due to some sort of relaxation process. When hydrogen is present relaxation peaks are observed which can be shown to be hydrogen concentration dependent. The effect has been attributed to diffusion. Unfortunately it is not always possible to prove that the observed peaks are due to hydrogen relaxation processes, or that the processes are linked with the individual steps involved in bulk diffusion.

(iv) Mössbauer Effect

The basic idea of the Mössbauer effect is as follows; a source nucleus in an excited state makes a transition to its ground state, emmitting a γ ray. The γ ray subsequently collides with an unexcited absorber nucleus of the same species, which ends up in the same excited state. Changes in the source energy, the absorber energy, or the energy of the γ ray in flight, will destroy the 'resonant' absorption even if the energy change is only a few parts in 10^{11}.

Mössbauer discovered that it is possible to observe resonant absorption if the source and absorber nuclei are in crystals at sufficiently low temperature. In such circumstances the crystals can recoil as units, with the emitting and absorbing nuclei remaining bound to their lattice sites and no phonons being excited. Being so massive, the crystals take up the required recoil momentum without taking up a significant amount of kinetic energy. This is known as a recoilless process and produces radiation with a precision in frequency of 3 parts in 10^{13}.

Mössbauer demonstrated resonant absorption by cooling a specimen of $^{77}Ir^{191}$ to a temperature of 88 K. He arranged for the source to move back

and forth along the line between the source and absorber. This motion produced positive and negative Doppler shifts in the frequency of the γ ray, which led to extremely small positive and negative changes in its energy.
Because of the accuracy in measured frequencies it is possible to detect the change in the natural frequency of radiation from atoms caused by other atoms in the neighbourhood and in this way analyse the interaction between the atom and the surrounding crystal.
The above techniques can only give information on the diffusion coefficient by derivation from the jump process. However, from a technological point of view it is not the detail of the jump processes which requires to be known, but rather the effect of a very large number of such processes in an imperfect crystal in a macroscopic system.

1.2.2 Macroscopic Techniques

The fundamental laws govering the transport of matter were formulated by Adolf Fick in 1855. Fick's two laws are:

$$J = -D\frac{\partial c}{\partial x} \tag{1.1}$$

and

$$\frac{\partial c}{\partial t} = D\frac{\partial^2 c}{\partial x^2} \tag{1.2}$$

where J is the flux, D is the diffusion coefficient and which is assumed to be invariant with concentration, c is the diffusant concentration per unit volume.
From these equations it may be seen that a macroscopic measurement of the diffusion coefficient can be achieved by observations of concentration of hydrogen within the metal, or by observations of the flux into the metal, out of the metal or through a membrane.
Methods of obtaining diffusion coefficient by macroscopic techniques can broadly be categorized as those in which a concentration distribution is measured and those in which a flux is measured.

1.2.3 Techniques which depend on concentration measurement

A number of techniques may be used to determine the diffusion coefficient by measurement of concentration, these include direct measurement of the hydrogen concentration within the specimen [13]; The Gorsky effect [14] [15]; neutron radiography [16] and resistivity relaxation [17].

i) Direct measurement of the hydrogen concentration.

Austin and Elleman [13] measured the diffusion of tritium in 304 and 316 stainless steels. They injected tritium into the surface of annealed specimens which were then diffusion annealed at constant temperature. The tritium concentration profiles were then determined by the successive removal of sections on which auto-radiography was carried out to determine the tritium concentration. The major disadvantages of this method are that the experiment must be halted so that sections may be removed and the measurement of the concentration results in the destruction of the specimen.

ii) The Gorsky effect.

A point defect, such as an interstitial hydrogen atom, gives rise to a diffusional relaxation process, the Gorsky effect, if two conditions are fulfilled.

(a) The point defects must cause a lattice distortion which changes the lattice volume.

(b) The defects must have high mobility.

If a specimen, with a uniform concentration of hydrogen, has a dilatation gradient applied to it, by bending for example, then the point defects (hydrogen atoms) follow the gradient by flowing from area of compression to areas of tension. This flow may be detected very sensitively and from the time required for diffusion across the specimen diameter, the absolute value of the diffusion coefficient can be determined.

(iii) Neutron radiography.

Neutron radiographiy is a relatively new and highly sensitive technique which depends upon the high attenuation of thermal neutrons by protons (H^1). Experimentally, a large, non-equilibrium hydrogen concentration is set up in a sheet of metal, usually electrolytically. The hydrogen is then allowed to dif-

fuse through the specimen and is observed by measuring the optical density of the sheet to neutrons using neutron radiography. From the time required for the hydrogen to reach an equilibrium concentration the diffusion coefficient can be determined.

(iv) Relaxation of resistivity.

The resistivity of a metal, which depends upon temperature and impurity concentration, can be measured very accurately. With accurate knowledge of the impurity concentration (hydrogen) and the temperature dependence of the resistivity of the metal it is possible to follow the the diffusion of a non-equilibrium concentration of hydrogen through a wire. Experimentally one half of the wire is loaded, usually electrolytically, with a uniform hydrogen concentration. The concentration is determined by measuring the resistance between two points in the loaded half of the wire. The wire is then held at the experimental temperature and the change in hydrogen concentration in the other, unloaded, half of the wire is determined by measuring the resistance between two points in this part of the wire. The diffusion coefficient can thus be determined.

The above methods are for measuring the diffusion rate without the effects of surfaces.

1.2.4 Techniques which depend on flux measurement

These techniques measure **the permeation** through a specimen. In the simplest form of permeation experiment, two chambers are separated by a membrane, the specimen. The hydrogen enters one side of the specimen from a stable supply (through gaseous permeation [18] [19] [20], electrochemistry [21] or ion injection [22] [23] [24]) and is detected on the other side.

The pressures of the diffusant gas in the two chambers are the quantities which are measured and these pressures are linked to the concentrations at the two metal surfaces.

In the the simplest case, the time taken for gas to dissolve is assumed to be rapid compared with the diffusion time. Richardson's law relates the flux to the pressure on each side of a membrane under conditions of **steady state**

permeation. The rate of flow, J per unit area is given by

$$J = \frac{P_m}{l}(p^{1/2} - p'^{1/2}) \tag{1.3}$$

where p and p' are the pressures on each side of the membrane, l is the thickness, P_m is **the permeability**. The permeability is the product of the diffusion coefficient with the **the Sieverts** constant K_{sm} defined as the equilibrium constant for the reaction

$$\tfrac{1}{2}H_2(gas) \rightleftharpoons H(Metal) \tag{1.4}$$

$$K_{sm} = \frac{C_H}{p_{H_2}^{1/2}} \tag{1.5}$$

Steady state permeation experiments can only provide values for the permeability. The diffusion coefficient can be obtained directly only by making use of measurements during transient conditions. One such method is the **"time-lag method"** [21] [25] [26] [27] [28] [29] [30]. The propagation time, or 'time-lag', for the change in pressure on one side of the specimen to reach the other side depends upon the diffusion coefficient but is independent of solubility. Therefore, from measurements of time-lag, the diffusion coefficient can be determined. A complementary form of the experiment is the **'outgassing'** experiment in which gas is removed rapidly from a chamber and the pressure rise due to the outgassing of the specimen is measured.

When $p' \ll p$, **The Richardson equation** becomes,

$$J = \frac{P_m}{l}p^{1/2} \tag{1.6}$$

and is valid when
(i) diffusion is the only rate limiting step,
(ii) the input pressure or surface concentration is so much greater than the output that the latter can be neglegted and
(iii) no processes occur in the solid which interfere with the Fickian diffusion.
The first two conditions are normally fulfilled when the specimen is thick and

the diffusion coefficient is small. When temperatures are high or pressures are low, then dissociation at the surface of the metal becomes the rate limiting process and the flux becomes proportional to the pressure.

A growing interest in transport properties in industrial alloys calls for some knowledge of processes such as trapping, precipitation, porosity etc. For **non-Fickian diffusion**, the model most often quoted is that of **Mc Nabb and Foster** [31]. This is a trapping model, whose parameters are: the concentration of the traps, N, the probability of atom release, p, a parameter related to the probability of atom capture, k and the fraction of occupied traps, n. By considering kinetics of the total trapped and dissolved hydrogen concentration, c, and applying Ficks law to the dissolved part of the total concentration, McNabb and Foster obtain the equations:

$$\frac{\partial c}{\partial t} + N\frac{\partial n}{\partial t} = \frac{\partial^2 c}{\partial x^2} \tag{1.7}$$

and

$$\frac{\partial n}{\partial t} = kc(1-n) - pn \tag{1.8}$$

As the above equations are non-linear, they can not be solved expilicitly. However, for small concentrations where the cross term $cn \ll c$, an analytic solution can be found. Robertson has presented a numerical solution of the above equations for the time lag method and has estimated trapping parameters for nickel-thoria [32]. He also presented a solution for the periodic pressure modulation (a square wave input pressure) using the assumption of dilute occupation of traps [40]. Cummings and Blackburn have also shown the analytic solution of these equations for an oscillating flux through a membrane [43].

Oriani [33] has reformulated the McNabb and Foster model in the contex of the assumption of local equilibrium between mobile and trapped populations. His approach does not allow actual rate constants to be evaluated but an apparent diffusion coefficient, D^{app} by writing Fick's first law:

$$J = -D^{app}\frac{\partial c_T}{\partial x} \tag{1.9}$$

where c_T is the total concentration of mobile and trapped populations.
The other equilibrium models, Ellerbrock *et al* [34], Kass [35] and Allen-Booth and Hewitt [36], assume that the traps consist of small voids in which hydrogen is present as gas, with local equilibrium between hydrogen in the lattice and in the voids.

Surface effects and trapping, both slow the transmission process and so delay the approach to the steady state in the time-lag technique. These delays may be partially due to slow surface reactions or trapping, but this is difficult to establish since these processes leave no obvious characteristics on the output trace of the time lag measurements.

The Modulation Technique

A recent development of the time lag technique is the modulation technique. This uses a **periodic modulation in the driving pressure or flux** [21] [37] [38] [39] [40]. This method has much to commend it over the time lag method. The diffusion coefficient can be derived from the phase difference between input and output modulation waveforms and the permeability can be determined from the relative amplitudes. Signal averaging of repeated modulations enables accurate measurements to be made and this makes it possible to identify more complex permeation processes, surface effects and trapping. This is the experimental method used in this project. In the next chapter the mathematical modeling of such an experimental system is presented. [41] [42] [43] [44] [45] [46]

1.3 The Effect of Surfaces and Trapping on Permeation

To verify that permeation being measured follows Richardson's law it is often demonstrated that the flux is proportional to square root of the input pressure, $p^{1/2}$ and inversely proportional to membrane thickness, l. If this is not the case, the measured permeability is lower than actual permeability. A major factor which can be responsible for this is the occurrence of slow surface processes. A useful way to present the data is to plot log solubility,

or log flux, against log pressure. If the $p^{1/2}$ law is followed then this graph has a slope 1/2.

Sawada et al [48] give slopes of approximately 1 for hydrogen in Nichrome and Kass and Andrzejewski [49] claim a slope of 1 for hydrogen in 309S stainless steel, both indicating surface limited diffusion. Not many authors describe surface limited diffusion but Kurakin et al [50] report 'it is proposed to atomize hydrogen in the gaseous phase in order to avoid the adsorption process becoming the limiting stage of permeation of hydrogen' in group I metals such as copper, silver and gold. This suggests that they believe the process is surface limited for the permeation of molecular hydrogen through these materials.

Tahara and Hayashi [51] state for nickel 'the permeation response deviates from that of diffusion control and the surface process is not negligible'.

While impurities, dislocations, grain and phase boundaries, voids, cracks or other such structural defects can act as traps for hydrogen and thereby have an effect on measured diffusion coefficients or effective solubilities, such traps have very little influence on steady state permeation rate. Consequently there is often much better accord among measurements of permeability than among measurements of diffusion coefficients or solubilities. Apart from cold worked iron and steels, trapping in the other materials is much less widely reported than surface effects; there are a few reports however. Lee and Lee [52] state that hydrogen evolution in annealed nickel is controlled by diffusion, but in cold worked nickel 'dislocations act as trapping sites of hydrogen.' They found no evidence of 'short-circuit pipe diffusion' in contrast with a study by Louthan et al [53]. In an another report by Louthan et al [54] on tritium absorption in 304L stainless steel an increase in permeability was observed, indicating that dislocations provide short-circuit diffusion paths rather than trap sites.

1.4 The Present Work

1.4.1 Aims

The aims set in this project are: experimental investigation and modelling of surface processes and internal trapping. This has been done in connection with the modulated hydrogen permeation technique of Blackburn and co-workers.

Surface contamination seems to be at the root of the scatter of permeability data and the modulation method has been proposed to isolate surface processes. On the one hand this makes it possible to pick out diffusivity irrespective of surface conditions: On the other it enables surface reaction rates such as dissolution and recombination to be determined. This is especially interesting for a hydrogen-related energy system which requires fast absorption and desorption rates. Divergency of the diffusivity at low temperatures from Arrhenius type behaviour of work hardened specimen can be understood by the so called trapping mechanism, where imperfections, impurity atoms, internal interfaces and voids may act as sites for the trapping of hydrogen. Previous studies on trapping have used the time lag method and show no feature on the time-pressure curve with which to identify the permeation characteristics, but the analyses of data have been based on assumptions such as dynamic equilibrium and unfillable traps. The modulated flow method, while isolating surface impedance from the bulk diffusion rate also clearly identifies the limited conditions under which the trapping takes place. This in turn may establish whether the customary assumptions used to find a closed form of solution to the non-linear differential equations of Mc Nabb and Foster theory are justified.

1.4.2 Choice of Materials for the present work

Two specimen materials have been used in this study: *Nickel* was chosen, because it is a well characterized metal for the purpose of detailed studies

of individual effects. Permeability and diffusivity data obtained for nickel show remarkable reproducibility. The investigation of the surface processes for nickel provide useful tests of the modulation technique. Reuben detected some surface effect on nickel by using a modulation technique [55].
Nickel thoria, NITD, was chosen to investigate trapping phenomena. Upon cold working, owing to the presence of dispersed 2% vol hard thorium oxide particles, voids and dislocation networks are introduced. This enables one to investigate the relative importance of the voids and dislocation networks in connection with hydrogen trapping. It also enables one to demonstrate that the modulation technique is useful in gaining a better insight into hydrogen trapping phenomena.

1.4.3 Format of This Thesis

Following this introduction, the second chapter describes in detail both the experimental system and the associated modelling of the pressure modulation method. Chapter 3 gives the experimental apparatus and operating procedure. Chapter 4 presents an extension of the mathematical modelling. Results of the experimental work are presented and discussed in chapter 5. The final chapter concludes this thesis with a review of the progress made and ideas for future work.

Chapter 2

Modulated Permeation: Method and Modelling

2.1 Introduction

The experiments undertaken in this work all depend on modulated flows of hydrogen through various thin metal foils. A mathematical approach to this problem which describes the propagation of flux and concentration modulations of a gaseous diffusant through a homogeneous foil under conditions of diffusion limited flow, surface limited flow (simplified two rate constant model) and internal trapping (linearized MacNabb and Foster model) have been developed by Cummings and Blackburn [41] [42] [43]. Their approach was to link fluxes with concentration and pressures by a series of linear equations in which the diffusivity, solubility, surface reaction rate and trapping rates appear as parameters. *Conditions in the solid, in the separate surfaces* and in the entry and exit chambers were expressed in matrix form, the product of these matrices giving the required relationship between the output and input.

In this chapter the model of Cummings and Blackburn is described and then critically reviewed in terms of its experimental applicability, especially with regard to surface and trapping phenomena. The model is extended to describe processes of greater complexity (six rate constant model) in chapter 4.

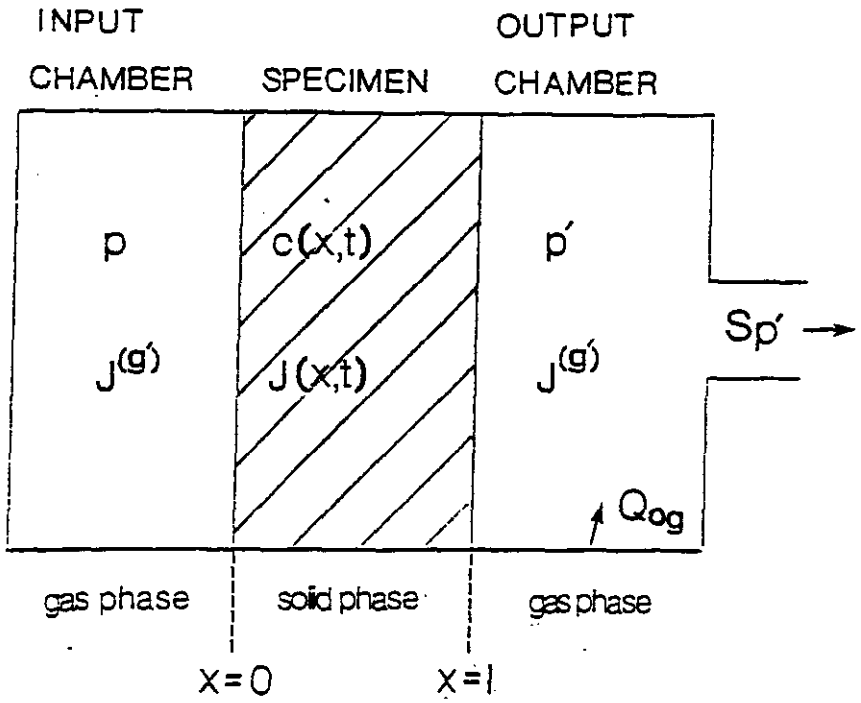

Figure 2.1 Schematic diagram of the experimental system to be modelled. It comprises three sections; the input chamber, the specimen membrane and the output chamber.

2.2 Representation of the System, Measured and Derived quantities

2.2.1 System

The experimental system to be modelled consists of three sections : input chamber, experimental membrane and output chamber, Fig 2.1. The membrane is considered to be a homogeneous isotropic solid of length l and uniform cross section γ in the plane perpendicular to the flow of the diffusing species. Diffusant enters this membrane from the input chamber, propagates by diffusion through the membrane and leaves the membrane to the output

chamber. The diffusant pressure in the input chamber is subject to modulation at angular frequency ω about a fixed central value p_s. The output chamber has volume V evacuated by a pump operating at constant speed S. Pressure in this chamber modulates with angular frequency ω about a central value p'_s whose magnitude represents a balance between diffusant flux from the membrane, outgassing of diffusant from the walls of the chamber at a rate Q_{og}, and the action of the pump. Conditions within the solid are described by the diffusant concentration $c(x,t)$ and its flux $J(x,t)$ where x is the position coordinate and t is the time. The position of the entry surface is represented by $x = 0$ and the exit surface is at $x = l$. Analysis of the above system is restricted to a condition of quasi-steady state such that all transient flows are supposed to have disappeared. The sole perturbations are the modulation of the input and its modulation is supposed not to alter the established steady state.

2.2.2 Measured and derived quantities

Once the modulation is established, the concentration, the flux and the pressures are each modulated at angular frequency ω about some fixed central value. Taking the concentration as an example, the variables can be represented as a sum of steady and oscillatory terms subscripts $_s$ and $_o$ respectively:

$$c(x,t) = c_s(x) + c_o(x,t) \tag{2.1}$$

or, with expilicit harmonic variation

$$c(x,t) = c_s(x) + c_o(x)\cos(\omega t + \phi) \tag{2.2}$$

where ϕ is the general phase lag, and subscript $_o$ denotes the harmonic quantity. Using complex notation this can be rewritten,

$$c = c_s + \Re(\mathbf{c}) \tag{2.3}$$

where $\mathbf{c} = c(x)\exp \mathbf{i}(\omega t + \phi)$ and $\Re(\mathbf{c})$ denotes the real part of the complex variable $\mathbf{c}$ and bold face type denotes the a time dependent quantity. Alternative expressions are

$$\mathbf{c} = |\mathbf{c}|\exp[\mathbf{i}(\omega t + \phi)] \quad and \quad c = c_s + |\mathbf{c}|\cos(\omega t + \phi)$$

Similar equations hold for J, p and p'. The use of prime $'$ being general to designate the exit chamber variables.

To describe the propagation of modulations, the diffusant concentration and flux characterize conditions at any point within a foil. Their time dependent parts are used to define **condition vectors** $P(\mathrm{x})$, within the foil and the corresponding quantities $P(g)$ and $P(g')$, within the entry and exit chambers. That is

$$P(x) = \begin{bmatrix} \mathrm{c}(x) \\ \mathrm{J}(x) \end{bmatrix} \tag{2.4}$$

$$P(g) = \begin{bmatrix} \mathrm{p} \\ \mathrm{J}(g) \end{bmatrix} \tag{2.5}$$

$$P(g') = \begin{bmatrix} \mathrm{p}' \\ \mathrm{J}(g') \end{bmatrix} \tag{2.6}$$

where $\mathrm{J}(g)$ is the time dependent part of the flux passing from the entry chamber to the entry surface and $\mathrm{J}(g')$ is that passing from the exit surface to exit chamber. Because attention is restricted to small fractional modulations, condition vectors may be related by the linear equations.

$$P(g) = SP(x = 0) \tag{2.7}$$

$$P(x = 0) = TP(x = l) \tag{2.8}$$

$$P(x = l) = S'P(g') \tag{2.9}$$

where T is the translation matrix relating condition vectors just below the entry and exit surfaces and S,S' are interface matrices linking the subsurface with those of the gas in the entry and exit chambers. A final pair of equations is required to link variables y and y', used in the experimental measurements, to the gas condition vectors. This is done through the entry and exit matrices, E and E', defined by:

$$\mathrm{y} = EP(g) \tag{2.10}$$

$$P(g') = E'\mathrm{y}' \tag{2.11}$$

In principle experimental variables may be the pressures, fluxes or any linear combination thereof. Working in terms of pressures, eqs.(2.7-2.11) may be combined to give

$$\mathbf{R} = \mathbf{p}/\mathbf{p}' = ESTS'E' \tag{2.12}$$

This equation relates the experimentally observable quantities through the coefficients which make up the matrices. The equation can be arranged to give (i) the phase lag ϕ, between the exit and entry chamber pressure modulation (ii) the ratio $|\mathbf{R}|^{-1}$, of exit end entry modulation amplitudes and the relative modulation amplitude ratio Λ. These are

$$\phi = \arg(\mathbf{R}) = \arctan[\Im(\mathbf{R})/\Re(\mathbf{R})] \tag{2.13}$$

$$|\mathbf{p}'| \,/\, |\mathbf{p}| = |\mathbf{R}|^{-1} \tag{2.14}$$

$$\Lambda = |\mathbf{R}|^{-1} \, (p_s/p_{s'}) \tag{2.15}$$

where $\Im(\mathbf{R})$ and $\Re(\mathbf{R})$ represent the imaginary and real components of the complex quantity $\mathbf{R}$. These last three quantities; phase lag, ϕ, modulation ratio, $|\mathbf{R}|$ and relative modulation amplitude ratio, Λ are supposed accessible to experimental determination. Three possible models of diffusant flow were considered by Cummings and Blackburn: flow limited by bulk diffusion, surface limited flow (simple two rate), internal trapping.

In the experimental work the following quantities are directly controlled; temperature, input pressure and angular frequency. The following quantities are measured during the experiment; (i) phase lag ϕ (ii) relative modulation amplitude ratio Λ with respect to angular frequency. Other quantities (diffusion coefficient, solubility, permeabilty, surface reaction rate, trapping rates etc.) are derived in the subsequent analysis.
In the coming sections the matrix coefficients will be specified in order to find expressions for phase lag, ϕ, amplitude ratio, $|\mathbf{R}|^{-1}$ and relative amplitude modulation ratio, Λ, for diffusion, surface reactions and internal trapping.

2.3 Diffusion Limited Permeation

2.3.1 Entry and Exit Matrices

The matrices are simple in form when diffusion is Fickian and the surface in equilibrium with an adjacent gas. The entry E and exit E' matrixes are idendical for the experimental system modelled. From (2.7)

$$\mathbf{y} = \mathbf{p} = E \begin{bmatrix} \mathbf{p} \\ \mathbf{J}^{(g)} \end{bmatrix} = \begin{bmatrix} 1 & 0 \end{bmatrix} \begin{bmatrix} \mathbf{p} \\ \mathbf{J}^{(g)} \end{bmatrix} \tag{2.16}$$

which identifies the entry matrix E. Pressure modulations in the output chamber are influenced in amplitude and phase by the chamber volume, the characteristics of the pump used and outgassing from the chamber walls. Changes of pressure are modelled by:

$$V\frac{dp'}{dt} = \sigma J^{(g')} + Q_{og} - Sp' \tag{2.17}$$

where $\sigma = \gamma RT$. This says that changes in the pressure may be due to the flux leaving the membrane, outgassing from other surfaces and pumping. Splitting (2.17) into steady state and harmonic parts as before gives:

$$p'_s = \frac{1}{S}(\sigma J_s + Q_{og}); \quad V\frac{dp'}{dt} = \sigma \mathbf{J}^{(g')} - S\mathbf{p}' \tag{2.18}$$

$$\mathbf{J}^{(g')} = \frac{1}{\sigma}[S + \mathrm{i}\omega V]\mathbf{p}' \tag{2.19}$$

Using the exit pressure $\mathbf{p}'$ as the detection variable, it follows from (2.8) that the exit matrix, E', is identified by:

$$P^{(g')} = \begin{bmatrix} 1 \\ (S + \mathrm{i}\omega V)/\sigma \end{bmatrix} (\mathbf{p}') = E'(\mathbf{p}') \tag{2.20}$$

2.3.2 The Phase Boundary Matrices, S and S'

Under the condition of surface equilibrium for a diatomic gas, the flux of diffusant entering or leaving the gas phase at all times equals the flux leaving or

entering the adjacent solid phase. That is, there is no surface accumulation. Thus at all times:

$$J^{(g)}(t) = J(0,t) \quad J^{(g')}(t) = J(l,t) \tag{2.21}$$

hence for the steady state part

$$J_s^{(g)} = J_s = J_s^{(g')} \tag{2.22}$$

and for the time dependent part

$$\mathbf{J}^{(g)}(t) = \mathbf{J}(0,t) \tag{2.23}$$

$$\mathbf{J}(l,t) = \mathbf{J}^{(g')}(t) \tag{2.24}$$

The subsurface diffusant concentrations may be written as providing equilibrium with the adjacent gas. Following Sieverts' law (1.5), this gives, for a diatomic gas:

$$c_s(0) = K_{sm} p_s^{1/2} \quad c_s(l) = K_{sm} p_s'^{1/2} \tag{2.25}$$

and for time dependent part

$$\mathbf{c}(0) = (K_{sm}/2p_s^{1/2})\mathbf{p} \quad \mathbf{c}(l) = (K_{sm}/2p_s'^{1/2})\mathbf{p}' \tag{2.26}$$

where K_{sm} is Sieverts coefficient.
Then the interface matrices, S and S'

$$\begin{bmatrix} \mathbf{p} \\ \mathbf{J}^{(g)} \end{bmatrix} = \begin{bmatrix} 2\sqrt{p_s}/K_{sm} & 0 \\ 0 & 1 \end{bmatrix} \begin{bmatrix} \mathbf{c}(0) \\ \mathbf{J}(0) \end{bmatrix} = S \begin{bmatrix} \mathbf{c}(0) \\ \mathbf{J}(0) \end{bmatrix} \tag{2.27}$$

and

$$\begin{bmatrix} \mathbf{c}(l) \\ \mathbf{J}(l) \end{bmatrix} = \begin{bmatrix} K_{sm}/2\sqrt{p_s'} & 0 \\ 0 & 1 \end{bmatrix} \begin{bmatrix} \mathbf{p}' \\ \mathbf{J}^{(g')} \end{bmatrix} = S' \begin{bmatrix} \mathbf{p}' \\ \mathbf{J}^{(g')} \end{bmatrix} \tag{2.28}$$

2.3.3 Translation Matrix

The translation matrix describes flow in the region $0 \leq x \leq l$ within the membrane and, in particular, it provides a means to relate concentration and flux at the $x = l$ surface to that at the $x = 0$ surface. A modulation of diffusant concentration at one surface of a membrane will propagate by diffusion. For the region $0 \leq x \leq l$, Fick's laws are assumed to be valid, so with diffusion coefficient D:

$$\frac{\partial c(x,t)}{\partial t} = D\frac{\partial^2 c(x,t)}{\partial x^2} \tag{2.29}$$

$$J(x,t) = -D\frac{\partial c(x,t)}{\partial x} \tag{2.30}$$

After splitting into steady state and harmonic parts: the general solutions for concentration and flux are:

$$\mathbf{c}(x) = \{\mathbf{A}\exp[\mathbf{a}(l-x)] + \mathbf{B}\exp[\mathbf{a}(x-l)]\}\exp \mathbf{i}\omega t \tag{2.31}$$

$$\mathbf{J}(x) = Da\{\mathbf{A}\exp[\mathbf{a}(l-x)] - \mathbf{B}\exp[\mathbf{a}(x-l)]\}\exp \mathbf{i}\omega t \tag{2.32}$$

The coefficients $\mathbf{A}$ and $\mathbf{B}$ can be eliminated when relating conditions at the front and rear surfaces of the membrane.

Then the translation matrix T, can be defined as;

$$T = \begin{bmatrix} \cosh \mathbf{a}l & (1/D\mathbf{a})\sinh \mathbf{a}l \\ D\mathbf{a}\sinh \mathbf{a}l & \cosh \mathbf{a}l \end{bmatrix} \tag{2.33}$$

where D is the diffusion coefficient and

$$\mathbf{a}l = (1+\mathbf{i})\zeta \tag{2.34}$$

with ζ a dimensionless representation of the frequency such that

$$\zeta = l(\omega/2D)^{1/2} \tag{2.35}$$

Note in passing that the translation matrix, T, has the property:

$$T(l_1)T(l_2) = T(l_1 + l_2) \tag{2.36}$$

2.3.4 Evaluation of R

Using the expressions obtained for E, S, T, S' and E', $\mathbf{R}$ can be evaluated to describe a pressure modulation experiment for diffusion limited flow:

$$\begin{aligned}
\mathbf{R} &= \mathbf{p}/\mathbf{p}' = ESTS'E' \\
&= \begin{bmatrix} 1 & 0 \end{bmatrix} \begin{bmatrix} 2p_s^{1/2}/K_{sm} & 0 \\ 0 & 1 \end{bmatrix} \begin{bmatrix} \cosh \mathbf{a}l & (1/D\mathbf{a}) \sinh \mathbf{a}l \\ D\mathbf{a} \sinh \mathbf{a}l & \cosh \mathbf{a}l \end{bmatrix} \\
&\quad \cdot \begin{bmatrix} K_{sm}/2p_s'^{1/2} & 0 \\ 0 & 1 \end{bmatrix} \begin{bmatrix} 1 \\ (S + \mathrm{i}\omega V/\sigma \end{bmatrix} \\
&= \left(\frac{p_s}{p_s'}\right)^{1/2} \cosh \mathbf{a}l + \frac{2p_s^{1/2}}{\sigma D K_{sm}} (S + \mathrm{i}\omega V) \frac{\sinh \mathbf{a}l}{\mathbf{a}}
\end{aligned} \tag{2.37}$$

When the output chamber pressure is low, that is $p_s' \ll p_s$, the basic assumption of rapid surface reaction means that Richardson's law of permeation (equation 1.6) applies in the form:

$$J_s = \frac{P_m p_s^{1/2}}{l} \tag{2.38}$$

$$P_m = D K_{sm} \tag{2.39}$$

where P_m is the permeability. Together with the pumping equation (2.18), (2.37) may be written:

$$\mathbf{R} = \left(\frac{p_s}{p_s'}\right)^{1/2} \left\{ \cosh \mathbf{a}l + 2 \left(\frac{p_s}{p_s'}\right) \left(\frac{S + \mathrm{i}\omega V}{S}\right) \left(\frac{1}{1 - Q_{og}/S p_s'}\right) \frac{\sinh \mathbf{a}l}{\mathbf{a}l} \right\} \tag{2.40}$$

Since $p_s \gg p_s'$, the cosh $\mathbf{a}l$ term remains negligible and if there is virtually no outgassing $Q_{og} \to 0$ then: Then the ratio $\mathbf{R}$ may then be written as:

$$\mathbf{R} = \frac{2\sqrt{p_s}l}{\sigma P_m} (S + \mathrm{i}\omega V) \frac{\sinh(1 + \mathrm{i})\zeta}{(1 + \mathrm{i})\zeta} \tag{2.41}$$

This form of the equation is used to obtain the variation of phase lag and relative modulation amplitude ratio.

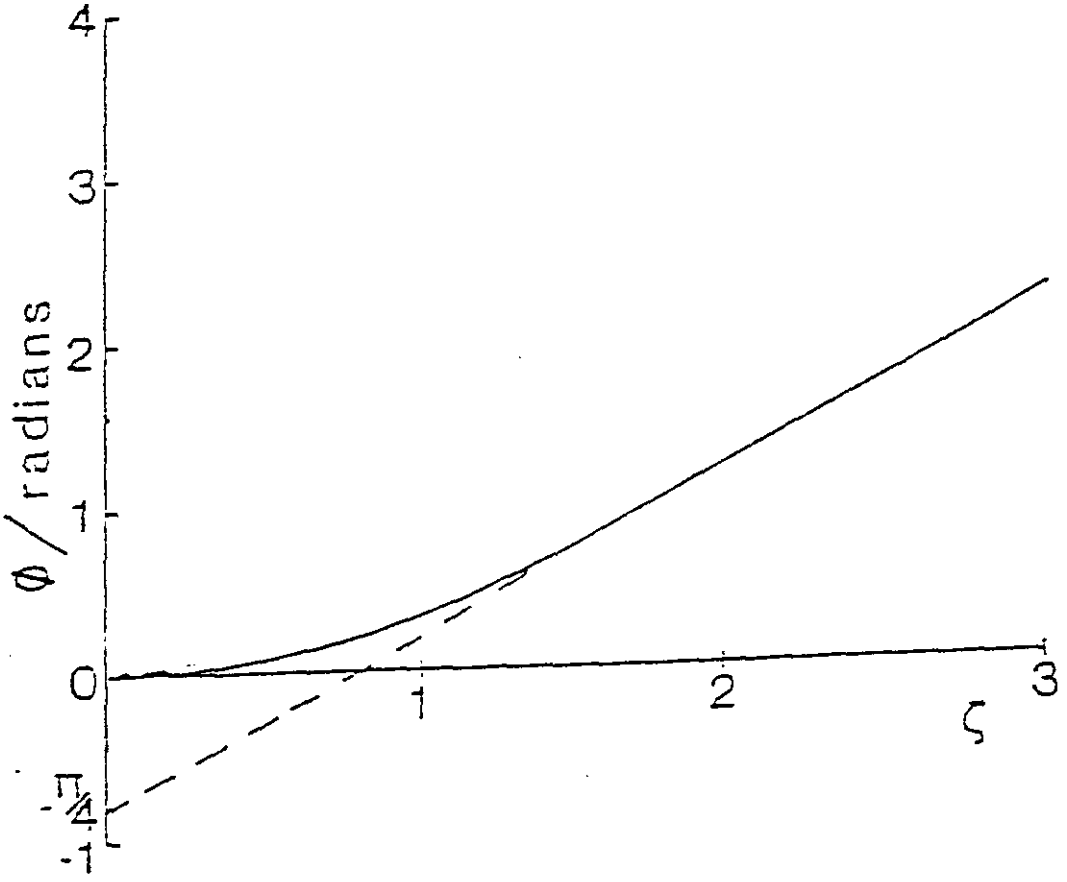

Figure 2.2 Variation of phase lag, ϕ, with frequency factor, ζ, for diffusion limited permeation.

2.3.5 The Variation of Phase Lag with Frequency

From (2.13) the phase lag is $\phi = \arg(\mathrm{R})$ so from (2.41):

$$\phi = \arctan\left(\frac{\tan\zeta}{\tanh\zeta}\right) - \frac{\pi}{4} + \arctan\left(\frac{\omega V}{S}\right) \tag{2.42}$$

The final term, $\varepsilon = \arctan(\omega V/S)$, is an equipment response time correction. The condition, $\varepsilon = 0$, is here referred to as the *hard pumping approximation* and it describes well the experimental conditions of the present work. In (2.42) it leads to:

$$\tan\phi = \frac{\tan\zeta - \tanh\zeta}{\tan\zeta + \tanh\zeta} \tag{2.43}$$

This functional relationship is of potential experimental importance, since it is independent of K_{sm} and so allows direct experimental evaluation of a diffusion coefficient. The behaviour of the function is shown in Fig (2.2), lower curve. Note that ζ has the value $\pi^{1/2}$ when the periodic time of the modulation equals the time l^2/D, characterizing diffusion through the foil.

High frequency limit

For higher frequencies, $\zeta > 3$, to a good approximation (2.43) reduces to:

$$\phi = \zeta - \frac{\pi}{4} = l\sqrt{\frac{\omega}{2D}} - \frac{\pi}{4} \tag{2.44}$$

Thus, the phase lag varies linearly with $\omega^{1/2}$ at high frequencies and, if this linear region is extrapolated back, gives an intercept of $-\pi/4$ on the ϕ axis.

Low frequency limit

In the low frequency limit, expanding (2.43) in powers of ζ gives, to a good approximation, for values of $\zeta < 1/2$:

$$\phi = \frac{\zeta^2}{3} = \frac{l^2\omega}{6D} \tag{2.45}$$

thus the phase lag, ϕ, should vary linearly with ω for low frequency modulation.

2.3.6 The Variation of Modulation Amplitude with Frequency

Measurement of pressure amplitudes also provides useful information about the permeation system. From (2.41):

$$|\mathbf{R}|^{-1} = \frac{DK_{sm}\zeta\sigma}{2p_s^{1/2}l}\left[\frac{1}{S^2+(\omega V)^2}\right]^{1/2}\left\{\frac{\sinh \mathbf{a}l \sinh \mathbf{a}^{*}l}{(1+\mathbf{i})(1-\mathbf{i})}\right\}^{-1/2} \tag{2.46}$$

It follows, using the hard pumping approximation $\omega V \ll S$:

$$|\mathbf{R}|^{-1} = \frac{|\mathbf{p}'|}{|\mathbf{p}|} = \frac{DK_{sm}\sigma}{p_s^{1/2}Sl}\frac{\zeta}{(\cosh 2\zeta - \cos 2\zeta)^{1/2}} \tag{2.47}$$

This result is of importance in two ways. First, it provides a separate way of evaluating the diffusion coefficient and hence, by comparison with the phase data, gives an internal consistency check. Second, it allows evaluation of the permeability, independent of the outgassing effects which can modify the precision of estimates based on the steady state pressures p_s and p_s'.

2.3.7 Relative Modulation Amplitude Ratio

Equation (2.47) can be simplified. Using the variable Λ to represent the relative modulation amplitude ratio and letting $Q_{og} \rightarrow 0$:

$$\Lambda = \frac{|\mathbf{p}'|}{p_s'}\frac{p_s}{|\mathbf{p}|} = \frac{\zeta}{[\cosh 2\zeta - \cos 2\zeta]^{1/2}} \tag{2.48}$$

This relationship is shown in Fig (2.3).

High frequency limit

In the high frequency limit, (2.48) approaches the curve:

$$\Lambda = \zeta \exp(-\zeta) \tag{2.49}$$

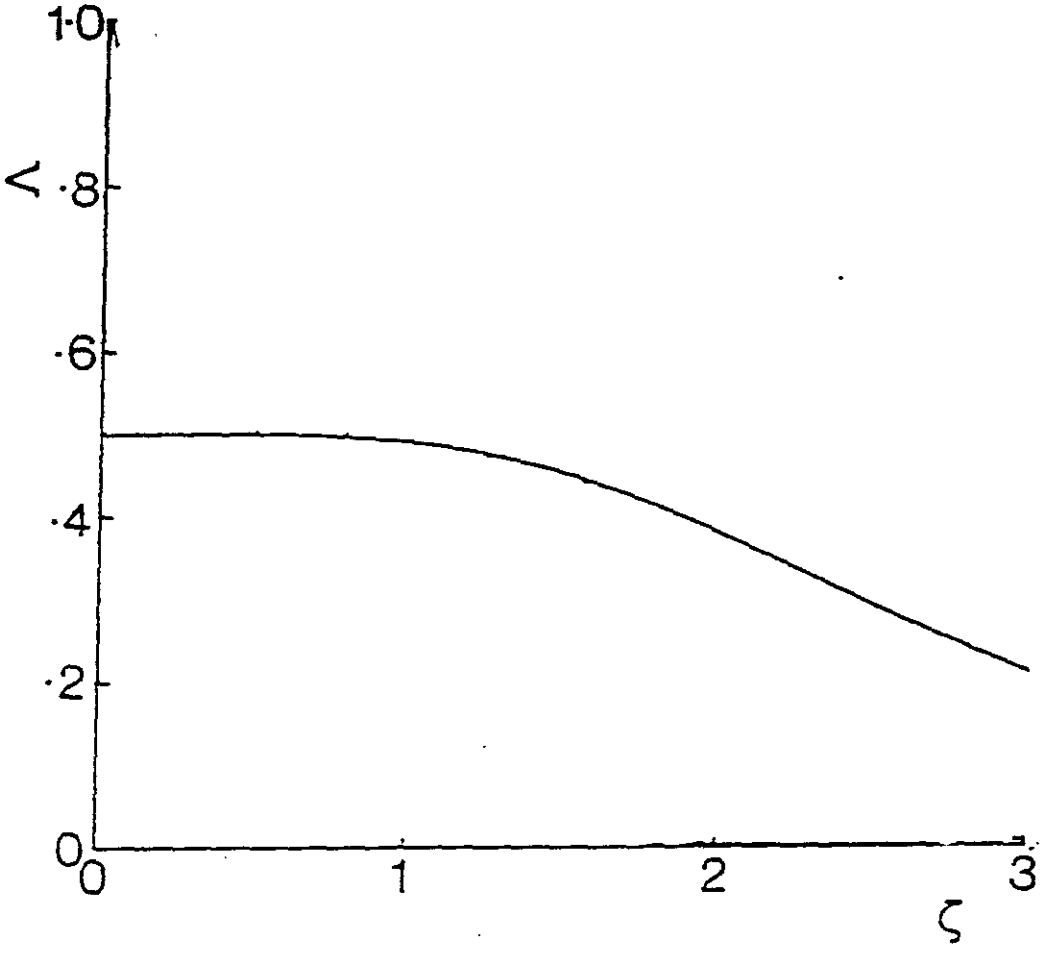

Figure 2.3 Variation of relative modulation amplitude ratio, $\Lambda = (|p'|p_s)/(p'_s|p|)$, with frequency factor, ζ, for diffusion limited permeation.

Low frequency limit

In the low frequency limit, the right-hand side of (2.48) approaches 1/2 and this constant value is a good approximation to the true curve over the range $0 < \zeta < \pi/4$.

$$\Lambda = \zeta \exp(-\zeta) \tag{2.50}$$

The low frequency limit of the relative modulation amplitude ratio (2.48) has particular significance. Consider the permeation pressure law in the exponent form:

$$J^{(g')} = kp^n \tag{2.51}$$

where the parameters k and n vary only slowly with pressure. On differentiating with respect to time, and taking the limit as $\omega \to 0$:

$$\frac{1}{J^{(g')}} \frac{\partial J^{(g')}}{\partial t} = \frac{n}{p} \frac{\partial p}{\partial t} \tag{2.52}$$

therefore, for sufficiently small modulation amplitudes:

$$\frac{\left|\mathbf{J}^{(g')}\right|}{J_s} = n \frac{|\mathbf{p}|}{p_s} \tag{2.53}$$

Thus, if outgassing is negligible, that is $Q_{og} \to 0$, using (2.18) and (2.19) gives:

$$\Lambda = \frac{|\mathbf{p}'|}{|\mathbf{p}|} \frac{p_s}{p'_s} = n \qquad \text{(for } \omega \to 0 \text{)} \tag{2.54}$$

This is an interesting result, the relative modulation amplitude ratio, extrapolated back to zero frequency, is simply the exponent n in the generalized permeation pressure law. For diffusion limited flow at small background pressures, when Richardson's law of permeation applies, the extrapolation of Λ to the zero frequency axis should lead to the value 1/2; under other conditions the measured value of n could be a useful indication of the mechanism which limits flow.

2.4 Surface Reactions

2.4.1 Two Rate Constant Model

To incorporate the effect of finite reaction rates, a model of minimal additional complexity is used. It has sufficient detail to describe deviations from equilibrium in the sub-surface concentrations and to describe the variation of permeation from a rate proportional to $p_s^{1/2}$ at high pressures, to one proportional to p_s at low pressures. However, it takes no account of any surface phase.

In this model the possible surface processes; adsorption, desorption, dissociation, association and de-solution; are all described by the single reversible reaction:

$$H_2 \text{ (gas phase)} \underset{k_2 c^2}{\overset{k_1 p}{\rightleftharpoons}} 2H \text{ (solid phase)} \tag{2.55}$$

where hydrogen is taken to be the diffusant gas and k_1 and k_2 are the rate constants. The same equilibrium applies at the output surface with rate constants k_1' and k_2'.

A change in surface properties calls for a change only in the phase boundary matrices, S and S'. The coefficients describing the translation, T, entry, E, and exit, E', matrices are retained. A new expression can be obtained for the vector pressure ratio, $\mathbf{R}$, and derivative expressions for the frequency variations of the phase lag, ϕ, the amplitude modulation ratio $|\mathbf{R}|^{-1}$, and the relative amplitude modulation, Λ. The calculation is made in the limit $p_s'/p_s \to 0$, which corresponds to the experimentally interesting condition of a rapidly pumped output chamber.

The rate constants k_1, k_2, k_1' and k_2' are such that at the entry surface:

$$J^{(g)} = k_1 p - k_2 c^2(0) = J(0) \tag{2.56}$$

and at the exit surface:

$$J(l) = k_2' c^2(l) - k_1' p' = J^{(g')} \tag{2.57}$$

the prime, $'$, being used to indicate that the exit surface coefficients may differ from those of the input.

Equilibrium

At equilibrium all fluxes are zero, $p = p'$, and for all x:

$$c(x) = K_{sm} p^{1/2} \tag{2.58}$$

Specifically:

$$c(0) = c(l) = K_{sm} p^{1/2} \tag{2.59}$$

so, using (2.56) and (2.57), the rate constants are related by:

$$K_{sm} = \left(\frac{k_1}{k_2}\right)^{1/2} = \left(\frac{k_1'}{k_2'}\right)^{1/2} \tag{2.60}$$

Steady state

In steady state flow there can be no accumulation of diffusant in the foil or in its surfaces, so all the fluxes in (2.56) and (2.57) can be set equal to some particular value, J_s, giving:

$$c_s(0) = K_{sm}(p_s - J_s/k_1)^{1/2} \tag{2.61}$$

$$c_s(l) = K_{sm}(p_s' + J_s/k_1')^{1/2} \tag{2.62}$$

Assuming Fick's laws to hold, the flux within the foil is:

$$J_s = \left(\frac{D}{l}\right)[c_s(0) - c_s(l)] \tag{2.63}$$

and so:

$$\frac{J_s l}{D K_{sm}} = \left(p_s - \frac{J_s}{k_1}\right)^{1/2} - \left(p_s' - \frac{J_s}{K_1'}\right)^{1/2} \tag{2.64}$$

Modulation

When modulation added to a steady flow, the flow equations, (2.56) and (2.57) become:

$$\left[J_s + \mathbf{J}^{(g)}\right] = k_1(p_s + \mathbf{p}) - k_2[c_s(0) + \mathbf{c}(0)]^2 = [J_s + \mathbf{J}(0)] \tag{2.65}$$

$$[J_s + \mathbf{J}(l)] = k_2'[c_s(l) + \mathbf{c}(l)]^2 - k_1'(p_s' + \mathbf{p}') = [J_s + \mathbf{J}^{(g')}] \tag{2.66}$$

Subject to the assumption that all modulations are of small amplitude, $|\mathbf{c}(x)| \ll c_s(x)$ and $|\mathbf{J}(x)| \ll J_s$, these last equations can be linearized to give for the time-dependent fluxes:

$$\mathbf{J}^{(g)} = k_1\mathbf{p} - 2k_2c_s(0)\mathbf{c}(0) = \mathbf{J}(0) \tag{2.67}$$

$$\mathbf{J}(l) = 2k_2'c_s(l)\mathbf{c}(l) - k_1'\mathbf{p}' = \mathbf{J}^{(g')} \tag{2.68}$$

2.4.2 Phase Boundary Matrixes, S, S'

Using (2.61) and (2.62) to substitute for $c_s(0)$ and $c_s(l)$, the phase boundary matrices, S and S', may be identified as:

$$S = \begin{bmatrix} (2/K_{sm})(p_s - J_s/k_1)^1/2 & 1/k_1 \\ 0 & 1 \end{bmatrix} \tag{2.69}$$

$$S' = \begin{bmatrix} (K_{sm}/2)(p_s' + J_s/k_1')^{-1/2} & (K_{sm}/2k_1')(p_s' + J_s/k_1')^{-1/2} \\ 0 & 1 \end{bmatrix} \tag{2.70}$$

2.4.3 No Backflow Approximation

In experiments where the output chamber is pumped so rapidly that $p_s \gg p_s'$, it can be assumed that there is no significant backflow to the

membrane from the diffusant in the output chamber. This allows (2.57) to be written as:

$$J(l) = k_2' c^2(l) = J^{(g')} \tag{2.71}$$

$$c_s(l) = K_{sm}(J_s/k_1')^{1/2} \tag{2.72}$$

so the steady state flow, (2.64),becomes:

$$\frac{J_s l}{P_m} = \left(p_s - \frac{J_s}{k_1}\right)^{1/2} - \left(\frac{J_s}{k_1'}\right)^{1/2} \tag{2.73}$$

where P_m is the permeability. It follows that:

$$p_s = J_s \left\{ \frac{1}{k_1} + \frac{1}{k_1'} + \left[\frac{2l}{P_m}\right] \left(\frac{J_s}{k_1'}\right)^{1/2} + J_s \left(\frac{l}{P_m}\right)^{1/2} \right\} \tag{2.74}$$

and (2.68) becomes:

$$\mathbf{J}(l) = 2k_2' c_s(l)\mathbf{c}(l) = \mathbf{J}^{(g')} \tag{2.75}$$

thus giving as the exit phase boundary matrix S':

$$S' \cong S_0' = \begin{bmatrix} 0 & (K_{sm}/2)(k_1' J_s)^{-1/2} \\ 0 & 1 \end{bmatrix} \tag{2.76}$$

where the suffix, $_0$, is used to denote the zero backflow approximation.

2.4.4 Evaluation of R.

Using the zero backflow approximation, multiplying out terms shows **R** to have the general form:

$$\mathbf{R} = \{(e + \mathbf{i}f)\cosh \mathbf{a}l + (g + \mathbf{i}h)\sinh \mathbf{a}l\} \frac{(S + \mathbf{i}\omega V)}{\sigma \mathbf{a}l} \tag{2.77}$$

with:

$$\begin{aligned} e &= f = \zeta \left\{ (p_s - J_s/k_1)^{1/2} (k_1' J_s)^{-1/2} + 1/k_1 \right\} \\ g &= (2l/DK_{sm})(p_s - J_s/k_1)^{1/2} \\ h &= \zeta^2 (DK_{sm}/lk_1)(k_1' J_s)^{-1/2} \end{aligned} \tag{2.78}$$

Since $\mathbf{a}l = (1+\mathrm{i})\zeta$, $\cosh \mathbf{a}l$ and $\sinh \mathbf{a}l$ can be expanded to give:

$$\begin{aligned}\mathbf{R} &= \frac{S+\mathrm{i}\omega V}{\sigma(1+\mathrm{i})\zeta} \\ &\quad .\{(e+\mathrm{i}f)[\cosh\zeta\cos\zeta+\mathrm{i}\sinh\zeta\sin\zeta] \\ &\quad +(g+\mathrm{i}h)[\sinh\zeta\cos\zeta+\mathrm{i}\sin\zeta\cosh\zeta]\} \end{aligned} \tag{2.79}$$

2.4.5 The Variation of Phase Lag with Frequency

Using (2.13) for the phase shift, ϕ, the above gives:

$$\phi = \arctan\left[\frac{e\tan\zeta\tanh\zeta+f+g\tan\zeta+h\tanh\zeta}{e-f\tan\zeta\tanh\zeta+g\tanh\zeta-h\tan\zeta}\right]+\varepsilon-\frac{\pi}{4} \tag{2.80}$$

where $\varepsilon = \arctan(\omega V/S)$ is the equipment response lag.

2.4.6 The Variation of Amplitude Ratio with Frequency

For the amplitude ratio, (2.79) gives:

$$\begin{aligned}|\mathbf{R}| &= \frac{|S+\mathrm{i}\omega V|}{\sqrt{2}\sigma\zeta} \\ &\quad .[(e^2+f^2)\,|\cosh\mathbf{a}l|^2+(g^2+h^2)\,|\sinh\mathbf{a}l|^2 \\ &\quad +2\Re[(e+\mathrm{i}f)(g-\mathrm{i}h)\cosh\mathbf{a}l\sinh\mathbf{a}^*l]]^{1/2} \end{aligned} \tag{2.81}$$

hence:

$$\begin{aligned}|\mathbf{R}| &= \frac{[S^2+\omega^2V^2]^{1/2}}{2\sigma\zeta} \\ &\quad .[(e^2+f^2+g^2+h^2)\cosh 2\zeta+(e^2+f^2-g^2-h^2)\cos 2\zeta \\ &\quad +2(eg+fh)\sinh 2\zeta+2(fg-eh)\sin 2\zeta]^{1/2} \end{aligned} \tag{2.82}$$

Although (2.80) and (2.82) with (2.79) are a complete description of the effect of surface rate constants on phases and amplitudes, they are not in a form which readily allows comparison. The difficulty is that, the coefficients e, f, g and h depend on both p_s and J_s.

2.4.7 The Variation of Phase lag and Amplitude ratio with Pressure

To show how the transmitted modulation varies with pressure it is convenient to express the flux in dimensionless form and the rate constants in a form which enhances effects which vary with the symmetry of the foil surfaces.

Dimensionless parameters, asymmetry of surface, reduced flux

To do this mean rates, $\overline{k}_1$ and $\overline{k}_2$, are formed with:

$$\overline{k}_1 = k_1 k_1' / (k_1 + k_1') \tag{2.83}$$

$$\overline{k}_2 = k_2 k_2' / (k_2 + k_2') \tag{2.84}$$

and the asymmetry of the surfaces is described by the parameter, μ, defined by the equivalent expressions:

$$\mu = (k_1 - k_1')/(k_1 + k_1') = (k_2 - k_2')/(k_2 + k_2') \tag{2.85}$$

In this formulation the condition $\mu = 0$ corresponds to $k_1 = k_1'$, $k_2 = k_2'$, and identity in the properties of the foil. The condition $\mu = 1$ corresponds to $k_1 \gg k_1'$ and a flux determined by the exit surface; $\mu = -1$ corresponds to $k_1' \gg k_1$ and a flux determined by the entry surface.

The flux is most conveniently put into dimensionless form, j, by dividing the steady state flux, J_s, by a reference flux, J_{ref}:

$$j = J_s / J_{ref} \tag{2.86}$$

To define J_{ref}, note first that in (2.73) at high pressures ($J_s \rightarrow \infty$) the steady state equation reduces to:

$$J_s(p \rightarrow \infty) = (P_m/l) p_s^{1/2} \tag{2.87}$$

that is to Richardson's law. At low pressures ($J_s \rightarrow 0$), (2.73) becomes:

$$J_s(p \to 0) = \overline{k}_1 p_s \qquad (2.88)$$

Extrapolation of these two limiting curves (2.87), (2.88) shows them to intersect when $p_s^{1/2} = (P_m/l)/\overline{k}_1$. The corresponding flux value is taken as the reference flux. That is:

$$J_{ref} = (P_m/l)^{1/2}/\overline{k}_1 \qquad (2.89)$$

and hence:

$$j = \overline{k}_1 (l/P_m)^{1/2} J_s \qquad (2.90)$$

Substitution into the steady state equation enables the pressure to be written:

$$p_s = j(P_m/\overline{k}_1 l)^{1/2} \left\{1 + [2j(1+\mu)]^{1/2} + j\right\} \qquad (2.91)$$

and the parameters e, f, g and h become:

$$\begin{aligned} e &= f = (\zeta/2\overline{k}_1)\left\{2 + [2j(1+\mu)]^{1/2}\right\} \\ g &= (1/\overline{k}_1)\left\{2j + [2j(1+\mu)]^{1/2}\right\} \\ h &= (\zeta^2/2\overline{k}_1)(1-\mu)[(1+\mu)/2j]^{1/2} \end{aligned} \qquad (2.92)$$

Of experimental interest is how the modulation amplitude and phase vary with frequency. The simplification of this section allows this readily to be done.

2.4.8 The Variation of Phase Lag with Pressure

The phase-frequency relationship of (2.80) is illustrated in Fig (2.4) for $\mu = 0$ (entry and exit surfaces are identical) and various values of j. There, the principle characteristic is the increase in phase lag that accompanies a reduction in flux or pressure. This is a direct consequence of the changeover from $p^{1/2}$, to p^1 permeation.

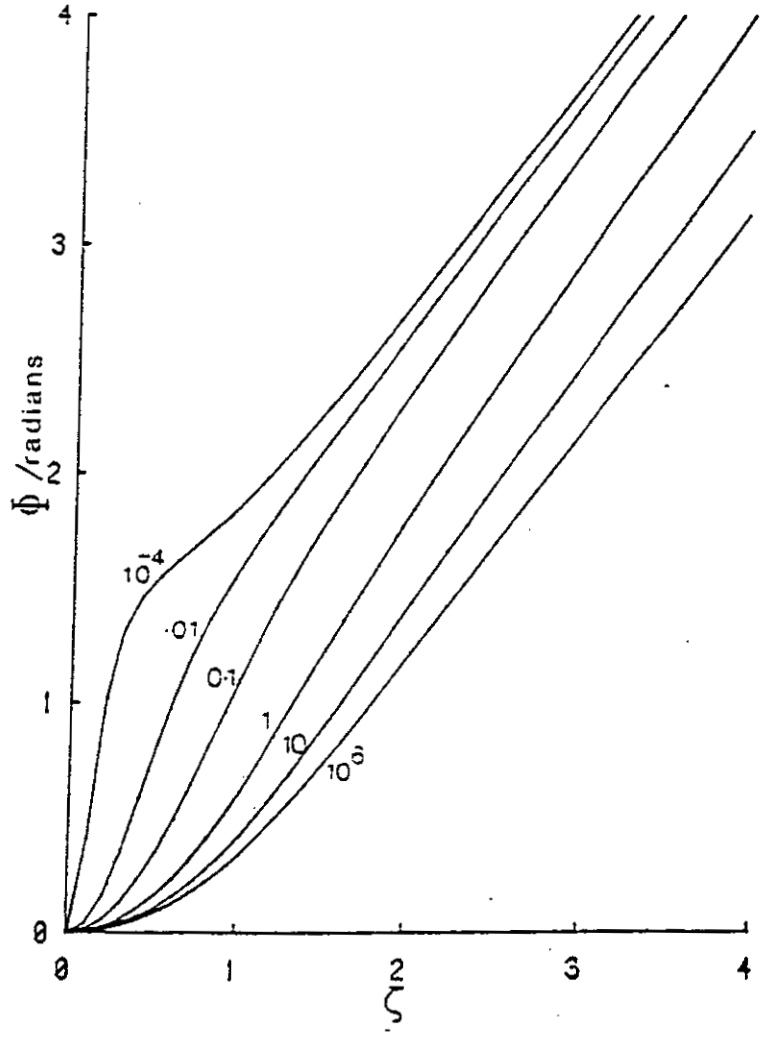

Figure 2.4 Diffusion with chemisorption: variation of phase lag ϕ with frequency factor ζ. Curves are for symmetric foils, $\mu = 0$, and specified values of the reduced flux j.

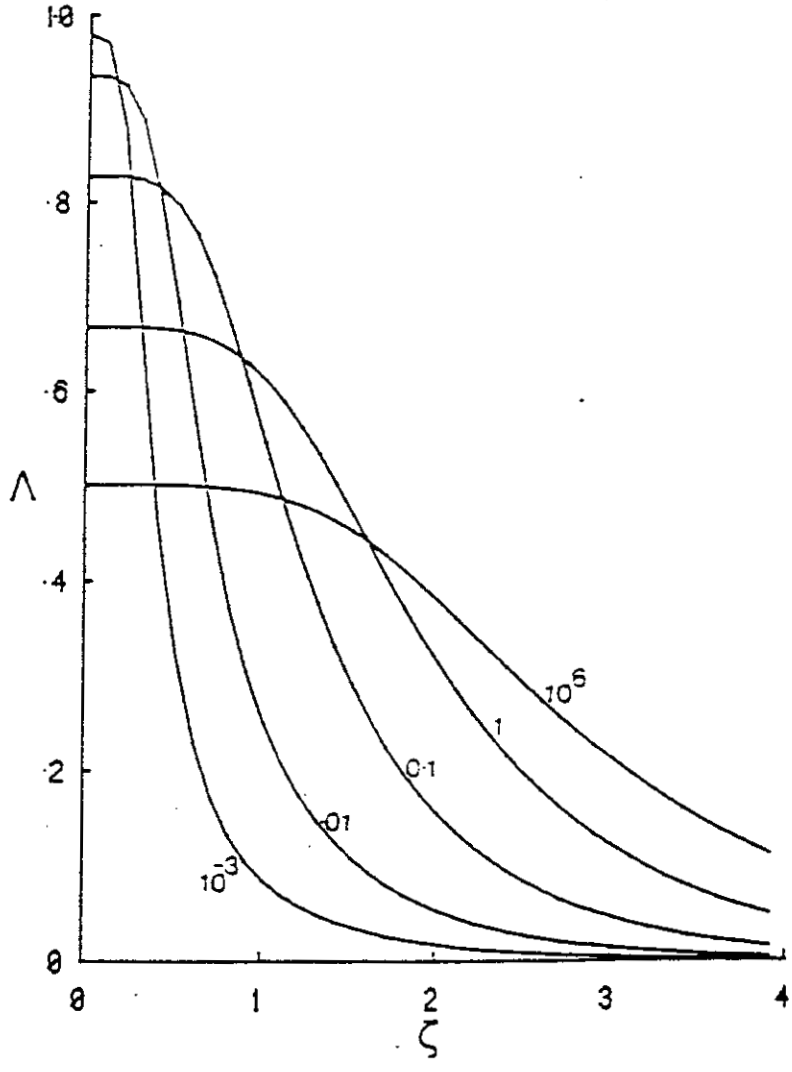

Figure 2.5 Diffusion with chemisorption: variation of relative modulation amplitude Λ with frequency factor ζ. Curves are for symmetric foils, $\mu = 0$, and specified values of the reduced flux j.

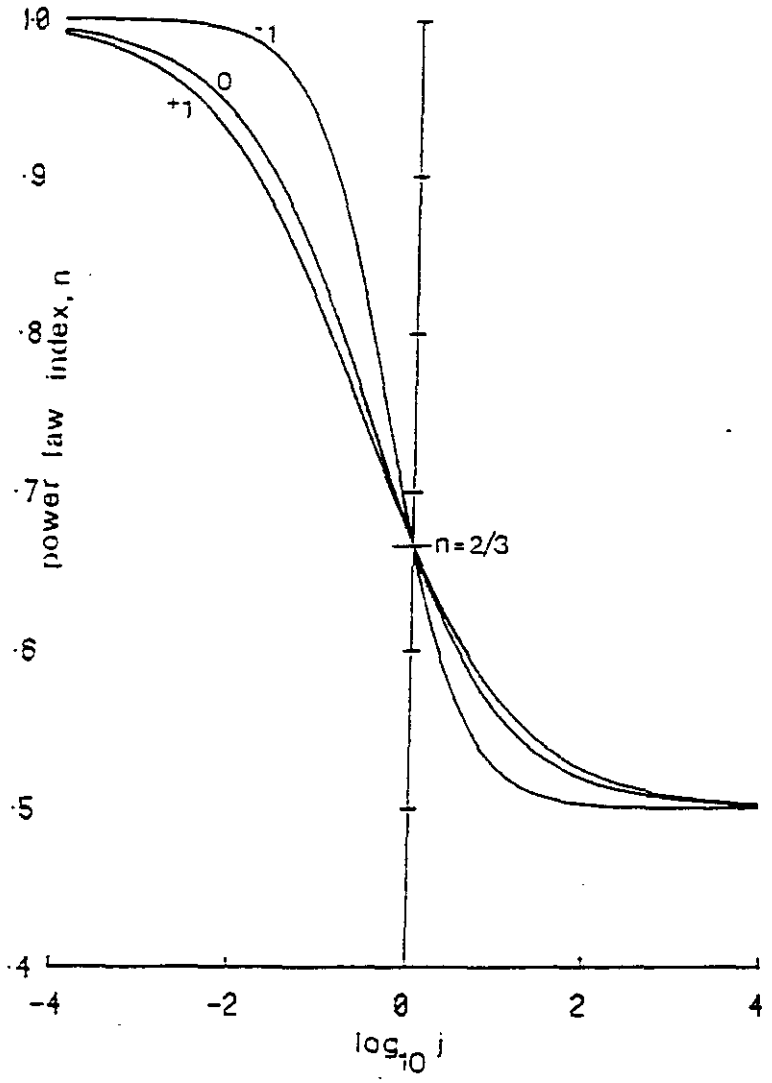

Figure 2.6 Diffusion with chemisorption:variation of the power law index, n, with reduced flux j, for $\omega = 0$ and $Q_{og} = 0$. Curves are for specified μ values and show a fall of index from 1 to 1/2 as the flux is increased to diffusion limited values.

High Frequency Limit

Analysis of the curves is simplified at high modulation frequencies for, with $\zeta > 3$, $\sinh \mathbf{a}l \approx \cosh \mathbf{a}l \approx \exp(\mathbf{a}l)$ and it follows that:

$$\mathbf{R} = [(e+g) + \mathbf{i}(f+h)] \exp \mathbf{a}l \frac{(S + \mathbf{i}\omega V)}{(1+\mathbf{i})\sigma\zeta} \tag{2.93}$$

Since this is in product form it follows immediately that:

$$\begin{aligned} \phi &= \arg[e+g+\mathbf{i}(f+g)] + \arg[\exp \mathbf{a}l] + \varepsilon - \pi/4 \\ &= \phi_s + \zeta + \varepsilon - \pi/4 \end{aligned} \tag{2.94}$$

where ϕ_s represents phase changes within the surfaces at high frequencies. The surface phase lag may be evaluated for any specified surface condition.

To explore the pressure dependence of the surface phase, consider a flux limited by the input surface with $\mu = -1$. Then from (2.93):

$$\phi = \arctan[\zeta/(\zeta + 2j)] \tag{2.95}$$

so at high pressures, when $j \gg 1$ and $n = 1/2$, $\phi_s = 0$; and at low pressures, when $j \ll 1$ and $n = 1$, $\phi_s = \pi/4$. Pressure reduction thus increases the phase lag by up to $\pi/4$. Intermediate surface conditions result in other values for ϕ_s. The principle point of note is that a single surface can produce a maximum phase change of $\pi/4$ on pressure variation so that when both surfaces limit the flux, a variation of $\pi/2$ is possible.

2.4.9 Variation of Relative Modulation Amplitude with Pressure

The variation of modulation amplitude with frequency is best described using the relative modulation amplitude ratio $\Lambda = |R|^{-1}(p_s/p_s')$. Neglecting equipment effects, $S \gg \omega V$, and assuming outgassing to be negligible, $Q_{og} = 0$, it follows from (2.82) and (2.91) that:

$$\Lambda = \frac{2\zeta}{\bar{k}_1} \frac{\{1 + [2j(1+\mu)]^{1/2} + j\}}{\left[\begin{array}{l} (e^2 + f^2 + g^2 + h^2)\cosh 2\zeta + (e^2 + f^2 - g^2 - h^2)\cos 2\zeta \\ +2(eg + fh)\sinh 2\zeta + 2(fg - eh)\sin 2\zeta \end{array} \right]^{1/2}} \tag{2.96}$$

This variation of relative amplitude modulation ratio, Λ, with frequency is shown in Fig (2.5) for $\mu = 0$ and specified values of j. Its characteristic feature is the changeover from a low frequency region where Λ falls with increasing pressure to a high frequency region where Λ increases with increasing pressure.

Low frequency limit

The value of Λ as $\omega \to 0$ is an especially useful indicator of the permeation process and, as described in the previous section, $\Lambda(\omega \to 0) = n$, where n is the power law index. This equality is subject to the condition that the outgassing terms can be ignored.

From (2.93) then, when $\omega \to 0$, one finds:

$$\Lambda(\omega \to 0) = \frac{\{1 + [2j(1+\mu)]^{1/2} + j\}}{\{1 + (3/2)[2j(1+\mu)]^{1/2} + 2j\}} \tag{2.97}$$

The form of this variation is shown in Fig 2.6 for $\mu = \pm 1$. It shows a gradual changeover in the power law index from the diffusion limited, high flux value of 1/2, when $j \gg 1$, to the surface limited, low flux value of 1, when $j \ll 1$. In passing it is of interest to note that when $j = 1$, that is when the flux is equal to the reference flux, $n = 2/3$ for all values of μ.

2.5 Internal Trapping

Atoms of a species subject to trapping during diffusion may be supposed to follow random paths through the solid interrupted by occasional pauses in the locations which are the traps. Traps which hold atoms of the diffusant species for times long relative to the time of an experiment are designated irreversible; traps which hold them for times comparable with the experiment

time are designated reversible. Experiments using modulation methods are sensitive to trapping times comparable with the period of the modulation and it is to this class of traps that the following calculation is addressed.

Diffusant atoms subject to trapping may be seen as belonging to one of two species: they are free and mobile so are part of the usual diffusant concentration c, or they are restricted and immobile and so part of a separate concentration z. Movement between the species is here described by the reversible reaction:

$$H(\text{mobile}) \underset{k_B z}{\overset{k_A c}{\rightleftharpoons}} H(\text{trapped}) \tag{2.98}$$

where k_A and k_B are rate constants.

Such effects appear only in the translation matrix T. The coefficients describing the phase boundary, S and S' and the entry, E and exit, E', matrices are the same as in the diffusion limited case. A new translation matrix, $T^{\dagger}$. will be used to provide a new expression for the vector pressure ratio, $\mathbf{R}$, and derived expressions for ϕ, $|\mathbf{R}|^{-1}$ and Λ. The calculation will be made in the limit $p'_s/p_s \rightarrow 0$, which corresponds to the experimental condition of a rapidly pumped output chamber.

2.5.1 Translation Matrix T

The rate equation corresponding to (2.98) can be written:

$$\frac{dz}{dt} = k_A c - k_B z \tag{2.99}$$

Since conservation of mass requires:

$$\frac{\partial c}{\partial t} = -\frac{\partial J}{\partial x} - \frac{\partial z}{\partial t} \tag{2.100}$$

it follows from Fick's law that:

$$J = -D\frac{\partial c}{\partial x} \tag{2.101}$$

$$\frac{\partial c}{\partial t} + \frac{\partial z}{\partial t} = D\frac{\partial^2 c}{\partial x^2} \tag{2.102}$$

Equations (2.99), (2.101) and (2.102) may be split into time dependent and steady state parts. This gives, respectively:

$$\frac{\partial \mathbf{z}}{\partial t} = k_A \mathbf{c} - k_B \mathbf{z} \quad ; k_A c_s = k_B z_s \tag{2.103}$$

$$\frac{\partial \mathbf{c}}{\partial t} + \frac{\partial \mathbf{z}}{\partial t} = D\frac{\partial^2 \mathbf{c}}{\partial x^2} \quad ; D\frac{\partial^2 c_s}{\partial x^2} = 0 \tag{2.104}$$

and

$$\mathbf{J} = -D\frac{\partial \mathbf{c}}{\partial x} \quad ; J_s = \frac{D}{l}[c_s(0) - c_s(l)] \tag{2.105}$$

The time dependent rate equation can be written:

$$\mathbf{z} = (\partial/\partial t + k_B)^{-1} k_A \mathbf{c} \tag{2.106}$$

and substituting into the time dependent conservation equation gives:

$$(\partial/\partial t + k_B + k_A)\frac{\partial \mathbf{c}}{\partial t} = D(\partial/\partial t + k_B)\frac{\partial^2 \mathbf{c}}{\partial x^2} \tag{2.107}$$

In effect, this is a diffusion equation describing the propagation of concentration modulations through the foil. Its solution is of the form:

$$\mathbf{c}(x) = \{\mathbf{F}\exp[\mathbf{b}(l-x)] + \mathbf{G}\exp[\mathbf{b}(x-l)]\}\exp(\mathbf{i}\omega t) \tag{2.108}$$

$$\mathbf{J}(x) = D\mathbf{b}\{\mathbf{F}\exp[\mathbf{b}(l-x)] - \mathbf{G}\exp[\mathbf{b}(x-l)]\}\exp(\mathbf{i}\omega t) \tag{2.109}$$

where $\mathbf{F}$ and $\mathbf{G}$ are determined by the imposed boundary conditions and $\mathbf{b}$ is a complex function of ω, k_A, k_B and D. Substitution of (2.108) into (2.107) provides the condition on $\mathbf{b}$ that:

$$D\mathrm{b}^2 = \frac{k_A\omega^2 + \mathrm{i}\omega(\omega^2 + k_B^2 + k_A k_B)}{(\omega^2 + k_B^2)} \tag{2.110}$$

and splitting b into real and imaginary parts using:

$$\mathrm{b}l = \xi + \mathrm{i}\chi \tag{2.111}$$

provides the two conditions:

$$(D/l^2)(\xi^2 - \chi^2) = k_A[1 - k_B^2/(\omega^2 + k_B^2)] \tag{2.112}$$

$$(2D/l^2)\xi\chi = \omega[1 + k_A k_B/(\omega^2 + k_B^2)] \tag{2.113}$$

Equations (2.108) and (2.109) can be written in matrix notation

$$\begin{aligned} \mathbf{P}(x) &= \begin{pmatrix} \mathrm{c}(x) \\ \mathrm{J}(x) \end{pmatrix} \qquad (2.114) \\ &= \begin{pmatrix} \exp[\mathrm{b}(l-x)] & \exp[\mathrm{b}(x-l)] \\ D\mathrm{b}\exp[\mathrm{b}(l-x)] & -D\mathrm{b}\exp[\mathrm{b}(x-l)] \end{pmatrix} \begin{pmatrix} \mathbf{F} \\ \mathbf{G} \end{pmatrix} \exp(\mathrm{i}\omega t) \end{aligned}$$

It is a simple matter to relate conditions at the $x = 0$ and $x = l$ surfaces in a way which is independent of F and G. The matrix, $T^{\dagger}$, which does this is given by:

$$P(0) = T^{\dagger}P(l) = \begin{pmatrix} \cosh \mathrm{b}l & (1/D\mathrm{b})\sinh \mathrm{b}l \\ D\mathrm{b}\sinh \mathrm{b}l & \cosh \mathrm{b}l \end{pmatrix} P(l) \tag{2.115}$$

where b is a complex function of ω, k_a, k_b and D and

$$\mathrm{b}l = \xi + \mathrm{i}\chi \tag{2.116}$$

Note that $T^{\dagger}$is identical with the translation matrix, T, which describes simple Fickian diffusion but for the substitution of b for a.

2.5.2 Evaluation of R

Assuming equilibrium conditions to hold at the surface and in the gas phase, $\mathbf{R} = \mathbf{p}/\mathbf{p}' = EST^{\dagger}S'E'$ becomes:

$$\mathbf{R} = \begin{pmatrix} 1 & 0 \end{pmatrix} \begin{pmatrix} 2p_s^{1/2}/K_{sm} & 0 \\ 0 & 1 \end{pmatrix} \begin{pmatrix} \cosh \mathrm{b}l & (1/D\mathrm{b}) \sinh \mathrm{b}l \\ D\mathrm{b} \sinh \mathrm{b}l & \cosh \mathrm{b}l \end{pmatrix} \cdot \begin{pmatrix} K_{sm}/2p_s'^{1/2} & 0 \\ 0 & 1 \end{pmatrix} \begin{pmatrix} 1 \\ (S + \mathrm{i}\omega V)/\sigma \end{pmatrix} \tag{2.117}$$

when , $p_s \gg p_s'$.

Splitting the bl term into its real and imaginary parts using (2.116), gives, after expansion of sinh bl:

$$\mathbf{R} = \frac{2p_s^{1/2}Sl}{DK_{sm}\sigma} \left[1 + \frac{\mathrm{i}\omega V}{S}\right] \frac{(\sinh \xi \cos \chi + \mathrm{i} \sin \chi \cosh \xi)}{(\xi + \mathrm{i}\chi)} \tag{2.118}$$

2.5.3 The Variation of Phase Lag with Frequency

The phase lag between output and input pressures is given by:

$$\phi = \arctan[\tan \chi / \tanh \xi] - \arctan[\chi/\xi] + \arctan[\omega V/S] \tag{2.119}$$

The final term, $\varepsilon = \arctan(\omega V/S)$ the equipment response term, may be neglected by setting $\varepsilon \to 0$ and after some rearrangement (2.119) becomes:

$$\tan \phi = \frac{\xi \tan \chi - \chi \tanh \xi}{\xi \tanh \xi + \chi \tan \chi} \tag{2.120}$$

2.5.4 The Variation of Modulation Amplitude with Frequency

Modulation amplitudes are given by:

$$|\mathbf{R}| = \frac{2p_s^{1/2}Sl}{DK_{sm}\sigma} \frac{|\sinh(\xi + \mathrm{i}\chi)|}{|\xi + \mathrm{i}\chi|} \tag{2.121}$$

so after normalizing and inverting:

$$|\mathbf{R}|^{-1} = \frac{|\mathbf{p}'|}{|\mathbf{p}|} = \frac{DK_{sm}\sigma}{2p_s^{1/2}Sl}\left[\frac{\xi^2+\chi^2}{\cosh^2\xi - \cos^2\chi}\right]^{1/2} \tag{2.122}$$

2.5.5 The Variation of Relative Modulation Amplitude Ratio with Frequency

To evaluate the relative modulation amplitude ratio, Λ, note that the steady state flux, J_s, still follows Richardson's equation:

$$J_s = DK_{sm}p_s^{1/2}/l \tag{2.123}$$

Using (2.18) then gives:

$$\Lambda = \frac{1}{2}\left[1 + \frac{Q_{og}}{\sigma J_s}\right]^{-1}\left[\frac{(\xi^2+\chi^2)}{\cosh^2\xi - \cos^2\chi}\right]^{1/2} \tag{2.124}$$

Dimensionless Trapping Parameters

To examine how, in general, trapping modifies the amplitude and phase of the transmitted pressure modulation, it is useful to replace the rate constants k_A and k_B by dimensionless parameters. Let:

$$A = k_A l^2/2D \tag{2.125}$$

$$B = k_B l^2/2D \tag{2.126}$$

Then when A is near unity the mean time taken for diffusant atoms to reach a trap is about equal to that taken to diffuse through the foil. When B is near unity the mean time to stay for diffusant atoms in a trap is about equal to that for diffusion through the foil.

Increases of A and B represent reductions in the time taken to reach a trap and in the time of stay within one. Using (2.112) and (2.113), it is convenient to note that:

$$\xi^2 = \left[\frac{\zeta^4 + (A+B)^2}{1 + B^2/\zeta^4}\right]^{1/2} + \frac{A}{1 + B^2/\zeta^4} \tag{2.127}$$

$$\chi^2 = \left[\frac{\zeta^4 + (A+B)^2}{1 + B^2/\zeta^4}\right]^{1/2} - \frac{A}{1 + B^2/\zeta^4} \tag{2.128}$$

Fig (2.7) shows this variation of ϕ with ζ for specified values of A and B. There are two principle points of interest: the strong maxima which vary in position with B, and the values of ϕ at higher ζ which show the curves describing flow through traps as giving lower phase values than for diffusion limited flow with $A = B = 0$.

Equation (2.120) can be expanded as a power series in ζ. To second order one finds:

$$\tan\phi = \xi\chi/3 \tag{2.129}$$

which gives a useful approximation for the maximum and minimum of the full curve. Differentiation of (2.129) gives as the condition for the existence of a full maximum and minimum that $A > 8B$. The corresponding position of the maximum of (2.129) is:

$$\zeta_{max} = B^{1/2} \tag{2.130}$$

or:

$$\omega_{max} = k_B \tag{2.131}$$

That of the minimum is:

$$\zeta_{min} = [AB]^{1/4} \tag{2.132}$$

or:

$$\omega_{min} = (k_A k_B)^{1/2} \tag{2.133}$$

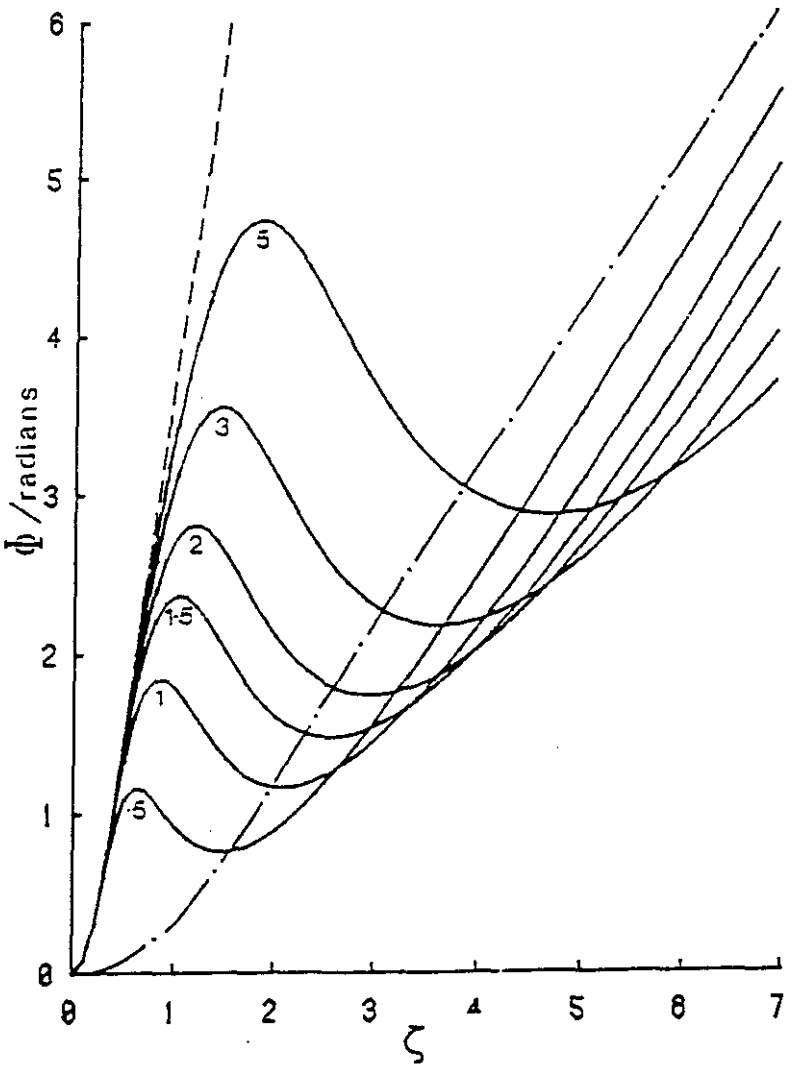

Figure 2.7 Diffusion with internal trapping: variation of phase lag ϕ with frequency factor ζ. Curves are shown for a fixed ratio of the trapping parameters, $A/B = 20$, with the specified values of B.

2.5.6 Low Frequency Asymptote: Dynamic Equilibrium

Also shown in Fig (2.7), is the low frequency asymptote of (2.120). For frequencies such that $\omega \ll k_B$, from (2.112) and (2.113) and remembering $\zeta = l(\omega/2D)^{1/2}$:

$$\chi = \xi = \zeta(1 + A/B)^{1/2} \tag{2.134}$$

and (2.120) becomes:

$$\tan\phi = \frac{\tan\chi - \tanh\chi}{\tan\chi + \tanh\chi} \tag{2.135}$$

This last result is of interest, since (2.135) has the same form as the phase shift one obtains when trapping is absent (since if $A = B = 0$ it follows from (2.112) and (2.113) that $\chi = \xi = \zeta$). Hence for frequencies such that $\omega \ll k_B$, the system with trapping behaves as the normal system but with a different effective diffusion coefficient.

Then when A is near unity the mean time taken for diffusant atoms to reach a trap is about equal to that taken to diffuse through the foil. When B is near unity the mean time of stay in a trap is about equal to that for diffusion through the foil.

Increases of A and B represent reductions in the time taken to reach a trap and in the time of stay within one. Fig (2.8) shows the variation of Λ with ζ described by (2.124), with the further assumption that outgassing is negligible ($Q_{og} \rightarrow 0$). General points to note are: Λ is greatest when $A = B = 0$; when B is small, Λ drops sharply from the value of $1/2$ at $\zeta = 0$ to a plateau region before falling away again with increasing ζ; the curves have a common value of A converge as ζ increases.

In detail, it may be shown that for curves satisfying the $A > 8B$ condition the position of steepest descent is close to the maximum in the corresponding curve for ϕ. The curves thus widen with increasing B. This calculation is again approximate to the precision of a series expansion. Examination of the plateau shows its height to be determined solely by the value of A and, when

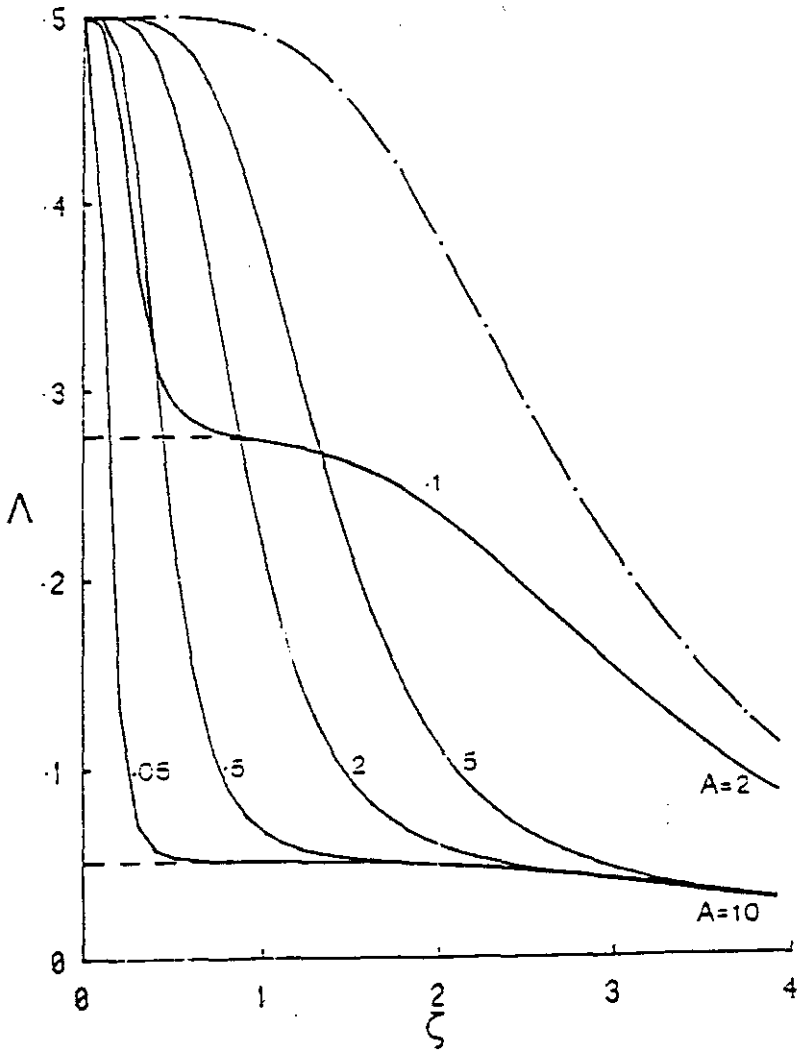

Figure 2.8 Diffusion with internal trapping: variation of relative modulation amplitude Λ with frequency factor ζ, assuming no outgassing ($Q_{og} = 0$). Curves are for specified values of the trapping parameter B for the cases $A = 2$ and $A = 10$.

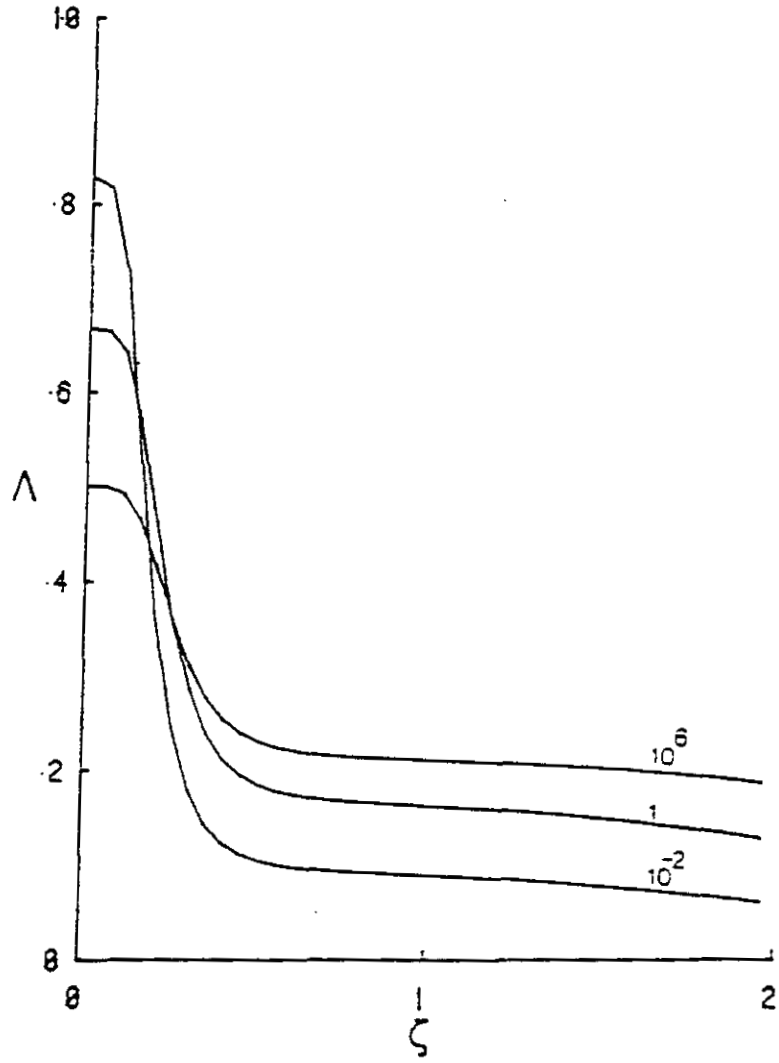

Figure 2.9 Diffusion with internal trapping and chemisorption: variation of phase lag ϕ with frequency factor ζ. Curves are for $A = 3$, $B = 0.1$, $\mu = 0$ and specified values of reduced flux j.

extrapolated back to the $\zeta = 0$ axis, to equal the intercept calculated for the case of $B = 0$. In the plateau region:

$$\begin{aligned} \Lambda(\text{plateau}) &\simeq \Lambda(\zeta = 0, B = 0) \\ &= \frac{1}{2}\left[\frac{2A}{\cosh^2[(2A)^{1/2}]} - 1\right]^{1/2} \end{aligned} \tag{2.136}$$

2.6 Aggregated Effects: Surfaces and Traps

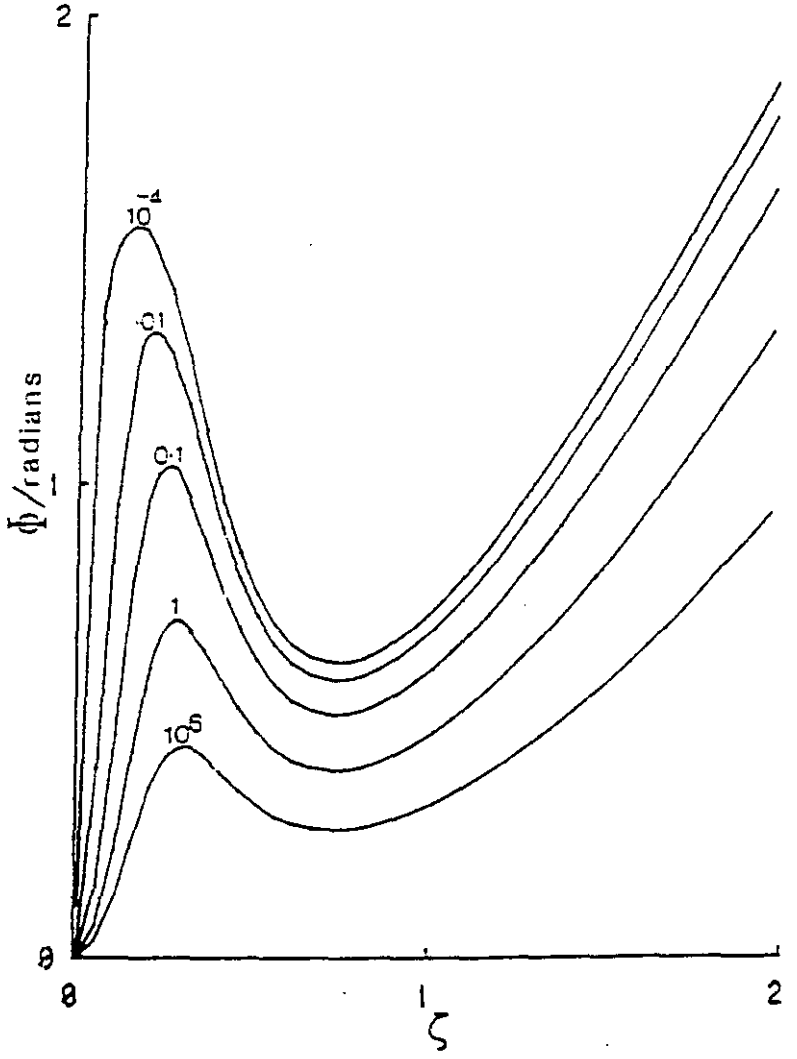

Figure 2.10 Diffusion with internal trapping and chemisorption: variation of relative modulation ratio Λ with frequency factor ζ. Curves are for $A = 3$, $B = 0.1$, $\mu = 0$ and various values of reduced flux j.

An advantage of the matrix formulation is that it is not difficult to extend the analysis of the last two sections to the treatment of a foil showing both trapping and surface inhibition of flux. So long as conditions lie within the range of the linear approximation, it is possible to relate output to input modulations by a matrix product. It is necessary merely to combine the translation matrix $T^{\dagger}$ of section [2.5] with the interphase matrices S and S' of section [2.4], that is to evaluate $\mathbf{R} = EST^{\dagger}S'_0E'$.

The product which results is just (2.77) with the substitution of **b** for **a** and consequential changes in the expressions for e, f, g and h. On multiplying out:

$$\mathbf{R} = \frac{(S + \mathrm{i}\omega V)}{(\xi + \mathrm{i}\chi)\sigma} \begin{bmatrix} (e + \mathrm{i}f)(\cosh\xi\cos\chi + \mathrm{i}\sin\chi\sinh\xi) \\ +(g + \mathrm{i}h)(\sinh\xi\cos\chi + \mathrm{i}\sin\chi\cosh\xi) \end{bmatrix} \tag{2.137}$$

with:

$$\begin{aligned} e &= (\xi/2\overline{k}_1)\{2 + [2j(1+\mu]^{1/2}\} \\ f &= (\chi/2\overline{k}_1)\{2 + [2j(1+\mu]^{1/2}\} \\ g &= \{2j + [2j(1+\mu)]^{1/2}/\overline{k}_1 \\ &\quad +(\xi^2 - \chi^2)(1+\mu)[(1+\mu)/2j]^{1/2}/4\overline{k}_1 \\ h &= (\xi\chi/2\overline{k}_1)(1-\mu)[(1+\mu)/2j]^{1/2} \end{aligned} \tag{2.138}$$

The phase shifts and amplitudes are then:

$$\begin{aligned} \phi &= \epsilon - \arctan(\chi/\xi) \\ &\quad + \arctan\left[\frac{e\tan\chi\tanh\xi + f + g\tan\chi + h\tanh\xi}{e - f\tan\chi\tanh\xi + g\tanh\xi - h\tan\chi}\right] \end{aligned} \tag{2.139}$$

and:

$$|\mathbf{R}|^{-1} = \frac{\sigma(\xi^2+\chi^2)^{1/2}\sqrt{2}}{(S^2+\omega^2V^2)^{1/2}} \left[\begin{array}{l} (e^2+f^2+g^2+h^2)\cosh 2\xi \\ +(e^2+f^2+g^2+h^2)\cos 2\chi \\ +2(eg+fh)\sinh 2\xi + 2(fg-eh)\sin 2\chi \end{array} \right]^{-1/2}$$

The relative modulation amplitude ratio:

$$\Lambda = \frac{\sqrt{2}\sigma(\xi^2+\chi^2)^{1/2}}{k_1} \frac{\{1+(2j+\mu)^{1/2}+j\}}{\left[\begin{array}{l} (e^2+f^2+g^2+h^2)\cosh 2\xi \\ +(e^2+f^2+g^2+h^2)\cos 2\chi \\ +2(eg+fh)\sinh 2\xi + 2(fg-eh)\sin 2\chi \end{array} \right]^{1/2}}$$

Graphical representations of these expressions are shown in Fig (2.9) and Fig (2.10). The case chosen is that for $A = 3$, $B = 0.1$, $\mu = 0$ with various values of j. It thus shows the combination of strong trapping with a range of surface rates varying from very rapid to very slow.

The curves retain the characteristics of the individual phenomena from which they derive. Trapping still shows in the maximum of the phase plot and in the shoulder of the amplitude variation; surface effects are to be seen in the high value of Λ at low frequencies and in the variation of phase with flux. Minor differences are that the range of phase change consequent on flux variation is no longer close to $\pi/2$ irespective of the frequency and the ratio of maximum to minimum phase lag is increased relative to the case for simple trapping.

2.6.1 Discussion of The Cummings and Blackburn Model

The matrix approach to the treatment of the diffusion equation provides a powerful way of describing the propagation of modulated diffusant fluxes. It is restricted to small fractional modulations but may readily be applied to different driving forces; pressure modulation, volume modulation or flux (ion current) modulation and to the analysis of surface reaction and trapping as well as that of diffusion limited flow.

The solutions show variations with modulation frequency and pressure which should make it possible to identify diffusion limited flow from flow influenced by surface reaction or trapping.

In diffusion limited flow the phase lag, ϕ, varies linearly with ζ at high frequencies and this linear region extrapolates back to give an intercept of $-\pi/4$ on the ϕ axis. The variation of the relative modulation amplitude ratio, Λ, with ζ provides a separate means to determine the diffusion coefficient, D. It also provides the permeability, P_m, which can be evaluated independently of outgassing effects by analysing $|\mathbf{R}|^{-1}$ versus ζ. In the low frequency limit $\Lambda = 1/2$: this corresponds to the permeation pressure law exponent for $p^{1/2}$ diffusion limited permeation.

The two rate constant surface model gives a maximum phase shift of $+\pi/2$; $+\pi/4$ per surface in the high frequency region, as flux is reduced. It must be stressed that this is a maximum phase shift, incomplete inhibition or single limiting surface resulting in smaller phase shifts. The two rate constant model describes the shift from $p^{1/2}$, diffusion limited permeation, to p^1, surface limited permeation, with reduction of flux. Values for $\Lambda(\omega \rightarrow 0)$ in excess of $1/2$ thus constitute strong evidence of surface effects. The low frequency increase in Λ is the most useful indicator of surface effects.

The processes of internal trapping are well characterized by pressure modulation experiments so long as the trapping is strong. A full maximum and minimum are found if the trapping parameters A and B obey $A \gg 8B$. If a full maximum and minimum are found, the position of the maximum, ω_{max}, gives a direct indication of the release rate constant, k_B, since $\omega_{max} \simeq k_B$. Similarly, the position of the minimum, ω_{min}, gives the trapping rate constant, k_A, from $\omega_{min} \simeq (k_A k_B)^{1/2}$. A useful indicator that traps may be present is the value for $\Lambda(\omega \rightarrow 0)$, obtained by extrapolating high frequency amplitude measurements back to the $\omega = 0$ axis. For deep traps, $A \gg 8B$, we shall be in the plateau region, and hence the apparent index, n, will be less than $1/2$. Since the solution is only applicable at very low concentration, phase lag ϕ and Λ are independent of input pressure. It is supposed that the trapping is directly proportional to the diffusant concentration. Therefore

this is not appropriate for the description of conditions when the fractional occupancy of traps is high.

When the fluxes are inhibited by both trapping and by surface reaction, only full curve fitting can give an effective analysis of the determining parameters.

Considering the experimental applicability of the Cummings and Blackburn model the followings can be pointed out;

Pressure, temperature, specimen geometry, pumping rate and data collection rates all impose constraints on the measurement of flux to an acceptable ratio of signal to noise. The experimental space within which measurements can usefully be made is limited by the resolution of amplitude of the pressure signals. The relative modulation amplitude ratio Λ is therefore limited by the signal to noise ratio.

To distinguish the limiting rate of the diffusant flow and derive reliable quantitative results for the permeation parameters, non-dimentional frequency ζ is also an important experimental parameter,

Relative modulation amplitude ratio less than 0.5 invalidates the determination of phase lag ϕ.

In diffusion limited permeation ζ from 0 to 5 may well give the necassary data to fit the model. However regard to trapping and surface model this will narrow the experimental space and pushes it to much lower frequencies.

Chapter 3

Experimental Equipment and Method

3.1 Introduction

The objectives of the experimental work were to measure permeation, diffusion, surface rate constants and trapping parameters by measurements of modulated macroscopic flow through thin metal foils using the mathemetical model of Cummings and Blackburn.

Previous experiments conducted on nickel were confined to temperatures over 573 K owing to poor signal to noise ratio, poor computer-controlled modulation and data sampling. To investigate internal trapping, which is likely to occur at temperatures below 550 K, the signal to noise ratio has been improved. The elimination of electronic noise has been achieved by improvement of the amplification and filtering, also reducing the mechanical noise around the rig has increased the signal to noise ratio. Changing the ion gauge filament to thoria-coated iridium has also reduced the outgassing in the output chamber. Longer cycle times are achieved by revising the control algorithm and redesigning the linear motion drive unit for modulation. This has made measurements down to 373 K possible.

The general requirements of the equipment were :

(i) to deliver to one side of the specimen a range of time dependent pressures.

(ii) detect time dependent flows emerging from the other side of this specimen.

Specific requirements were :to use an ultra high vacuum system with input and output chamber separated by a foil specimen; to arrange pumping kinetics and pressure control systems so that the diffusion time (l^2/D) would be an appreciable fraction of the period of oscillation for a useful range of temperatures and pressures, ensuring sufficient structure for a curve fit analysis; to control the input side pressure so as to follow a chosen series of modulations.

The following sections describe: the vacuum systems; pressure control, modulation and measurement; specimen and furnace configuration and temperature control; specimen choice, materials and preparation; measurement and analysis of experimental variables.

3.2 Vacuum Systems

Fig (3.1) illustrates the double ultra high vacuum system, in which a foil specimen separates the two chambers. Much of the basic vacuum equipment has been used by earlier workers [45]. In this system the input chamber volume may be changed so providing a means to control the diffusant flux. The output chamber, of fixed volume, is continuously pumped into an ion pump via a calibrated leak ($0.714 \pm 0.002 ls^{-1}$), this leak acting as a choke to minimise pressure variations arising from ion pump fluctuations.

The ultra high vacuum components were constructed of stainless steel and sealed with OFHC copper gaskets on conflat knife-edges. This system was outgassed by baking at 440 K for a minimum of 24 hours after each new specimen was installed. During bakeout, gas released from the system was taken through a liquid nitrogen trap to a diffusion pump. After bakeout the output chamber was pumped by a 25 ls^{-1} ion pump, the input chamber continuing to be pumped by the diffusion pump. The residual partial pressure after bakeout was typically of the order of 10^{-9} torr.

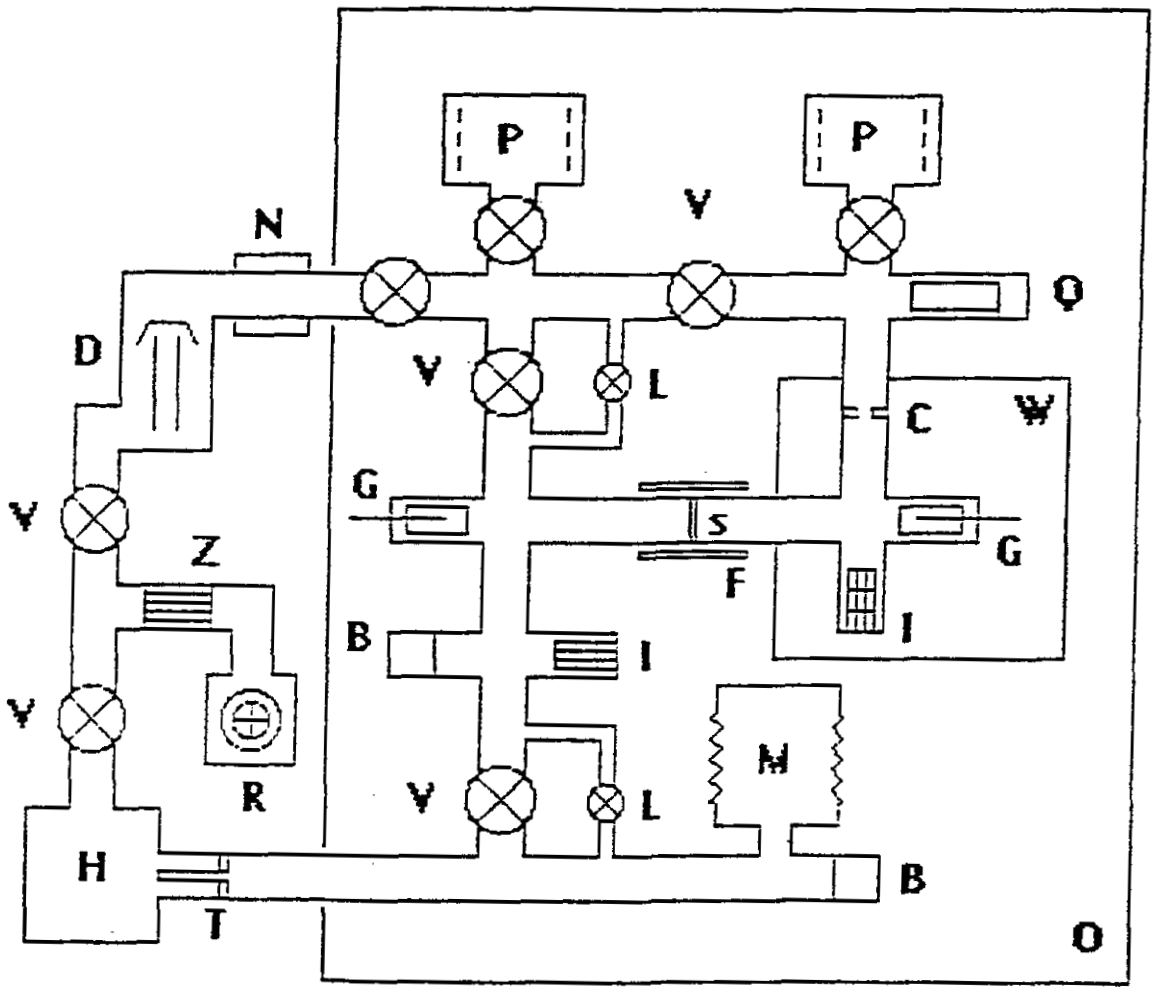

Figure 3.1 Schematic of the permeation rig vacuum system. Key to symbols: B - Baratron manometer; C - calibrated leak; D - diffusion pump; F - furnace; G - ion gun; H - hydrogen reservoir; I - ion gauge; L - leak valve; M - modulator bellows; N - liquid nitrogen trap; O - bakeout oven; P - ion pump; Q - quadrupole mass spectrometer; R - rotary pump; S - specimen; T - palladium thimble; V - valve; W - water cooled exit chamber; Z - zeolite vapour trap.

3.3 Pressure Control, Modulation and Measurement

3.3.1 Measurement and control of the input base pressure

The input chamber pressure was monitored using Baratron capacitance manometers [56] with full scales of 10 torr and 100 torr. The 100 torr Baratron (B100) was readable to a precision of three and a half digits while the 10 torr Baratron (B1) was readable to four and a half digits. Thus the B100 Baratron was used in the range 100 to 1 torr $\pm$ 0.05 torr, while the B1 Baratron was used in the range 10 to 10^{-3} torr $\pm 5 \times 10^{-5}$ torr. Both Baratrons were calibrated against an NBS standard.

To provide a diffusant of suitable purity, hydrogen was bled into the input chamber from a supply reservoir using a palladium diffuser; Fig (3.2). The diffuser was surrounded by a small thermocoax furnace and was heated to $\approx$ 500 K. Conductance at this temperature and for a supply pressure of 500 torr was $\approx 10^{-4}$ ls^{-1}. The base pressure was set by admitting hydrogen through the heated palladium diffuser until the required pressure was reached.

3.3.2 Modulation of the input chamber pressure

Modulation of the input pressure was provided by harmonic variation of the chamber volume. A large stainless steel bellows fitted to the input chamber provided the means of change; Fig (3.3). To change the volume, an a.c. motor was used to drive a linear motion vacuum feedthrough. This feedthrough was connected to a position transducer to provide a feedback signal for the control of the system. Pressure was assumed to be linear with position for this control. The bellows was contained within a low vacuum cylinder maintained at a pressure close to that inside the bellows thus reducing the power required of the motor. The transducer followed a sinusoidal reference signal generated by the computer program and fed via a 12 bit digital-to-analogue converter.

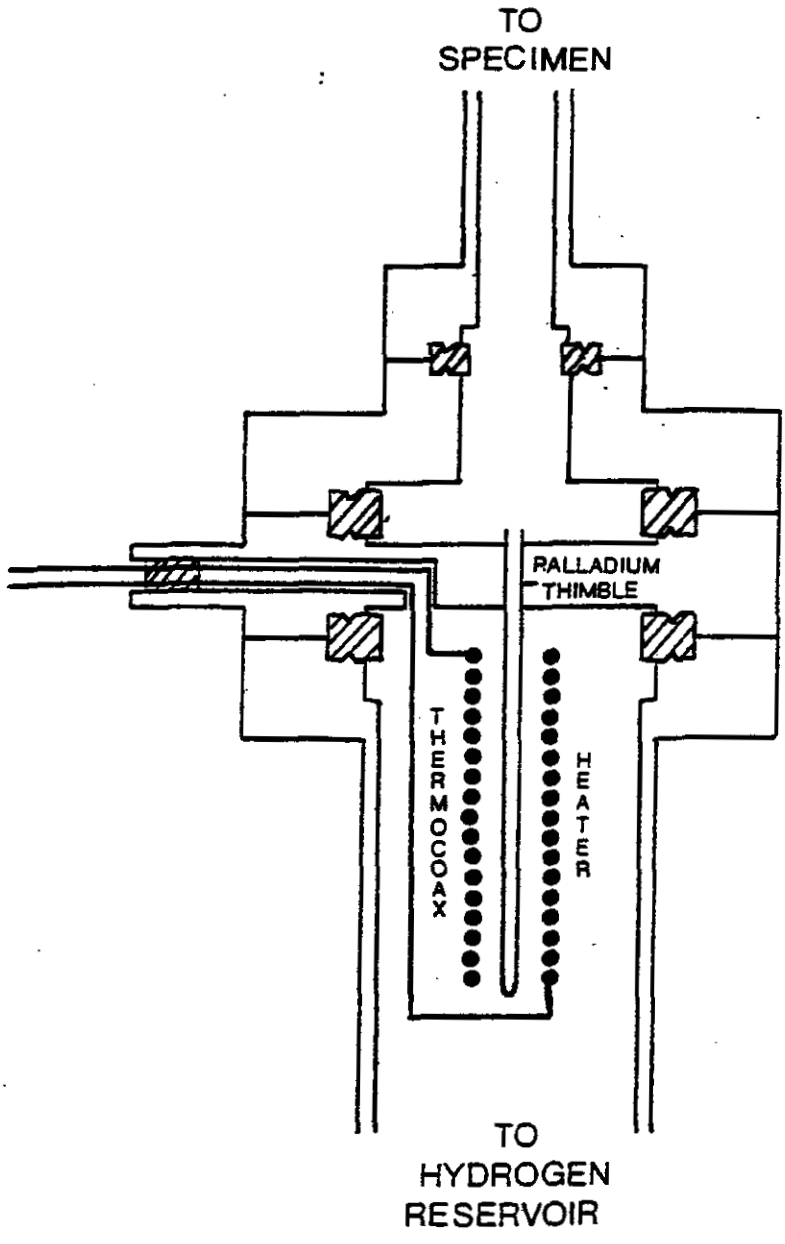

Figure 3.2 Schematic of the palladium thimble assembly

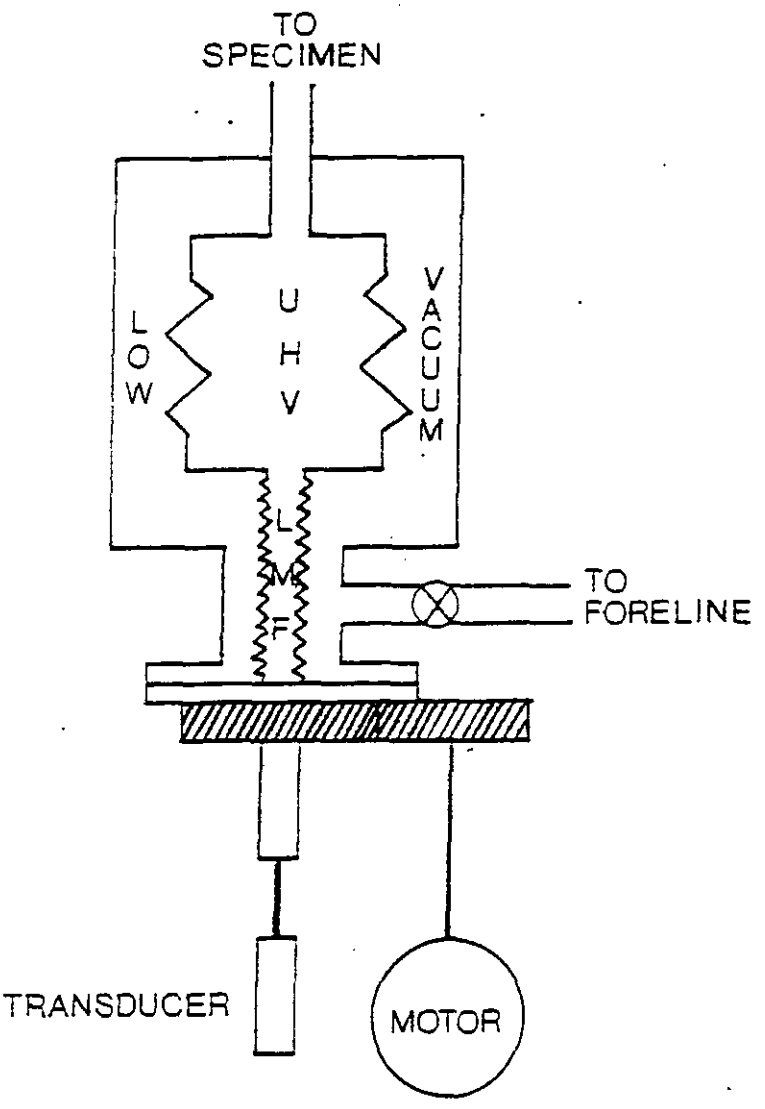

Figure 3.3 Schematic of the stainless steel bellows, linear motion feedthrough, A.C. motor and transducer

3.3.3 Measurement of the output chamber pressure

The output chamber pressure was monitored using an ion gauge. This gauge was calibrated for hydrogen against a Baratron by measurement of the rate of rise of pressure in a measured volume through a calibrated leak. The result was a correction multiplier of 3.1 ± 0.1, and is in good agreement with the multiplier, 3.1, predicted by Dennis and Heppel [57]. The gauge head was of a Bayard Alpert type, [58], range 10^{-2} to 10^{-11} torr, with a sensitivity of 25 per torr and an X-ray limit of 2×10^{-11} torr. The output of this ion gauge was fed into a second 16 bit analogue-to-digital converter, from where it was stored.

3.4 Temperature Control

3.4.1 Specimen mount and furnace design

Fig(3.4) shows the design used. The specimen was sealed, depending on thickness and hardness, between an annealed copper gasket and one conflat knife edge or between two annealed copper gaskets.

The furnace heating element took the form of two 4m lengths of 0.5mm diameter thermocoax cable - a nickel resistance wire surrounded by an insulant and enclosed within an inconel sheath - fitted with cold junctions at each end. This was wound around formers, Fig(3.5), so that the heater was in two separate parts, allowing easy removal when necessary. This external heater was placed around the specimen holding flange with copper blocks between the flange and heater to reduce gradients in temperature and to act as a heat reservoir, to reduce short term specimen temperature fluctuations.

3.4.2 Temperature measurement and furnace control

Temperatures were measured using chromel/alumel thermocouples, each calibrated against an NPL Pt/PtRh standard. Typically four thermocouples were used. All were of 0.5 mm diameter insulated and sheathed in inconel.

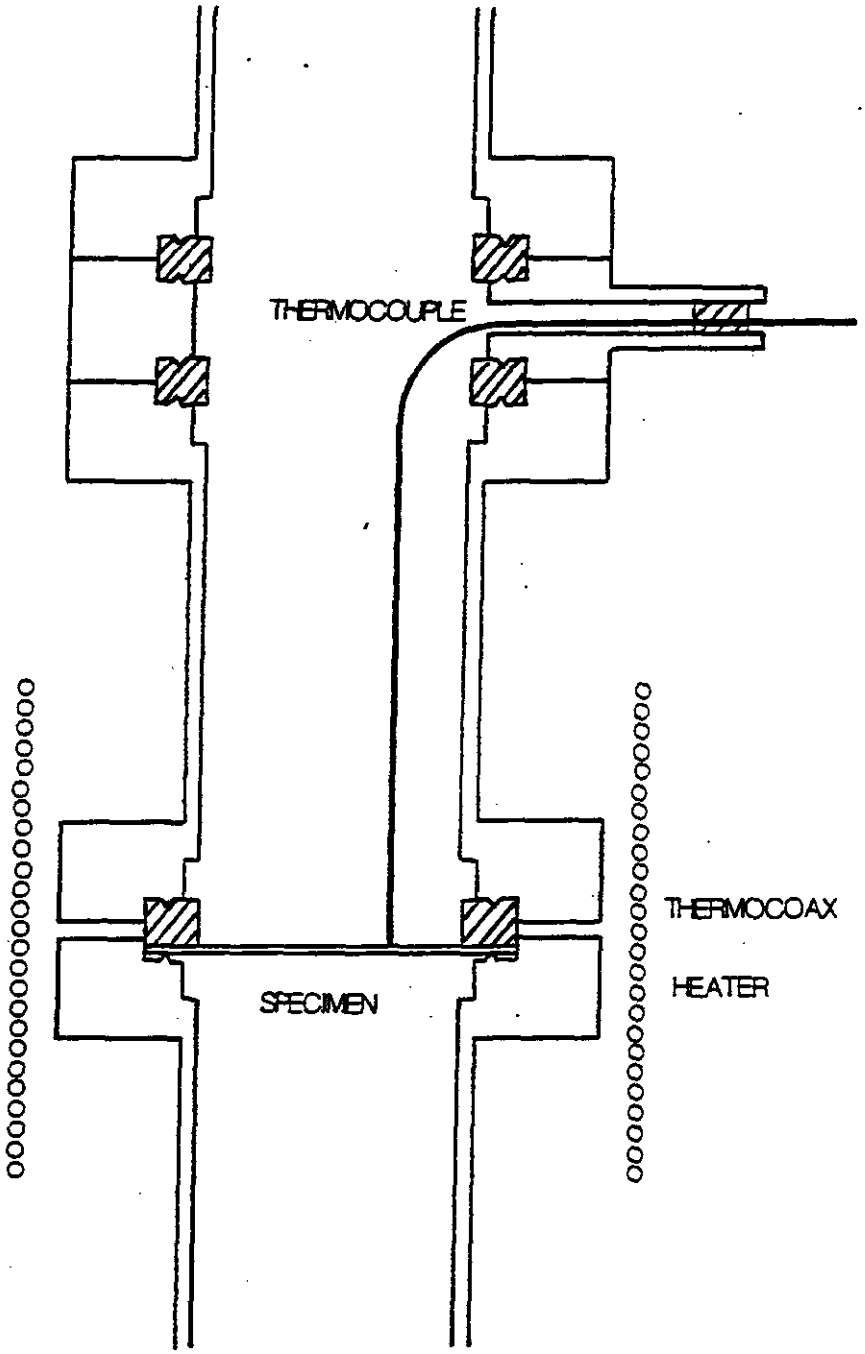

Figure 3.4 Schematic of specimen mount.

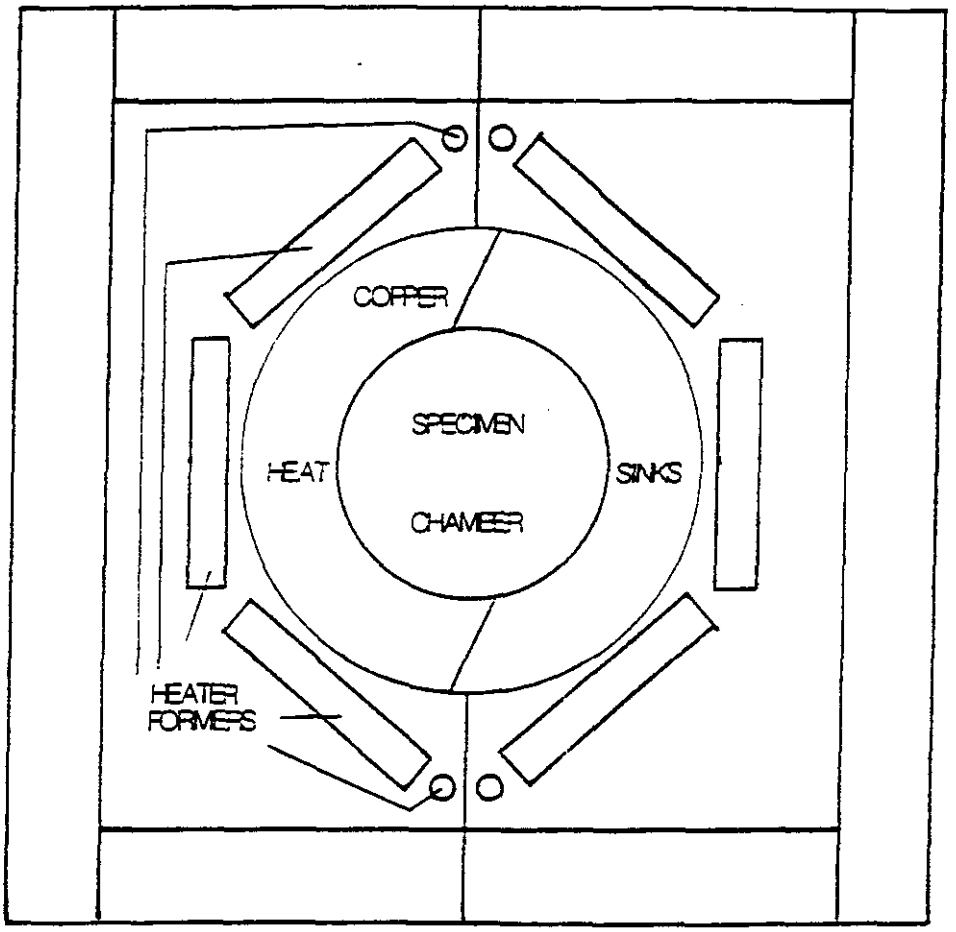

Figure 3.5 Schematic of furnace.

The thermocouples were brazed into a conflat flange and arranged on the input side of the specimen. One thermocouple was used for control, two were used to measure the temperature of the specimen and one was a spare. The spare thermocouple was occasionally used to check the readings of the others. The reference junction for all thermocouples was a continuously maintained 318 K cell. The control thermocouple was connected to a three term controller which, when adjusted, could control temperature to ± 0.1 K.

Temperature measurements were derived from two thermocouples. In normal operation these were consistent to better than 1K. Temperatures quoted for experimental runs are the mean of the two experimental values read.

3.4.3 Temperature control program

The requirements of the temperature control system were to:

(1) ramp the temperature under computer control to any temperature in the range 300 - 900K.

(2) maintain the temperature to ± 0.1 K throughout each set of frequency modulation runs.

These requirements were met by the use of a 12 bit digital to analogue converter to provide the reference signal for the specimen furnace temperature controller. This signal was floated, divided and sent to the furnace controller in such a way that 1 bit $\equiv 1\mu$V. In principle, therefore, the temperature could be ramped in steps of 0.25K. Since each digital to analogue conversion took $\approx$ 100ms to complete the time increments were limited to the response of the furnace controller. This limit is in excess of 1Ks^{-1} but presented no impediment to control since the prime concern was to limit the ramp rate to 0.1Ks^{-1} and avoid leaks caused by rapid thermal expansion of vacuum seals.

The temperature control signal provided by the two thermocouples, was measured with a digital voltmeter. Voltages were interpreted as temperatures using a Lagrange interpolating polynomial of degree three with a stored table

of calibrated values. Sensitivity by this method was better than 0.1K The digital-to-analogue bit value was adjusted so that the set temperature was centred on the nearest bit value.

3.5 Specimen Materials and Preparation

The materials investigated were foils of nickel, nickel thoria and palladium. The purity ,chemical composition and preparation of each material is detailed in separate sections. The following cleaning procedure were used for each foil:
(i) degreased in a solvent in an ultrasonic bath
(ii) polished with diamond lapping compounds
(iii) polished with alumina powder in distilled water
(iv) cleaned in distilled water in an ultrasonic bath
(v) dried in an oven at 400 K for about 15 minutes.
The specimen foils were then sealed between the conflat flanges.

3.5.1 Nickel

The 99.98% nickel,0.125 mm and 0.5 mm thick, were supplied by Goodfellow Metals in an annealed condition. The as-received 0.5 mm thick foil was cold rolled down to 0.075 mm.

The chemical analysis was as follows:

Cobalt	8 ppm
Chromium	8 ppm
Copper	10 ppm
Iron	10 ppm
Silicon	2 ppm
Tin	1 ppm

3.5.2 Nickel Thoria

The nickel thoria specimens were supplied by J.S. Chinn Co. Ltd as 1.00 mm thick sheet. These specimens were cold rolled down to 0.075, 0.125 , 0.3 and

of calibrated values. Sensitivity by this method was better than 0.1K The digital-to-analogue bit value was adjusted so that the set temperature was centred on the nearest bit value.

3.5 Specimen Materials and Preparation

The materials investigated were foils of nickel, nickel thoria and palladium. The purity ,chemical composition and preparation of each material is detailed in separate sections. The following cleaning procedure were used for each foil:
(i) degreased in a solvent in an ultrasonic bath
(ii) polished with diamond lapping compounds
(iii) polished with alumina powder in distilled water
(iv) cleaned in distilled water in an ultrasonic bath
(v) dried in an oven at 400 K for about 15 minutes.
The specimen foils were then sealed between the conflat flanges.

3.5.1 Nickel

The 99.98% nickel,0.125 mm and 0.5 mm thick, were supplied by Goodfellow Metals in an annealed condition. The as-received 0.5 mm thick foil was cold rolled down to 0.075 mm.

The chemical analysis was as follows:

Cobalt	8 ppm
Chromium	8 ppm
Copper	10 ppm
Iron	10 ppm
Silicon	2 ppm
Tin	1 ppm

3.5.2 Nickel Thoria

The nickel thoria specimens were supplied by J.S. Chinn Co. Ltd as 1.00 mm thick sheet. These specimens were cold rolled down to 0.075, 0.125 , 0.3 and

0.5 mm and each specimen was subsequently annealed at different annealing temperatures.
The chemical composition was as follows;

Titanium	10 ppm
Chromium	10 ppm
Cobalt	10 ppm
Iron	20 ppm
Sulfer	20 ppm
Corbon	50 ppm
Thoria	1.92 vol%
Nickel	balance

3.5.3 Palladium

The palladium foil was supplied by Goodfellow Metals. It was 99.99% palladium and 0.25 mm thick.
The chemical analysis was as follows:

Silver	2 ppm
Copper	1 ppm
Platinum	2 ppm
Silicon	2 ppm
Iron	2 ppm

3.6 Experimental run

The control system is illustrated in Fig(3.6). Control of equipment during an experiment was fully automated. With the pressure set, the control program called a sequence in which the temperature ramped up to the first set temperature. The step temperature was held for a period of 90 minutes, to allow the temperature, input pressure, output pressure and gauges to stabilize. Within this plateau ten measurements of temperature and input and output pressures were taken using the $7\frac{1}{2}$ digits volt meter.

For analysis of the time varying diffusant flux the signal from the gauges

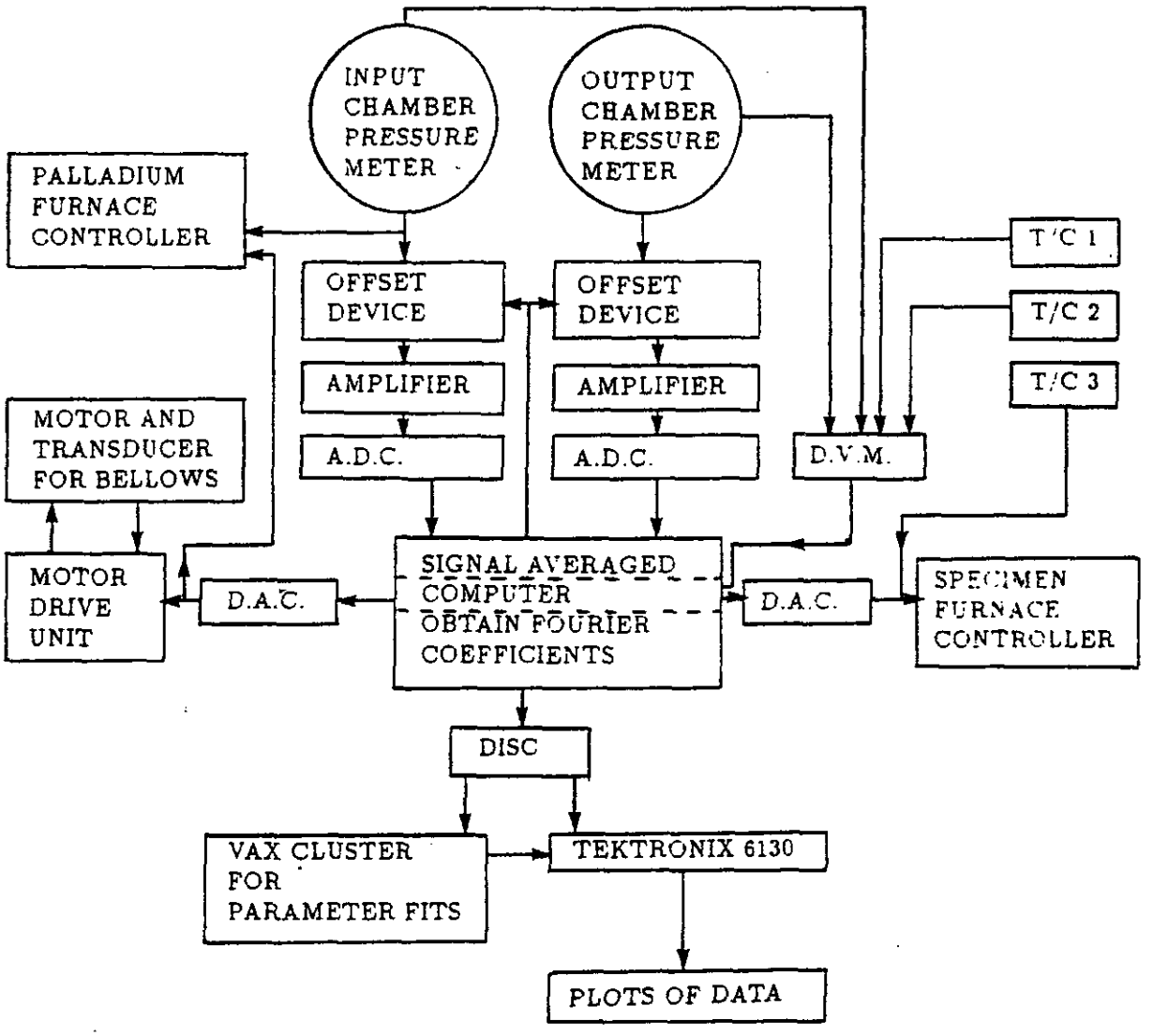

Figure 3.6 Diagram of the experimental control system

was sent to an offset device which measured the steady state pressure. The reference signal for the first frequency was sent to the motor drive unit of the volume modulator via a 12 bit digital to analogue converter as described in section 3.3. The frequency was controlled using the time base driving the digital-to-analogue converter. After sufficient time had elapsed to allow transients to decay, measurements of the pressure wave form in the input and output chambers were compared with the offset value and the difference captured by 16 bit analogue to digital converters. 16384 measurements were taken with four cycles for each frequency. Cycle times ranged from 20 s to 8000 s. A least-squares fit was performed on the resulting waveforms, to give the Fourier coefficients and their standard errors. The Fourier coefficients were converted into terms of phase lag, ϕ, and relative amplitude modulation ratio, Λ. After all the frequencies at a given temperature had been run, the temperature was ramped to the next set value and the process repeated.

After an experimental run, the refined phase lag and relative modulation amplitude data for each combination of frequency, temperature and pressure, was transferred to a graphics terminal for plotting. The data was then sent to a mainframe computer for least-squares fitting of the parameters of the model being used.

Experiments were performed on nickel and nickel thoria in the temperature range 373 K - 623 K. Mean pressures for as-recieved nickel were 6.65 Pa, 66.5 Pa and 6.65 kPa. mean pressure for cold worked nickel was 6.65 kPa.

Experiments were performed on nickel thoria foils in the temperature range 473 K - 913 K. Mean pressures were lowest 100 Pa, highest 10^5 Pa.

Experiments were performed on palladium for three temperatures, 395, 493 and 560 K.Mean pressure was 800 Pa.

3.6.1 The derivation of Fourier coefficients using a least squares method

Analytic expressions for the input and output waveforms were obtained by least squares fit of the data to the equation:

$$y_i = a \sin x_i + b \cos x_i \tag{3.1}$$

It is useful to express this as:

$$(y_i - \overline{y}) = a\left[\sin x_i - \sum(\sin x_i)/N\right] + b\left[\cos x_i - \sum(\cos x_i)/N\right] \tag{3.2}$$

where $\overline{y}$ refers to the mean value of y.
In matrix notation (3.2) may be written $\forall i = 1$ to N:

$$\begin{bmatrix} \vdots \\ y_i - \overline{y} \\ \vdots \end{bmatrix} = \begin{bmatrix} \vdots & \vdots \\ (\sin x_i - \sum \sin x_i) & (\cos x_i - \sum \cos x_i) \\ \vdots & \vdots \end{bmatrix} \begin{bmatrix} a \\ b \end{bmatrix} \tag{3.3}$$

$$Y \quad = \quad J \quad P$$

Hence:

$$\tilde{J}Y = \tilde{J}JP \tag{3.4}$$

Therefore:

$$P = (\tilde{J}J)^{-1}\tilde{J}Y \tag{3.5}$$

Thus the parameter matrix P containing the Fourier coefficients a and b can be found. Also a variance co-variance matrix can be defined to obtain the standard error of a and b, such that:

$$\sigma_a^2 = (\tilde{J}J)_{11}^{-1}\sigma_y^2 \tag{3.6}$$

and,

$$\sigma_b^2 = (\tilde{J}J)_{22}^{-1}\sigma_y^2 \tag{3.7}$$

where σ_a and σ_b are the standard errors on a and b and σ_y^2 is the residual sum of squares such that:

$$\sigma_y^2 = \sum (y^{obs} - y^{calc})^2 / N \tag{3.8}$$

By this method the Fourier coefficients a and b and their standard errors were found for both input and output waveforms. For further analysis the coefficients were put into phase and amplitude form.

3.7 Iterative non-linear curve fitting of experimental variables

The least-square method presented above can be extended to cases where the proposed relationship between the variables is not linear.
The experimental variables are Λ, and ϕ. For eample, at a given frequency, phase lag ϕ and relative modulation amplitude ratio Λ can be written as

$$\phi = f(D, K_{sm}, k_1, k_2 ....)$$

$$\Lambda = f(D, K_{sm}, k_1, k_2 ....)$$

This functions can be expanded in a Taylor series about the value of the function corresponding to a first estimate of the parameters D_0, k_0 etc. The correct values of parameters D, k_1 etc. Thus for ϕ

$$\phi = \phi_0 + \left[\frac{\partial f}{\partial D}\right]_0 (D - D_0) + \left[\frac{\partial f}{\partial k}\right]_0 (k - k_0) + ... \tag{3.9}$$

where subscrip $_0$ denotes evaluation at $D = D_0, k = k_0$.
If the quantity $Y = \phi^{obs} - \phi$ is defined

$$Y = \phi^{obs} - \phi_0 - \left[\frac{\partial f}{\partial D}\right]_0 (D - D_0) - \left[\frac{\partial f}{\partial k}\right]_0 (k - k_0) + ... \tag{3.10}$$

The values of the parameters for a given value of frequency are therefore given by $Y = 0$,

$$\phi - \phi_0 = - \left[\frac{\partial f}{\partial D}\right]_0 (D - D_0) - \left[\frac{\partial f}{\partial k}\right]_0 (k - k_0) + ... \tag{3.11}$$

For a set of frequencies the set of simultaneous equations for evaluation of $(D - D_0)$ and $k - k_0$ can be written in a way analoguos to linear regression

$$Y = JP \tag{3.12}$$

$$\begin{bmatrix} \vdots \\ \phi_i - \phi^{obs} \\ \vdots \end{bmatrix} = \begin{bmatrix} -[\frac{\partial f}{\partial D}]_0^1 & -[\frac{\partial f}{\partial k}]_0^1 \cdots \\ \vdots & \vdots \\ -[\frac{\partial f}{\partial D}]_0^n & -[\frac{\partial f}{\partial k}]_0^n \cdots \end{bmatrix} \begin{bmatrix} (D - D_0) \\ (k - k_0) \\ \vdots \end{bmatrix} \tag{3.13}$$

P is the solution matrix, since J is non-square, it cannot be inverted directly. Multiplying both side by $\tilde{J}J$

$$P = (\tilde{J}J)^{-1}\tilde{J}Y \tag{3.14}$$

Then the best values of D and k can be found by iterating until $P \rightarrow 0$.

Chapter 4

Six rate surface model

4.1 Introduction

In this chapter the algebra becomes particularly complicated owing to there being four rate equations to be solved simultaneously. In the first part, manipulations are performed to obtain a general form from which special cases are subsequently identified. These special cases provide valuable limits in which the physical consistency can be checked out and to which real experiments can usefully be directed.

The principal feature of the two rate constant model described in chapter 2, is the ability to describe the changeover from high pressure, diffusion limited permeation to low pressure surface limited flow. It takes no account, however, of any adsorbed surface phase of atoms or molecules. To investigate the possibility that such a surface layer might be detected in a modulation experiment the basic three stage surface processes that are essential for permeation are considered.

(i)- adsorption of molecules onto the surface from the gas phase and their desorption from the surface

(ii)- molecular dissociation on the surface to atoms and their recombination to molecules

(iii)- absorption of adsorbed atoms into solution in the surface layer of the solids and their reverse passage out of solution.

In some cases, dissociation may occur simultaneously with adsorption so that

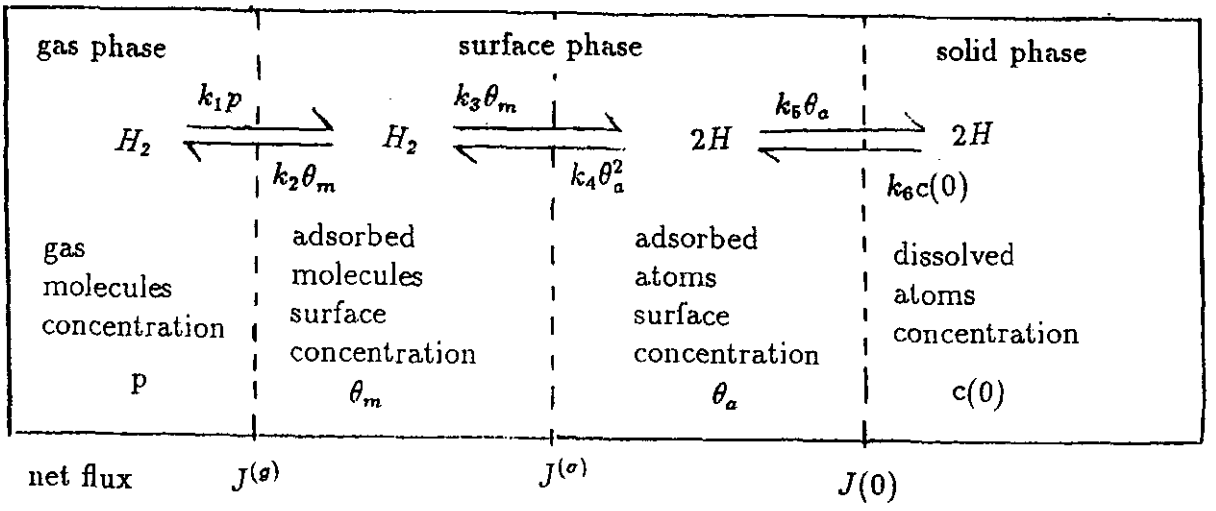

Figure 4.1 Three stage surface processes

the processes (i) and (ii) become a single process there is then no identifiable molecular phase on the surface; this is direct dissociative chemisorption and is believed to occur for hydrogen adsorbtion on many transition metals.

4.2 Three Stage Surface Processes

The three stages are given in figure (1). where hydrogen is taken to be the diffusant gas and k_1 , k_2, k_3, k_4, k_5, k_6 are the rate constants.

4.2.1 Input surface rate equations

The six independent rate constants are defined by the following flow equations;

The flux in to the molecular surface phase,

$$J^{(g)} = k_1 p - k_2 \theta_m \tag{4.1}$$

The accumulation of adsorbed molecules in molecular surface phase,

$$\partial\theta_m/\partial t = J^{(g)} - k_3\theta_m + k_4\theta_a^2 \tag{4.2}$$

The flux, $J^{(\sigma)} = k_3\theta_m - k_4\theta_a^2$ (in figure 4.1) is defined as the flux to the atomic surface phase thus $\partial\theta_m/\partial t$ is the difference between the two fluxes, J^g and J^σ, $\partial\theta_m/\partial t = J^{(g)} - J^{(\sigma)}$.

The accumulation of atoms in the atomic surface phase

$$\partial\theta_a/\partial t = k_3\theta_m - k_4\theta_a^2 - J(0) \tag{4.3}$$

This is the difference between the flux $J^{(\sigma)}$ and the flux $J^{(0)}$ through the solid phase;

$$J(0) = k_5\theta_a - k_6 c(0) \tag{4.4}$$

4.2.2 Output surface rate equations

The above set of relations applies to the input surface; for the output interface by analogy;

$$J(l) = k_6' c(l) - k_5'\theta_a' \tag{4.5}$$

$$\partial\theta_a'/\partial t = J(l) - k_4'\theta_a'^2 + k_3'\theta_m' \tag{4.6}$$

$$\partial\theta_m'/\partial t = k_4'\theta_a'^2 - k_3'\theta_m' - J^{(g')} \tag{4.7}$$

$$J^{(g')} = k_2'\theta_m' - k_1' p' \tag{4.8}$$

4.2.3 Modulation

When modulation is added to the steady state

$$[J_s + \mathbf{J}^{(g)}] = k_1[p_s + \mathbf{p}] - k_2[\theta_{ms} + \theta_\mathbf{m}] \tag{4.9}$$

$$\mathrm{i}\omega[\theta_\mathbf{m}] = [J_s + \mathbf{J}^{(g)}] - k_3[\theta_{ms} + \theta_\mathbf{m}] + k_4[\theta_{as} + \theta_\mathbf{a}]^2 \tag{4.10}$$

$$\mathrm{i}\omega[\theta_\mathbf{a}] = k_3[\theta_{ms} + \theta_\mathbf{m}] - k_4[\theta_{as} + \theta_\mathbf{a}]^2 - [J_s + \mathbf{J}(0)] \tag{4.11}$$

$$[J_s + \mathbf{J}(0)] = k_5[\theta_{as} + \theta_\mathbf{a}] - k_6[c_s + \mathbf{c}(0)] \tag{4.12}$$

For the output surface;

$$[J_s + \mathbf{J}^{(l)}] = k_6'[c_s + \mathbf{c}(l)] - k_5'[\theta_{as}' + \theta_\mathbf{a}'] \tag{4.13}$$

$$\mathrm{i}\omega[\theta'_{\mathrm{a}}] = [J_s + \mathrm{J}^{(l)}] - k'_4[\theta_{as} + \theta_{\mathrm{a}}]^2 + k'_3[\theta_{ms} + \theta_{\mathrm{m}}] \tag{4.14}$$

$$\mathrm{i}\omega[\theta'_{\mathrm{m}}] = k'_4[\theta_{as} + \theta'_{\mathrm{a}}]^2 - k'_3[\theta'_{ms} + \theta'_{\mathrm{m}}] - [J_s + \mathrm{J}(g')] \tag{4.15}$$

$$[J_s + \mathrm{J}(g')] = k'_2[\theta'_{ms} + \theta'_{\mathrm{m}}] - k'_1[p'_s + \mathrm{p}] \tag{4.16}$$

The time dependent part of the flow equations, subject to assumption that all modulation amplitudes are small $|\mathrm{c}| \ll c_s$ and $|\mathrm{J}(x)| \ll J_s$, can be written as;

$$\mathrm{J}^{(\mathrm{g})} = k_1\mathrm{p} - k_2\theta_{\mathrm{m}} \tag{4.17}$$

$$\mathrm{i}\omega\theta_{\mathrm{m}} = \mathrm{J}^{(\mathrm{g})} - k_3\theta_{\mathrm{m}} + k_{4p}\theta_{\mathrm{a}} \tag{4.18}$$

$$\mathrm{i}\omega\theta_{\mathrm{a}} = k_3\theta_{\mathrm{m}} - k_{4p}\theta_{\mathrm{a}} - \mathrm{J}(0) \tag{4.19}$$

$$\mathrm{J}(0) = k_5\theta - k_6\mathrm{c}(0) \tag{4.20}$$

and for the output surface;

$$\mathrm{J}^{(\mathrm{l})} = k'_6\mathrm{c}(l) - k'_5\theta_{\mathrm{a}} \tag{4.21}$$

$$\mathrm{i}\omega\theta'_{\mathrm{a}} = \mathrm{J}^{(\mathrm{l})} - k'_{4p}\theta_{\mathrm{a}} + k'_3\theta_{\mathrm{m}} \tag{4.22}$$

$$\mathrm{i}\omega\theta'_{\mathrm{m}} = k'_{4p}\theta_{\mathrm{a}} - k'_3\theta_{\mathrm{m}} - \mathrm{J}(\mathrm{g}') \tag{4.23}$$

$$\mathrm{J}(g') = k'_2\theta_{\mathrm{m}} - k'_1\mathrm{p} \tag{4.24}$$

For convenience $k_{4p} = 2k_4\theta_{as}$ and $k'_{4p} = 2k_4\theta'_{as}$ are introduced and it is straighforward to show that from the steady part of the (4.9-4.16):

$$k_{4p} = 2k_4\left(\frac{k_1k_3}{k_2k_4}\right)^{1/2}\left[p_s - J_s\left(\frac{k_2+k_3}{k_1k_3}\right)\right]^{1/2} \tag{4.25}$$

and

$$k'_{4p} = 2k'_4\left(\frac{k'_1k'_3}{k'_2k'_4}\right)^{1/2}\left[p'_s + J_s\left(\frac{k'_2+k'_3}{k'_1k'_3}\right)\right]^{1/2} \tag{4.26}$$

4.2.4 Steady State Flow

In the steady state flow there can be no accumulation of diffusant in the foil or in its surface so all the fluxes can be set to J_s, from (4.1-4.4)

$$\frac{J_s}{K_{sm}}\left(\frac{1}{D} + \frac{1}{k_6} + \frac{1}{k'_6}\right) = \left[p_s - J_s\left(\frac{k_2+k_3}{k_1k_3}\right)\right]^{1/2} - \left[p'_s + J_s\left(\frac{k'_2+k'_3}{k'_1k'_3}\right)\right]^{1/2} \tag{4.27}$$

4.2.5 Equilibrium

At equilibrium, all fluxes (equations 4.1-4.4) are zero, entry and exit chamber pressures are equal, and the concentration may be described using a Sievert' law solubility coefficient, K_{sm} with;

$$K_{sm} = \frac{k_5}{k_6}\left(\frac{k_1 k_3}{k_2 k_4}\right)^{1/2} \tag{4.28}$$

4.2.6 Phase boundary Matrices S and S'

Rearranging the time dependent flow equations (4.17-4.24) in matrix form from the flow equations:

$$\begin{bmatrix} \mathbf{p} \\ \mathbf{J}^{(g)} \end{bmatrix} = \begin{bmatrix} k_2/k_1 & 1/k_1 \\ 0 & 1 \end{bmatrix} \begin{bmatrix} \theta_{\mathbf{m}} \\ \mathbf{J}^{g} \end{bmatrix} \tag{4.29}$$

$$\begin{bmatrix} \theta_{\mathbf{m}} \\ \mathbf{J}^{(g)} \end{bmatrix} = \begin{bmatrix} 1 & 0 \\ k_3 + \mathrm{i}\omega & -k_{4p} \end{bmatrix} \begin{bmatrix} \theta_{\mathbf{m}} \\ \theta_{\mathbf{a}} \end{bmatrix} \tag{4.30}$$

$$\begin{bmatrix} \theta_{\mathbf{m}} \\ \theta_{\mathbf{a}} \end{bmatrix} = \begin{bmatrix} (k_{4p} + \mathrm{i}\omega)/k_3 & 1/k_3 \\ 1 & 0 \end{bmatrix} \begin{bmatrix} \theta_{\mathbf{a}} \\ \mathbf{J}(0) \end{bmatrix} \tag{4.31}$$

$$\begin{bmatrix} \theta_{\mathbf{a}} \\ \mathbf{J}^{(0)} \end{bmatrix} = \begin{bmatrix} k_6/k_5 & 1/k_5 \\ 0 & 1 \end{bmatrix} \begin{bmatrix} \mathbf{c}(0) \\ \mathbf{J}(0) \end{bmatrix} \tag{4.32}$$

Multiplying out the above four equation yields the interface matrices S for entry and S' for the exit chamber

$$S = \frac{1}{k_1 k_3 k_5} \begin{bmatrix} k_2 k_{4p} k_6 & k_2 k_{4p} + k_2 k_5 \\ -\omega^2 k_6 & +k_3 k_5 - \omega^2 \\ +\mathrm{i}\omega k_6 (k_2 + k_3 + k_{4p}) & +\mathrm{i}\omega (k_2 + k_3 + k_{4p} + k_5) \\ \\ -\omega^2 k_1 k_6 & k_1 k_3 k_5 - \omega^2 k_1 k_6 \\ \mathrm{i}\omega k_1 k_6 (k_3 + k_{4p}) & +\mathrm{i}\omega k_1 (k_3 + k_{4p} + k_5) \end{bmatrix} \tag{4.33}$$

To obtain S' we can repeat the process for the

output surface and find;

$$S' = \frac{1}{k_2' k_{4p}' k_6'} \begin{bmatrix} k_1' k_3' k_5' & k_2' k_{4p}' + k_2' k_5' \\ -\omega^2 k_1' & +k_3' k_5' - \omega^2 \\ +\mathrm{i}\omega k_1'(k_3' + k_{4p}' + k_5') & +\mathrm{i}\omega(k_2' + k_3' + k_{4p}' + k_5') \\ \\ -\omega^2 k_1' k_6' & k_2' k_{4p}' k_6' - \omega^2 k_6' \\ \mathrm{i}\omega k_1' k_6'(k_3' + k_{4p}') & +\mathrm{i}\omega k_6'(k_2' + k_{4p}' + k_3') \end{bmatrix} \tag{4.34}$$

4.2.7 Evaluation of R

Extension of the two-rate constant model into the six-rate constant model calls for a change only in the phase boundary matrixes S and and S' . The coefficients describing the translation matrix T, entry E and exit E' matrixes are retained. Multiplying out the matrices $ESTS'E'$ give the formal solution for R. It is apparent that the general solution for the phase lag and relative modulation amplitude ratio will contain a large number of terms. But it is possible to predict the frequency response of a foil to pressure modulation for any given set of $\{k_i, k_i'\}, D, K_{sm}, p_s, l, \gamma$. This has been done by a matrix multiplication routine for the matrices $ESTS'E'$

4.3 General Solution for Phase lag and Relative Modulation Amplitude ratio

It may also be useful to give a general solution which describes the experimental conditions throughout this work. First, we can rewrite the $\mathbf{R} = |\mathbf{p}'| / |\mathbf{p}| = ESTS'E'$;

$$\mathbf{R} = \begin{pmatrix} E_{11} & E_{12} \end{pmatrix} \begin{pmatrix} S_{11} & S_{12} \\ S_{21} & S_{22} \end{pmatrix} \begin{pmatrix} \cosh \mathbf{a}l & (1/D\mathbf{a}) \sinh \mathbf{a}l \\ D\mathbf{a} \sinh \mathbf{a}l & \cosh \mathbf{a}l \end{pmatrix}$$

$$\cdot \begin{pmatrix} S'_{11} & S'_{21} \\ S'_{21} & S'_{22} \end{pmatrix} \begin{pmatrix} 1 \\ (S+\mathrm{i}\omega V)/\sigma \end{pmatrix} \tag{4.35}$$

When $p_s \gg p'_s$, under hard pumping conditions, exit surface, $J(l,t)$ and $c(l,t)$ are independent of $\mathbf{p}$, in effect, there will be no back flow, then coefficient S'_{11} and S'_{21} can be set to zero. Also because of the coefficient $E_{12} = 0$ and $E_{11} = 1$, then $\mathbf{R}$ can be written as;

$$\mathbf{R} = \begin{pmatrix} S_{11} & S_{12} \end{pmatrix} \begin{pmatrix} \cosh \mathbf{a}l & (1/D\mathbf{a}) \sinh \mathbf{a}l \\ D\mathbf{a} \sinh \mathbf{a}l & \cosh \mathbf{a}l \end{pmatrix} \cdot \begin{pmatrix} S'_{21} \\ S'_{22} \end{pmatrix} \begin{pmatrix} 1 \\ (S+\mathrm{i}\omega V)/\sigma \end{pmatrix} \tag{4.36}$$

Multiplication out of these matrices gives:

$$\mathbf{R} = \frac{(S+\mathrm{i}\omega V)}{(1+\mathbf{i})\zeta\sigma} \begin{bmatrix} (e+\mathrm{i}f)(\cosh\zeta\cos\zeta + \mathbf{i}\sin\zeta\sinh\zeta) \\ +(g+\mathrm{i}h)(\sinh\zeta\cos\zeta + \mathbf{i}\sin\zeta\cosh\zeta) \end{bmatrix} \tag{4.37}$$

where the coefficient of the interface matrixes has also an imaginary part; in this case the coefficients, e,f, g, and h become;

$$\begin{aligned} e &= \zeta\Re[S_{11}S'_{12} + S_{12}S'_{22}] - \zeta\Im[S_{11}S'_{12} + S_{12}S'_{22}] \\ f &= \zeta\Im[S_{11}S'_{12} + S_{12}S'_{22}] + \zeta\Re[S_{11}S'_{12} + S_{12}S'_{22}] \\ g &= \frac{l}{D}\Re[S_{11}S'_{22}] - \frac{2D}{l}\zeta^2\Im[S_{12}S'_{12}] \\ h &= \frac{l}{D}\Im[S_{11}S'_{22}] + \frac{2D}{l}2\zeta^2\Re[S_{12}S'_{12}] \end{aligned} \tag{4.38}$$

The phase shifts and amplitudes are then:

$$\begin{aligned} \phi &= \varepsilon - \pi/4 \\ &\quad + \arctan\left[\frac{e\tan\zeta\tanh\zeta + f + g\tan\zeta + h\tanh\zeta}{e - f\tan\zeta\tanh\zeta + g\tanh\zeta - h\tan\zeta}\right] \end{aligned} \tag{4.39}$$

and:

$$|\mathbf{R}| = \frac{(S^2+\omega^2V^2)^{1/2}}{2\sigma\zeta} \cdot \left[\begin{array}{l} (e^2+f^2+g^2+h^2)\cosh 2\zeta \\ +(e^2+f^2-g^2-h^2)\cos 2\zeta \\ +2(eg+fh)\sinh 2\zeta + 2(fg-eh)\sin 2\zeta \end{array} \right]^{1/2} \quad (4.40)$$

then the relative amplitude modulation ratio Λ;

$$\Lambda = \frac{|\mathbf{p}'|}{|\mathbf{p}|}\frac{p_s}{p_s'} = |\mathbf{R}|^{-1}\frac{p_s}{p_s'} \quad (4.41)$$

4.3.1 High frequency approximation

At high modulation frequencies, with $\zeta > 3$, $\sinh \mathbf{a}l \approx \cosh \mathbf{a}l \approx \exp(\mathbf{a}l)$ and it follows that:

$$\mathbf{R} = [(e+g)+\mathbf{i}(f+h)]\exp \mathbf{a}l\frac{(S+\mathbf{i}\omega V)}{(1+\mathbf{i})\sigma\zeta} \quad (4.42)$$

Since this is in product form it follows immediately that:

$$\begin{aligned} \phi &= \arg[e+g+\mathbf{i}(f+g)] + \arg[\exp \mathbf{a}l] + \varepsilon - \pi/4 \\ &= \phi_s + \zeta + \varepsilon - \pi/4 \end{aligned} \quad (4.43)$$

where ϕ_s represents phase changes within the surfaces at high frequencies. The surface phase lag may be evaluated for any specified surface condition.

4.3.2 Low frequency approximation

Of experimental interests also is the value of $|\mathbf{R}|^{-1}$ when $\omega \to 0$, this can be simplified as;

$$\left|\mathbf{R}^{-1}\right|(\omega \to 0) = \frac{\sigma}{S}(S_{11}S_{12}' + S_{12}S_{22}' + \frac{l}{D}S_{11}S_{22}')^{-1} \quad (4.44)$$

When the imaginary part of the above equations set to zero, one can recover the e, f, g, and h terms for the solution of phase lag and amplitude ratio of the simple two rate constant model given in chapter 2.

4.4 Possible Limiting Surface Processes

In some cases diffusant flow may be inhibited by one step in the three-stage surface process. This in turn may identify the certain characteristics of the metal hydrogen interaction. The following limiting cases are all of potential interest:

(i) The rate is limited by molecular adsorbtion/desorption, that is, k_1 is the slow step.

(ii)The rate limited by dissociation, that is, k_3, is the slow step.

(iii)There could be accumulation at the surface such that the adsorbed molecules lie in deep potential wells, requiring large activation energies both to evaporate, k_2 and to dissociate, k_3, in other words there can be a molecular surface phase.

(iv) Similar to (iii); there could be an atomic surface phase such that, when the atoms are strongly absorbed (chemisorbed) to the surface, then the process of re-association k_4 and solution into the bulk phase k_5 are the slowest

(v)Surface penetration, from the surface phase to the solid phase can be the slowest step such that k_5 and k_6 are the slowest. In the following section the forms of S and S' for these five limiting cases are presented.

4.4.1 Molecular adsorbtion/desorption limited

When adsorption on the surface and desorption of the molecules from the surface are slow compared to the other surface processes and to the bulk diffusion, there will be no accumulation of atoms or molecules on the surface. Since the flow equations (4.2-4.4) will be in equilibrium. The flux equation can be written as:

$$\mathrm{J}^{(g)} = k_1 p - k_2 \theta_m = \mathrm{J}(0) \tag{4.45}$$

Since $k_3\theta_m = k_4\theta_a^2$ and $k_5\theta_a = k_6 c(0)$ the time dependent part of the flow equation will be:

$$\mathrm{J}^{(g)} = k_1 p - \frac{k_2 k_{4p} k_6}{k_3 k_5} \mathrm{c}(0) \tag{4.46}$$

and then the interphase matrices S and S' will be

$$S = \begin{bmatrix} \frac{k_2 k_{4p} k_6}{k_1 k_3 k_5} & \frac{1}{k_1} \\ 0 & 1 \end{bmatrix} \tag{4.47}$$

$$S' = \begin{bmatrix} \frac{k'_1 k'_3 k'_5}{k'_2 k'_{4p} k'_6} & \frac{k'_3 k'_5}{k'_2 k'_{4p} k'_6} \\ 0 & 1 \end{bmatrix} \tag{4.48}$$

Using equations (4.25-4.28)

$$S_{11} = \frac{2}{K_{sm}} (p_s - J_s/k_1)^{1/2} \quad and \quad S_{12} = 1/k_1 \tag{4.49}$$

and

$$S'_{12} = \left(\frac{K_{sm}}{2}\right) (k'_1 J_s)^{-1/2} and \quad S'_{22} = 1 \tag{4.50}$$

The solution is of exactly the same form as Cummings and Blackburn's simple two rate constant model. Here k_1 defines the molecular adsorption rate, in the simple two rate constant model it is the chemisorption rate. This case, therefore, can not be picked out experimentally.

4.4.2 Dissociation/association limited

When the dissociation process becomes the rate limiting step, and if there is no molecular or atomic phase, for the time dependent part, the flow equation can be written as

$$\mathbf{J}^{(g)} = \frac{k_3 k_1}{k_2} \mathbf{p} - \frac{k_{4p} k_6}{k_5} \mathbf{c}(0) = \mathbf{J}(0) \tag{4.51}$$

Then the interphase matrices S and S' become;

$$S = \begin{bmatrix} \frac{k_2 k_{4p} k_6}{k_1 k_3 k_5} & \frac{k_2}{k_1 k_3} \\ 0 & 1 \end{bmatrix} \tag{4.52}$$

$$S' = \begin{bmatrix} \frac{k'_1 k'_3 k'_5}{k'_2 k'_{4p} k'_6} & \frac{k'_5}{k'_{4p} k'_6} \\ 0 & 1 \end{bmatrix} \tag{4.53}$$

Then the matrix coefficients;

$$S_{11} = \frac{2}{K_{sm}} \left(p_s - J_s \left(\frac{k_2}{k_1 k_3}\right)^{1/2} and \quad S_{12} = \frac{k_2}{k_1 k_3}\right. \tag{4.54}$$

and

$$S'_{12} = \left(\frac{K_{sm}}{2}\right)\left(\frac{k'_1}{k_2 k_3} J_s\right)^{-1/2} and \quad S'_{22} = 1 \tag{4.55}$$

Again same form of solution as molecular adsorption/desorption and Cummings and Blackburn two rate constant model. When one compares this result with Cummings and Blackburn's two rate constant model it can be easily seen that the surface reaction rates are related by;

$$k_1^{2r} = k_3 k_1 / k_2 \;\; and \;\; k_2^{2r} = k_4 \left(\frac{k_6}{k_5}\right)^2 \tag{4.56}$$

so the phase lag and amplitude variation with frequency will show the same behaviour as in the simple two rate constant model. Therefore experimental separation of the above two cases not possible.

The experimental interest of the six rate model, of course, is not to complicate the issue with many parameters which cannot be estimated quantitatively. It is mainly intended to separate the possible surface inhibition by atoms or molecules, in other words, the possibility of the accumulation of atoms or molecules on the surface and the slow surface penetration. The next sections are the simplified solutions of these limiting cases.

4.4.3 Strongly bound molecules/molecular surface phase

Suppose that adsorbed molecules lie in deep potential wells, requiring large activation energies to evaporate, rate k_2 and dissociate, rate k_3. If all other rate constants are faster compared to the diffusion process, then there will be an identifiable molecular surface phase.
Again using the no backflow approximation provides a simplified solution, the interface matrix coefficients S_{11}, S_{12}, S'_{12} and S'_{22} are necessary to find the solution for phase lag and amplitude ratio are then found from (4.33 and 4.34).

$$S_{11} = \frac{2p_s^{1/2}}{K_{sm}} + i\omega \frac{2p_s^{1/2}}{K_{sm} k_2} \quad and \quad S_{12} = 0 \tag{4.57}$$

and

$$S'_{12} = 0 \quad and \quad S'_{22} = 1 + \mathrm{i}\omega/k_2 \tag{4.58}$$

Then the terms e, f , g, h from (4.38) are:

$$\begin{aligned} e &= f = 0 \\ g &= \frac{l2p_s^{1/2}}{DK_{sm}}\left[1 - \frac{\omega^2}{k_2 k'_2}\right] \\ h &= \frac{l2p_s^{1/2}}{DK_{sm}}\left[\frac{\omega}{k_2} + \frac{\omega}{k'_2}\right] \end{aligned} \tag{4.59}$$

then using equations (4.39-4.41) for phase lag ϕ, $|\mathbf{R}|^{-1}$ and Λ

$$\begin{aligned} \phi &= \varepsilon - \pi/4 \\ &\quad + \arctan\left[\frac{\tan\zeta}{\tanh\zeta}\right] + \arctan\left(\frac{\omega}{k_2}\right) + \arctan\left(\frac{\omega}{k'_2}\right) \end{aligned} \tag{4.60}$$

$$|\mathbf{R}|^{-1} = \frac{\sigma DK_{sm}}{Slp_s^{1/2}}\zeta\left[\cosh 2\zeta - \cos 2\zeta\right]^{-1/2}\left[1 + \left(\frac{\omega}{k_2}\right)^2\right]^{-1/2}\left[1 + \left(\frac{\omega}{k'_2}\right)^2\right]^{-1/2} \tag{4.61}$$

Remembering Richardson's equation (1.6) and the pumping equation (2.18),

$$J_s = \frac{DK_{sm}}{l}p_s^{1/2} \quad and \quad p'_s = \frac{\sigma}{S}J_s$$

Then the relative modulation amplitude ratio Λ,

$$\Lambda = \zeta\left[\cosh 2\zeta - \cos 2\zeta\right]^{-1/2}\left[1 + \left(\frac{\omega}{k_2}\right)^2\right]^{-1/2}\left[1 + \left(\frac{\omega}{k'_2}\right)^2\right]^{-1/2} \tag{4.62}$$

Figures 2 and 3 show the variation of phase lag and relative amplitude modulation ratio versus frequency factor ζ for various values of dimensionless parameter $2D/k_2 l^2$, which provides approximate measure of the time of stay of an undissociated molecule on the surface to time an atom spends diffusing through the bulk of the foil.

Both phase lag and relative modulation amplitude ratio are independent of pressure.

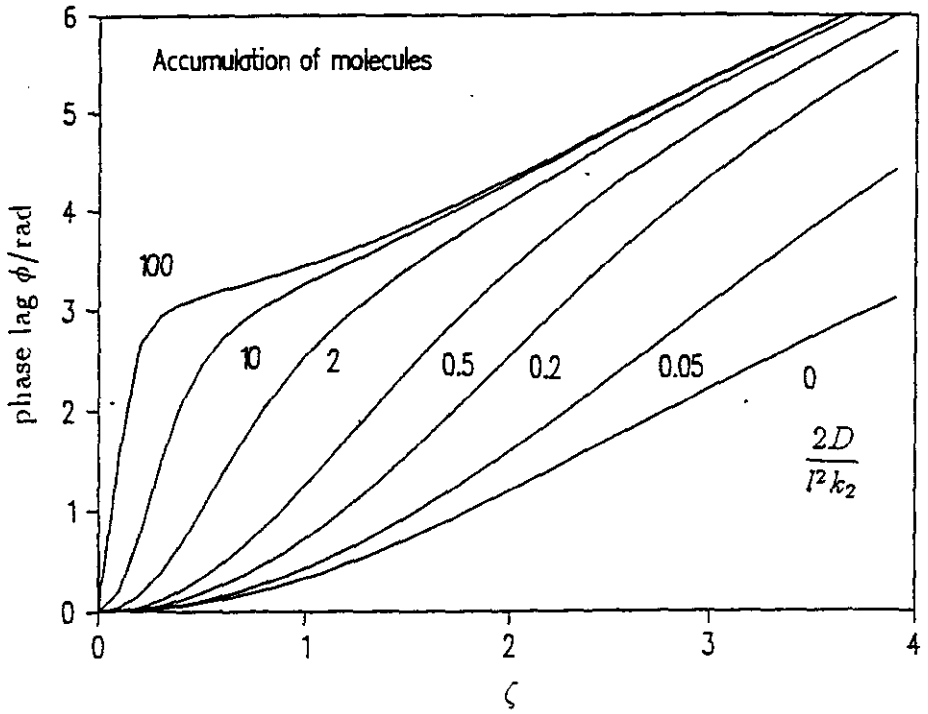

Figure 4.2 The variation of phase lag versus frequency factor ζ for various values of dimensionless parameter $2D/k_2 l^2$ for symmetric foils, $k_2 = k_2'$

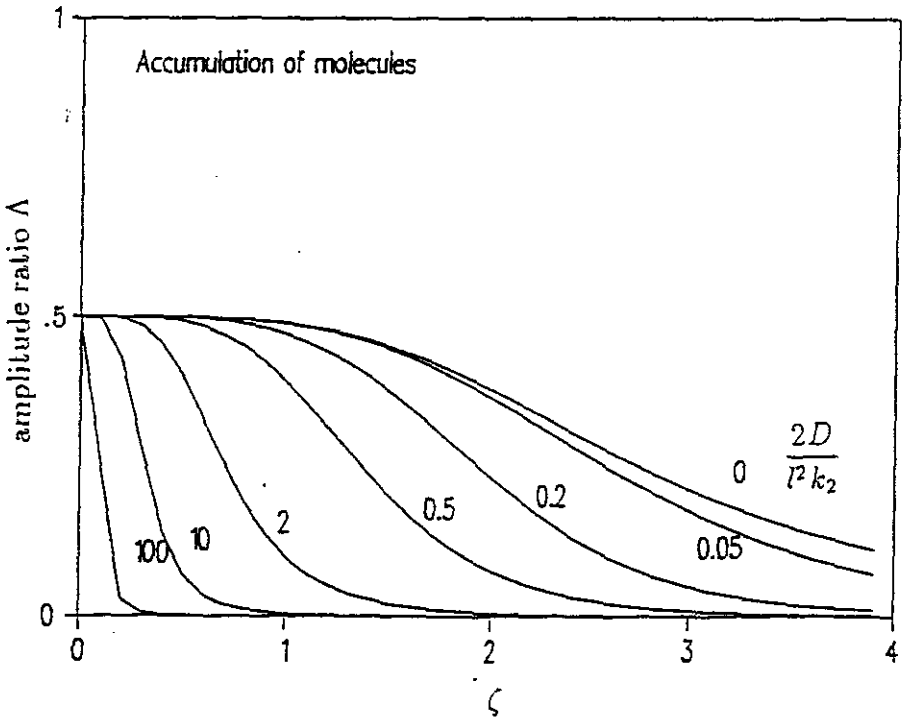

Figure 4.3 The variation of relative amplitude modulation ratio Λ, versus frequency factor ζ for various values of dimensionless parameter $2D/k_2 l^2$ for symmetric foils, $k_2 = k_2'$

The limits of phase lag at high frequencies and modulation ratio at zero frequencies give useful information for identifying the surface process.

High frequency approximation

From (4.42) ϕ_s maximum phase lag introduced by slow surface process as k_2 and $k_2' \rightarrow 0$ is π. then extrapolated intercept at the zero frequency is $3\pi/4$ (figure 2).

Low frequency approximation

From equation (4.44) or also from (27) only $p^{1/2}$ permeation can occur The low frequency approximation leads $|\mathbf{R}|^{-1}$ and Λ:

$$|\mathbf{R}|^{-1} = \frac{1}{2}\frac{\sigma}{S}\frac{DK_{sm}}{lp_s^{1/2}} \tag{4.63}$$

$$\Lambda = \frac{1}{2} \tag{4.64}$$

4.4.4 Atomic surface phase

When the atoms are strongly chemisorbed to the surface, the process of reassociation k_4 and the solution in the bulk phase, k_5 are necessarily much slower than any of the other process.

More speficially for both surfaces $k_1, k_2, k_3, k_6 \gg k_{4p}, k_5$

$$S_{11} = \frac{2p_s^{1/2}}{K_{sm}} + \mathrm{i}\omega\frac{2p_s^{1/2}}{K_{sm}k_{4p}}\left(\frac{k_2+k_3}{k_2}\right) \; and \quad S_{12} = 0 \tag{4.65}$$

and

$$S_{12}' = 0 \; and \quad S_{22}' = 1 + \frac{\mathrm{i}\omega}{k_{4p}'}\left(\frac{k_2+k_3'}{k_2'}\right) \tag{4.66}$$

the terms e, f, g and h become:

$$e = f = 0$$

$$g = \frac{l2p_s^{1/2}}{DK_{sm}}\left[1 - \frac{\omega^2}{k_{4p}k_{4p}'}\left(\frac{k_2+k_3}{k_2}\right)\left(\frac{k_2'+k_3'}{k_2'}\right)\right]$$

$$h = \frac{l2p_s^{1/2}}{DK_{sm}}\left[\frac{\omega}{k_{4p}}\left(\frac{k_2+k_3}{k_2}\right) + \frac{\omega}{k_{4p}'}\left(\frac{k_3'+k_2'}{k_2'}\right)\right. \tag{4.67}$$

In comparison with the previous example, the terms, e, f, g and h are analogous, in which ω/k_2 is replaced by $(\omega/k_{4p})(k_2+k_3)/k_2$ Then the phase shifts and amplitudes are :

$$\phi = \varepsilon - \pi/4 + \arctan\left[\frac{\tan\zeta}{\tanh\zeta}\right] + \arctan\left(\frac{\omega}{k_{4p}}\left(\frac{k_2+k_3}{k_2}\right)\right) + \arctan\left(\frac{\omega}{k'_{4p}}\left(\frac{k'_2+k'_3}{k'_2}\right)\right) \tag{4.68}$$

$$|\mathbf{R}|^{-1} = \frac{\sigma D K_{sm}}{S l p_s^{1/2}}\zeta\left[\cosh 2\zeta - \cos 2\zeta\right]^{-1/2} \left[1+\left(\frac{\omega}{k_{4p}}\left(\frac{k_2+k_3}{k_2}\right)\right)^2\right]^{-1/2}\left[1+\left(\frac{\omega}{k'_{4p}}\left(\frac{k'_2+k'_3}{k'_2}\right)\right)^2\right]^{-1/2} \tag{4.69}$$

and as previous case relative modulation amplitude ratio Λ

$$\Lambda = \zeta\left[\cosh 2\zeta - \cos 2\zeta\right]^{-1/2} \left[1+\left(\frac{\omega}{k_{4p}}\left(\frac{k_2+k_3}{k_2}\right)\right)^2\right]^{1/2}\left[1+\left(\frac{\omega}{k'_{4p}}\left(\frac{k'_2+k'_3}{k'_2}\right)\right)^2\right]^{1/2} \tag{4.70}$$

Fig. 4 and 5 show the variation of phase lag ϕ and relative modulation amplitude ratio, Λ for various values of $2D/l^2k_{4p}$ with respect to frequency factor ζ

The phase lag and relative amplitude modulation ratio are both dependent on pressure through the pressure dependence of k_{4p}.

High frequency approximation

Comparison with the molecular surface phase it shows that a maximum phase lag of π can be introduced, It should perhaps be pointed out that this surface effect is in addition to the $\pi/2$ phase lag introduced when the changeover from $p^{1/2}$ to p^1 permeation occurs.

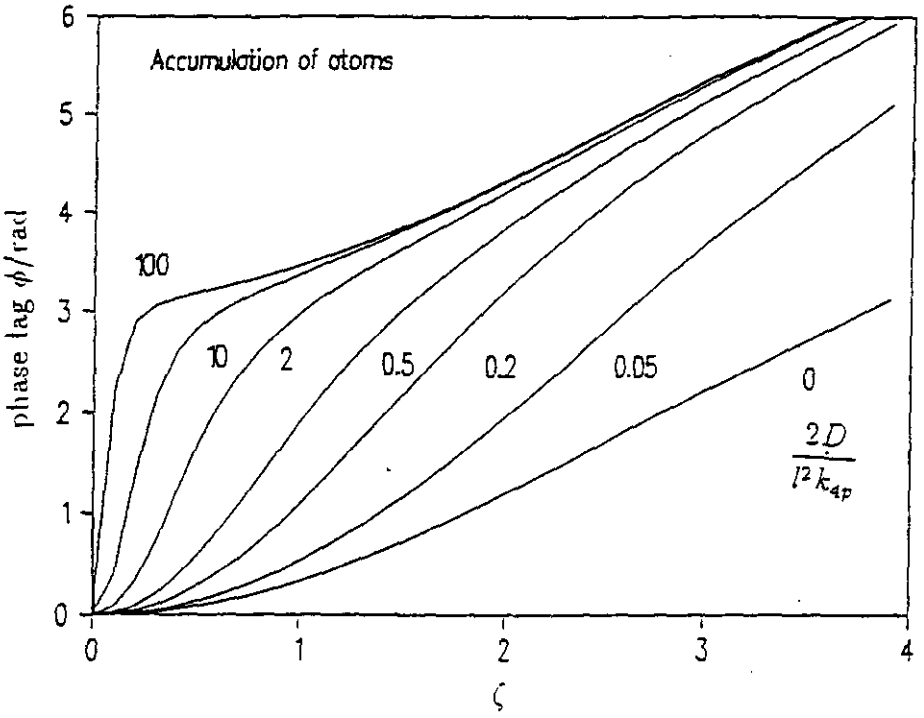

Figure 4.4 The variation of phase lag, ϕ versus frequency factor ζ for various values of dimensionless parameter $2D/k_{4p}l^2$ for symmetric foils, $k_4 = k_4'$

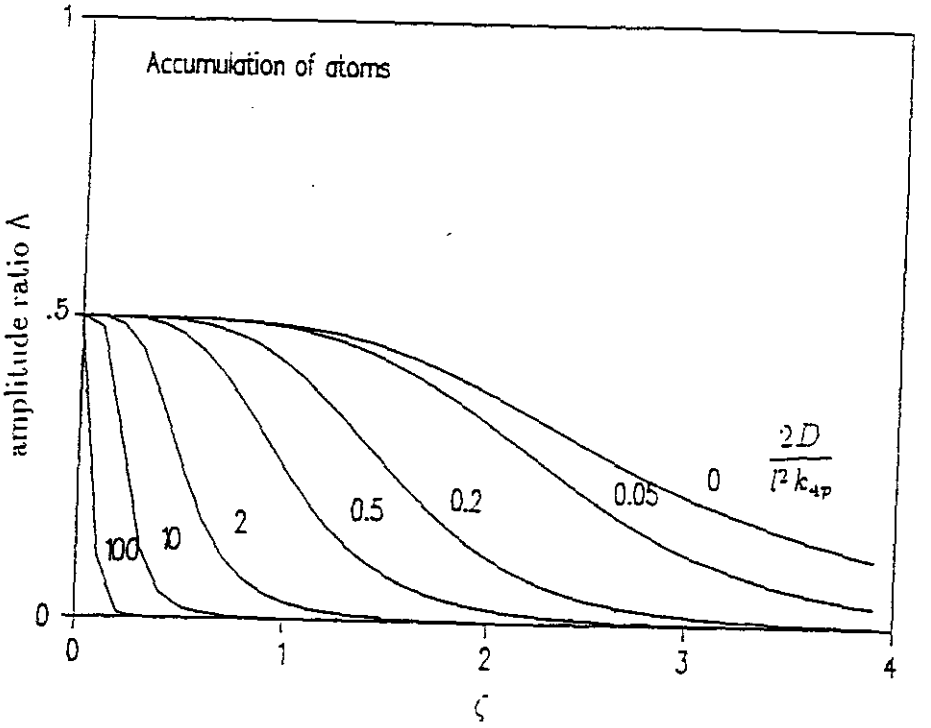

Figure 4.5 The variation of relative amplitude modulation ratio, Λ versus frequency factor ζ for various values of dimensionless parameter $2D/k_{4p}l^2$ for symmetric foils, $k_4 = k_4'$

Low frequency approximation

By comparison with the atomic surface case the low frequency approximation leads $|\mathbf{R}|^{-1}$ and Λ:

$$|\mathbf{R}|^{-1} = \frac{1}{2}\frac{\sigma}{S}\frac{DK_{sm}}{lp_s^{1/2}} \tag{4.71}$$

$$\Lambda = \frac{1}{2} \tag{4.72}$$

4.4.5 Surface penetration slow step

When transition between the surface and solid phases are relatively slow, more specifically, k_1, k_2, k_3, k_4 are much slower than k_5 and k_6, then the flow equations (4.1-4.3) will be in equilibrium. The time dependent part of the flow equation can be written as:

$$\mathbf{J}^{(g)} = k_5\theta_{\mathbf{a}} - k_6\mathbf{c}(0) \tag{4.73}$$

where $\theta_{\mathbf{a}} = \left(\frac{k_1 k3}{k_2 k_4}\right)^{1/2} \frac{\mathrm{p}}{2p_s^{1/2}}$, the interface matrices can be defined as;

$$S = \begin{bmatrix} \frac{2p_s^{1/2}}{K_{sm}} & \frac{2p_s^{1/2}}{k_6 K_{sm}} \\ 0 & 1 \end{bmatrix} \tag{4.74}$$

and S'

$$S' = \begin{bmatrix} \frac{K_{sm}}{2p_s^{1/2}} & \frac{1}{k_6'} \\ 0 & 1 \end{bmatrix} \tag{4.75}$$

Experimentally the hard pumping condition is of particular interest. This enables one to use the general form of solution. From (4.38), the terms e, f, g and h become:

$$\begin{aligned} e &= \zeta\left(\frac{2p_s^{1/2}}{K_{sm}}\frac{1}{k_6'} + \frac{1}{k_6}\frac{2p_s^{1/2}}{K_{sm}}\right) \\ f &= e \\ g &= \frac{l}{D}\left(\frac{2p_s^{1/2}}{K_{sm}}\right) \\ h &= \frac{2D\zeta^2}{l}\left(\frac{p_s^{1/2}}{k_6 k_6' K_{sm}}\right) \end{aligned} \tag{4.76}$$

the phase lag, ϕ from (4.39) is:

$$\phi = \arctan\left[\frac{\zeta\left(\frac{1}{k_6}+\frac{1}{k_6'}\right)(\tan\zeta\tanh\zeta+1)+\frac{l}{D}\tan\zeta+\frac{2D\zeta^2}{l}\left(\frac{1}{k_6k_6'}\right)\tanh\zeta}{\zeta\left(\frac{1}{k_6}\frac{1}{k_6'}\right)(\tan\zeta\tanh\zeta-1)+\frac{l}{D}\tanh\zeta-\frac{2D\zeta^2}{l}\left(\frac{1}{k_6k_6'}\right)\tan\zeta}\right] + \varepsilon - \pi \quad (4.77)$$

and:

$$|\mathbf{R}| = \frac{(S^2+\omega^2V^2)^{1/2}}{2\sigma\zeta} \cdot \left[\begin{array}{l}(e^2+f^2+g^2+h^2)\cosh 2\zeta \\ +(e^2+f^2-g^2-h^2)\cos 2\zeta \\ +2(eg+fh)\sinh 2\zeta + 2(fg-eh)\sin 2\zeta\end{array}\right]^{1/2} \quad (4.78)$$

then the relative amplitude modulation ratio Λ;

$$\Lambda = \frac{|\mathbf{p}'|}{|\mathbf{p}|}\frac{p_s}{p_s'} = |\mathbf{R}|^{-1}\frac{p_s}{p_s'} \quad (4.79)$$

High frequency approximation

From equation (4.43) the surface phase lag ϕ_s is $\pi/2$ so the extrapolated intercept at zero frequency is $\pi/4$.

Low frequency approximation From equation (4.44)

$$|\mathbf{R}|^{-1} = \frac{1}{2}\frac{K_{sm}}{p_s^{1/2}}\left[\frac{1}{k_6}+\frac{1}{k_6'}+\frac{l}{D}\right]^{-1} \quad (4.80)$$

This result suggest that when $k_6, k_6' \gg D/l$ then the permeation is wholly diffusion limited. If this condition does not prevail permeation still follows the $p^{1/2}$ but varies more slowly with $1/l$

In the limit that $k_6, k_6' \ll D/l$ the permeation becomes independent of both D and l. There are experimental results (Silberg and Bachman) [59] for which this parameter range is appropriate and indeed it is observed that for Pd/H, fluxes are proportional to $p_s^{1/2}$ and independent of thickness, that is surface penetration appears to be the rate limiting in the high pressure regime.

Fig. 6 and 7 show variation of phase lag and amplitude ratio for various values of $\frac{2D}{lk_6}$

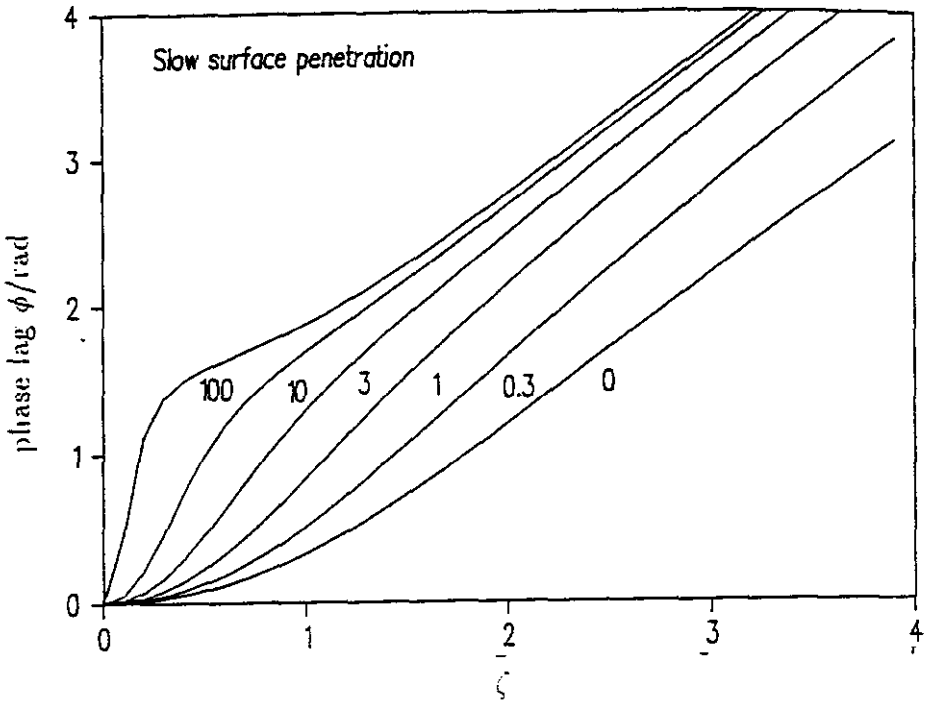

Figure 4.6 The variation of phase lag ϕ versus frequency factor ζ for various values of dimensionless parameter $2D/k_6 l$ for symmetric foils, $k_6 = k_6'$

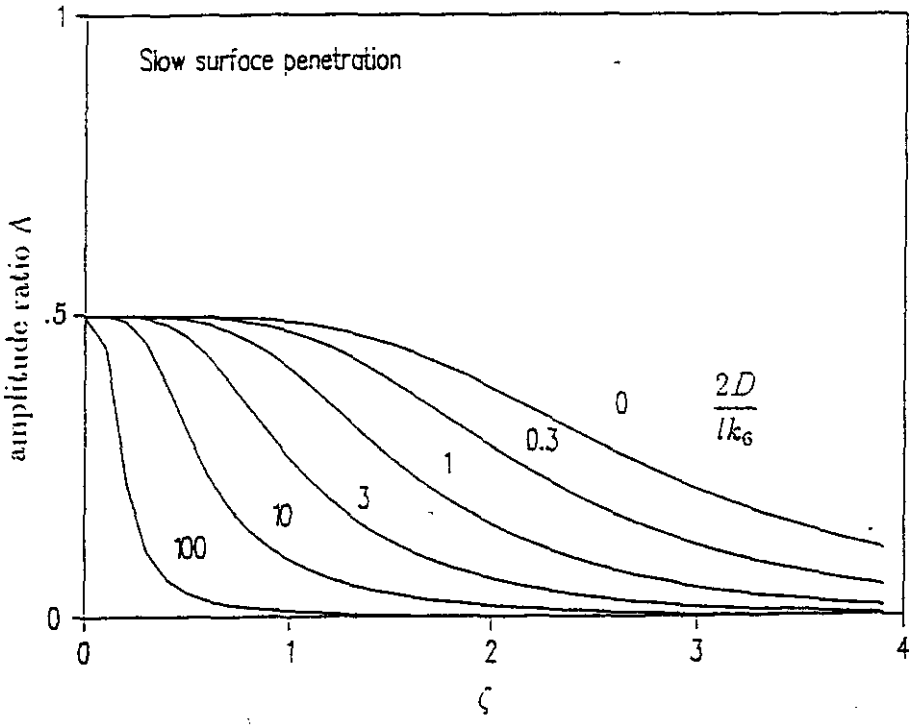

Figure 4.7 The variation of relative modulation amplitude ratio, Λ versus frequency factor ζ for various values of dimensionless parameter $2D/k_6 l$ for symmetric foils, $k_6 = k_6'$

4.5 Discussion

The six rate constant model makes it possible to predict the frequency response of a foil to pressure modulation for any given set of $\{k_i, k_i'\}$, K_{sm}, D, $and p_s$. More difficult is the reverse analysis which extracts the rate constant from the observed frequency response of phase lag and amplitude.

Five limiting cases relevant to experimental conditions have been identified. Results for these limiting cases are summarized in table 4.1.
For " Diffusion limited flow ", the ϕ and Λ are pressure independent their variation with frequency solely determined by a diffusion coefficient and the permeation law for diatomic gas has a $p^{1/2}$ dependence.
When parameters correspond with other than diffusion limited conditions, the characteristics are less distinct, but some cases at least are amenable to experimental analysis and a degree of separation is always possible. The frequency analysis of ϕ and Λ are both needed for an effective analysis and data must be available over a substantial pressure range.

When flow is limited by surface processes, the identification of the rate limiting step can be followed in the pressure dependence of the frequency response of the phase lag and amplitude ratio.

Pressure dependency suggests that the flow may be limited by molecular adsorption/desorption, dissociation or accumulation of atoms on the surface. For each case an increase in pressure should always reduce the phase lag.
When the flow is rate limited by adsorbtion/desorption or dissociation separation of these two cases is very difficult. Then the combination of these two steps as dissociative chemisorption can be clearly distingushed from the accumulation of atoms by observing the zero frequency intercept of the relative modulation amplitude ratio.
When atoms are accumulated on the surface; $\Lambda(\omega = 0) = 1/2$, whereas dissociative chemisorption will always give $1/2 < \Lambda < 1$.

The extrapolated intercept of phase lag at high frequencies also shows different limits as pressure is lowered. Under limitation by dissociative chemisorption, the phase lag intercept at $\omega = 0$, will be up to $\pi/4$ whereas accumulation of atoms will have an intercept at $3\pi/4$. This allows definite separation of k_1 and k_4. On the other hand it should be remembered that at very low pressures k_1 limitation must always prevail. If this happens within the range of k_4 influence then the data are probably too complicated to allow satisfactory separation. Above some pressure, the data should be independent of pressure and flow becomes diffusion limited.

Pressure independence suggests that the flow may be limited by accumulation of molecules, surface penetration or diffusion through the bulk. Permeation follows a $p^{1/2}$ law in both limiting cases. An extrapolated intercept of phase lag between $\pi/4$ and $3\pi/4$ unaffected by pressure is a clear indication of a molecular surface phase, or, accumulation of molecules. If the intercept is lower than this, then the experiments should include a check on the steady state flux with foil thickness. If surface penetration limits the flow, then the steady state flux is no longer inversily proportional to the foil thickness.

Limiting Rate	Phase Characteristic		Amplitude Characteristic		Steady State Flux Limit	Limiting process
	$\phi(\omega = 0)$ high ω limit	remarks $\phi(\omega)$	$\Lambda(\omega = 0)$ exponent n	remarks $\Lambda(\omega)$		
K_{sm}	$-\pi/4$	solely depends on D	1/2	solely depends on D	$\frac{DK_{sm}}{l} p_s^{1/2}$	diffusion
k_1, k_2	$\leq +\pi/4$	pressure dependent	$1/2 < n < 1$	pressure dependent	$\frac{p_s}{1/k_1 + 1/k_1'}$	adsorption
k_3, k_4	$\leq +\pi/4$	pressure dependent	$1/2 < n < 1$	pressure dependent	$\frac{p_s}{1/k_3 + 1/k_3'}$	dissociation
k_2, k_3	$\leq +3\pi/4$	pressure independent	1/2	pressure independent	$\frac{DK_{sm}}{l} p_s^{1/2}$	accumulation (molecules)
k_4, k_5	$\leq +3\pi/4$	pressure dependent	1/2	pressure dependent	$\frac{DK_{sm}}{l} p_s^{1/2}$	accumulation (atoms)
k_5, k_6	$\leq +3\pi/4$	pressure independent	1/2	pressure independent	$\frac{K_{sm}}{1/k_6 + 1/k_6'} p_s^{1/2}$	surface penetration

Table 4.1 Six rate constant model results

Chapter 5

Results and Discussion

5.1 Introduction

Measurements were made of modulated hydrogen flow through nickel and nickel-2% thoria in the cold worked and annealed conditions. Other measurements were made on palladium. The results are detailed in a separate section for each material.

The raw experimental data are in the form of ϕ and Λ both against square root of frequency $\omega^{1/2}$. The experimental parameter space was explored in order to reveal how the permeation is affected by surface reaction and internal trapping. Then the phase lag ϕ and Λ were fitted to the appropriate model to obtain the permeation parameters at each temperature. These parameters in turn are analysed in the form of Arrhenius plots to find the activation energy and pre-exponential factor of each temperature dependent rate.

5.2 Pure Nickel and Palladium

Experiments were performed on pure nickel in the as-received and 87 % cold worked state in the temperature range of 373K-623 K.

5.2.1 As received Nickel

The raw experimental data are in the form of phase lag, ϕ, and amplitude ratio, Λ both against square root of frequency, $\omega^{1/2}$, in the pressure range

6.65 Pa to 7.3 kPa and for temperatures between 373 K and 623 K.

Figures 5.1 and 5.2 show the isothermal variation of the phase lag, ϕ and relative modulation amplitude ratio, Λ with the square root of the modulation frequency $\omega^{1/2}$, for the three pressures 6.65 Pa, 66.5 Pa and 6.65 kPa for as-received nickel(well-annealed) at 548 K. These curves are typical of those obtained for other temperatures. This data show excellent support for the surface inhibition model presented in the chapter 2. The low frequency increase in Λ to above 1/2 and cross-over with respect to reduction of pressure is strong evidence of surface inhibition along with 0.4π increase in ϕ, which approaches the maximum possible increase of $\pi/2$ when both surfaces limit the flow. Also the detailed analysis of the three stage surface processes presented in modelling chapter 4 justifies the assumptions made in the Cummings and Blackburn simple two rate canstant surface model. Their model takes no account of any surface phase and describes the possible surface processes; adsorption/desorption, dissociation/association, solution/de-solution by a single reversible reaction, absorption/desorption. In other words, the model they presented can decribe the dissociative-chemisorption of hydrogen on the surface. Extended analysis of surface processes in chapter 4, has shown that the low frequency increase in Λ to above 1/2 and cross-over with respect to reduction of pressure can only be the case of dissociative-chemisorption. As concluded in chapter 4, it is more useful to analyse these results using Cummings and Blackburn's simple two rate constant model. Both the variation of phase lag and relative modulation amplitude ratio with frequency supports the view that hydrogen is dissociatively chemisorbed in nickel. All the results were simultaneously subjected to a non-linear least square fitting of curves for ϕ and Λ vs. $\omega^{1/2}$. To derive the coefficients, the data set consisted of pairs of ϕ and Λ covering 35-40 frequencies at the three pressures for a particular temperature. The standard errors of input and output chamber modulations higher than 0.5%, and relative modulation amplitude ratio less than 0.5 were rejected from the curve fitting procedures. Then the iteration proceeded until 0.1% accuracy was obtained in the parameters.
Analysing the temperature variation of these parameters on the assumption of an Arrhenius model also gives the activation energies as well as the pre-exponential factors.

Figure 5.3 shows the variation of P_m, D and k_1 with inverse temperature (1000/T(K)). The best fit values from these Arrhenius plots of D, P_m and

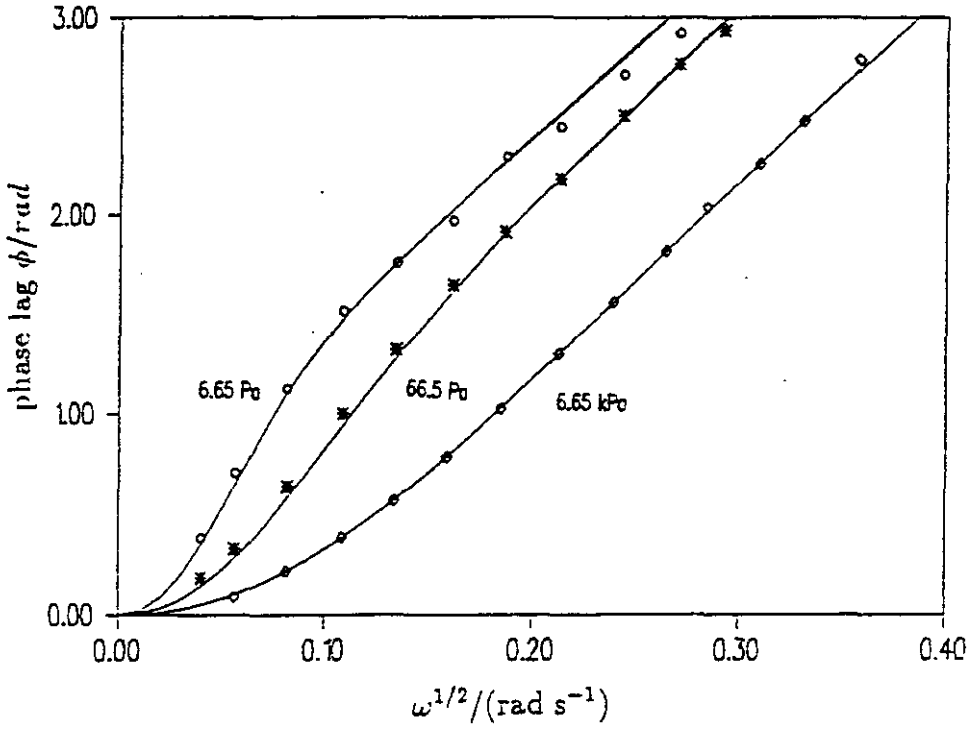

Figure 5.1 Measured variation of phase lag ϕ with square root of modulation frequency, $\omega^{1/2}$ for pure nickel at 548 K for pressures of o–6.65 Pa, *–66.5 Pa and ◇–6.65 kPa

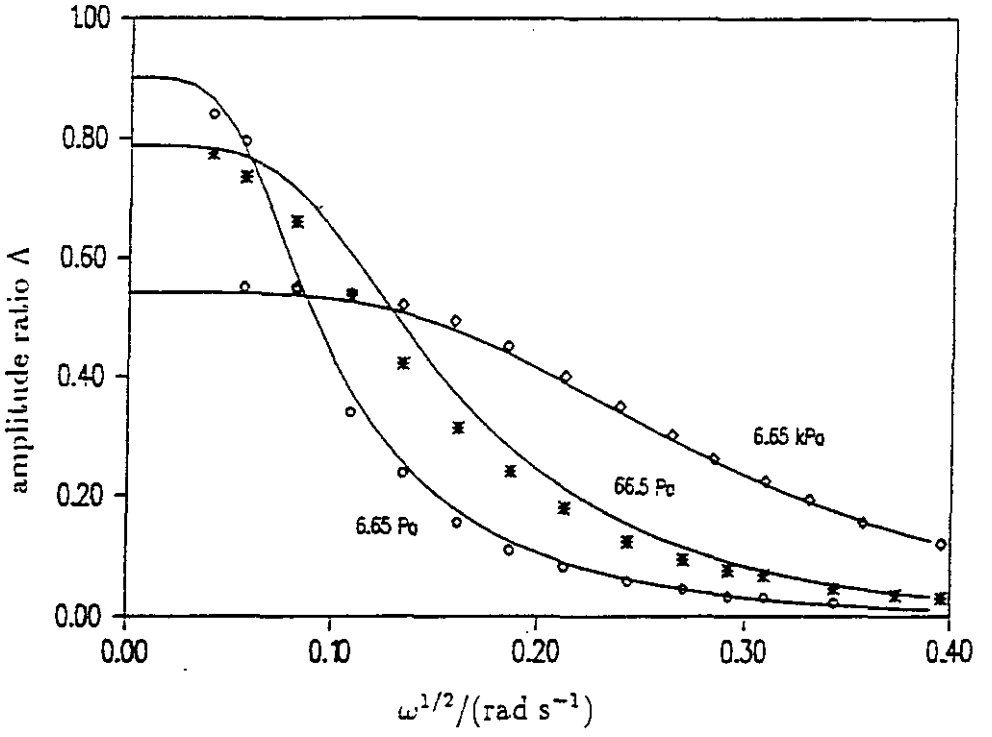

Figure 5.2 Measured variation of modulation amplitude ratio Λ with square root of modulation frequency, $\omega^{1/2}$ for pure nickel at 548 K for pressures of o–6.65 Pa , *–66.5 Pa and ◇–6.65 kPa

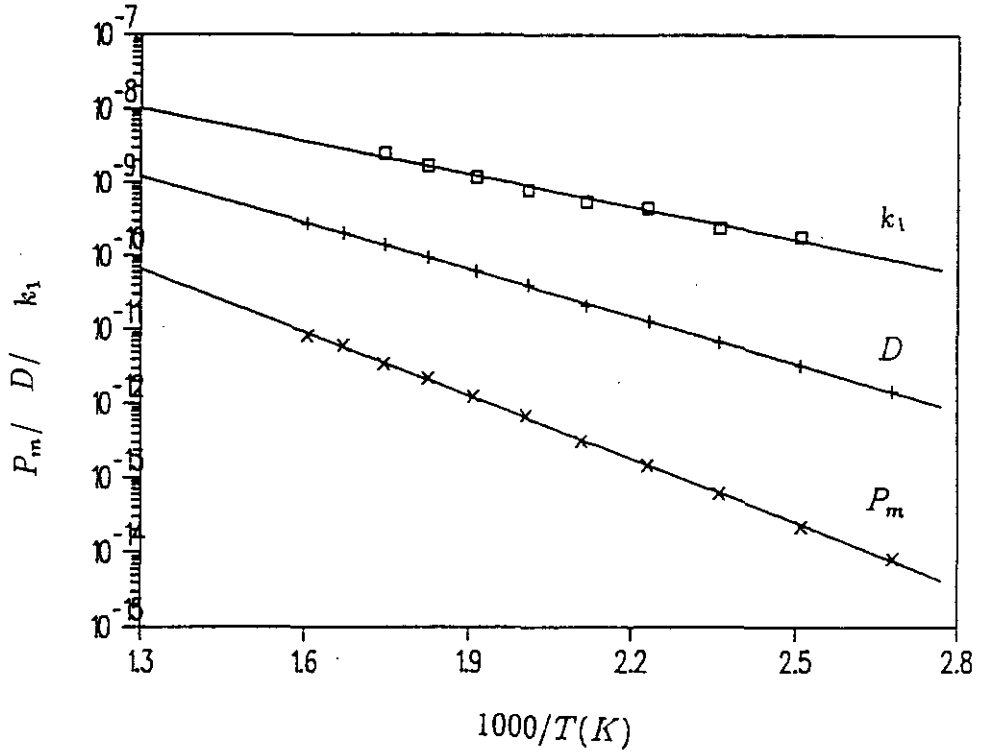

Figure 5.3 The Arrhenius plots of measured $P_m/(molH_2m^{-1}s^{-1}Pa^{-1/2})$, $D/(m^2s^{-1})$ and $k_1/(molH_2m^{-2}s^{-1}Pa^{-1})$ for pure nickel

k_1 are:

$$D/(m^2s^{-1}) = 7.12 \times 10^{-7} \exp\left[-40.64 \times 10^3/RT(K)\right]$$

$$P_m/(molH_2m^{-1}s^{-1}Pa^{-1/2}) = 3.35 \times 10^{-7} \exp\left[-54.25 \times 10^3/RT(K)\right]$$

$$K_{sm}/(molH_2m^{-3}Pa^{-1/2}) = 0.47 \exp\left[-13.6 \times 10^3/RT(K)\right]$$

$$k_1/(molH_2m^{-2}s^{-1}Pa^{-1}) = 1.44 \times 10^{-6} \exp\left[-29.68 \times 10^3/RT(K)\right]$$

Where $R = 8.314 Jmol^{-1}$. gas constant

The pre-exponential factor and the activation energy for diffusivity are in agreement with Robertson's best-fit line values of $D_0 = 6.44 \times 10^{-7} m^2 s^{-1}$ and $E_D = 40.2 kJmol^{-1}$ [64] and with the assessments by Volkl and Alefeld of $D_0 = 6.9 \times 10^{-7} m^2 s^{-1}$ and $E_D = 40.5 kJmol^{-1}$ [4]. Excellent agreement is found with the permeation coefficients of Robertson [64] and Le Claire [65]. They are $P_{m0} = 3.32 \times 10^{-7} (molH_2) m^{-1} s^{-1} Pa^{-1/2}$, $E_P = 54.8 KJmol^{-1}$ and $P_{m0} = 3.38 \times 10^{-7} (molH_2) m^{-1} s^{-1} Pa^{-1/2}$ respectively. These results are also consistent with the previous work on nickel by the periodic modulation technique [41]. The Arrhenius behaviour of k_1 suggests that the proposed model is adequate. No other values of k_1 have been reported against which to make comparision. However, Baskes [60] and Pick and Sonenberg [63] have estimated the so called recombination rate k_r theoretically which is equiva lent to k_2/σ, where σ is the roughness factor, defined as the ratio of the true surface area to the geometrical one. According to their theory the rate of adsorption, $k_1 p$, is given by the kinetic theory of gases, with $k_1 = \Phi s$, through the sticking coefficient, s, and with $\Phi = 4.385/(2T)^{1/2} molm^{-2}s^{-1}Pa^{-1}$. Using the relationship.

$$K_{sm} = \left(\frac{k_1}{k_2}\right)^{1/2} \tag{5.1}$$

Then the recombination rate k_2 which is equivalent to $\Phi s/K_{sm}$

$$k_2/(m^4.s^{-1}molH_2^{-1}) = 6.51 \times 10^{-6} \exp\left[-2.32 \times 10^3/RT/(K)\right] \tag{5.2}$$

Baskes model relates the activation energy for recombination is the sum of the activation energies of the diffusion and solubility such that;

$$k_r = k_{r0} \exp(2E_S - (E_C)/kT) \tag{5.3}$$

where $E_C = E_D + E_S$ for metals in which hydrogen disolution is endothermic, otherwise $E_C = 0$

On the other hand, Pick and Sonnenberg report:

$$k_r = k_{r0} \exp(2E_S/kT) \tag{5.4}$$

Taking $E_C = 0$ this assumption implies that the sticking probability, s=1, that is k_1 takes its maximum value, such that all arriving molecules are absorbed. For metal in which hydrogen disolution is exothermic, predicted recombination coefficients are essentially the same for the Baskes and the Pick and Sonnenberg model. But for endothermic metals Baskes model predicts a significantly lower recombination coefficient.

Any estimation of recombination coefficient depends on the value of sticking probability which will vary with the amount of surface impurity and also the kind of surface impurity. So without any experimental justification of the model they presented, either their calculated values or the comparison with this work will have limited value.

In order to enhance the surface effect experiments were performed at 648 K on a nickel foil which had previously been oxidized at 770 K. The results are shown in figures 5.4 and 5.5. The resulting phase lag ϕ and relative modulation amplitude ratio Λ show a solely surface limited permeation at 8 kPa. The low frequency value of $\Lambda = 1$ and the high frequency extrapolate of ϕ at zero frequency, $\pi/2$ are evidence of permeation being proportional to pressure. This shows that impurities such as oxides on the surface can affect the permeation rate and support the view that hydrogen is dissociatively chemisorbed in nickel.

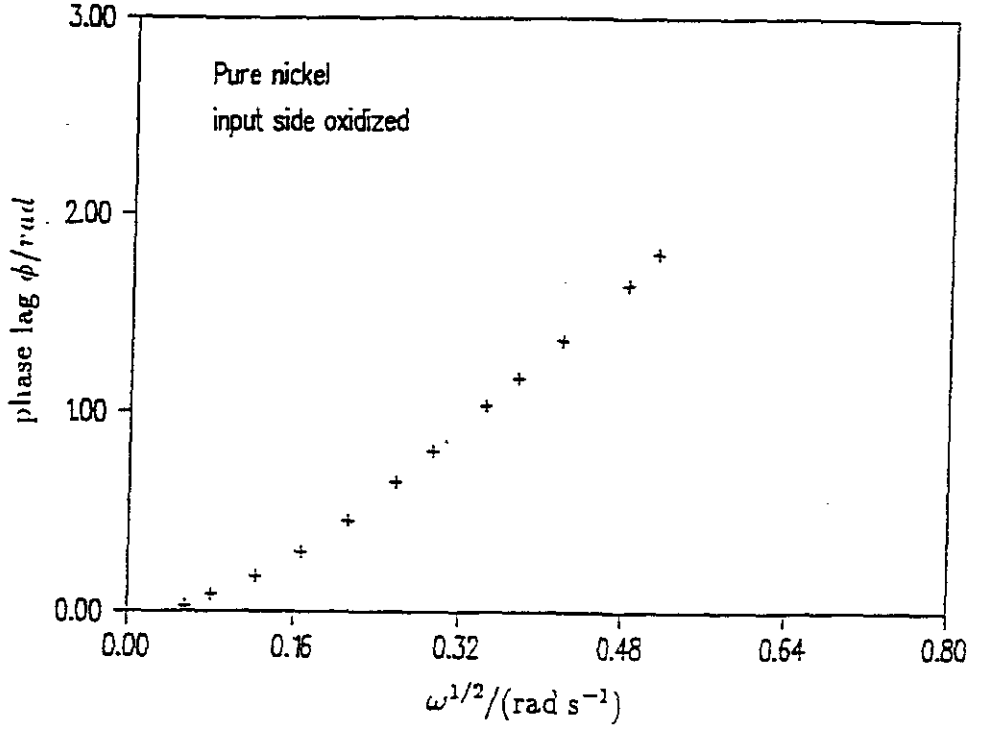

Figure 5.4 Measured variation of phase lag ϕ with root frequency $\omega^{1/2}$ for oxidized nickel at 450 K, 8 kPa

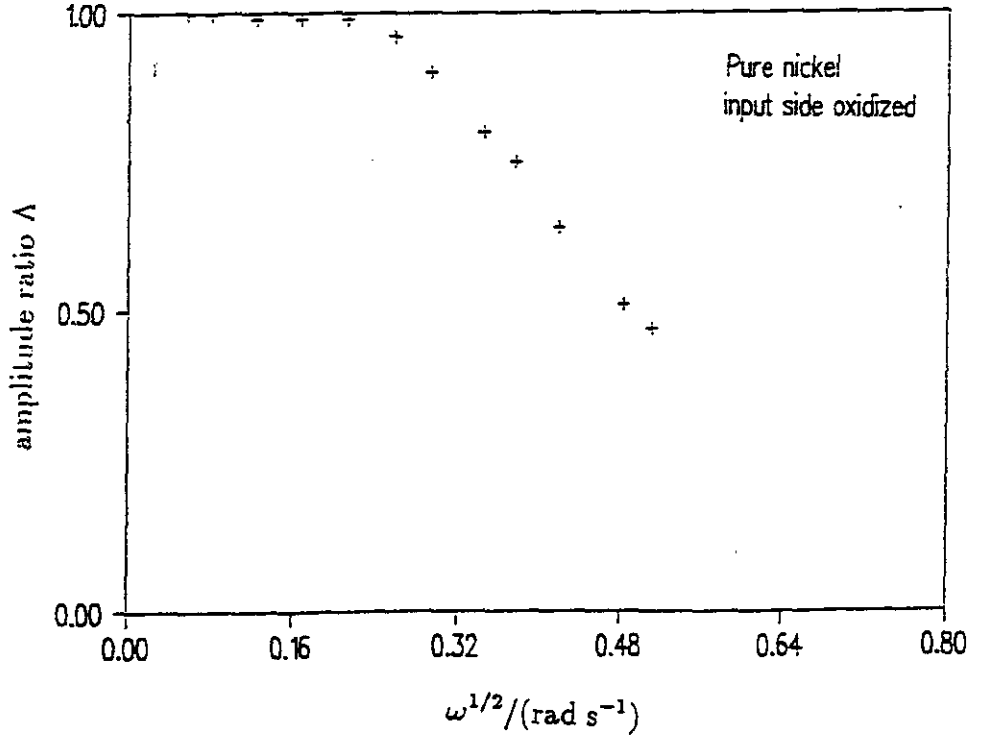

Figure 5.5 Measured variation of relative amplitude modulation ratio Λ with root frequency $\omega^{1/2}$ for oxidized nickel, 450 K, 8 kPa

5.2.2 Palladium

Experiments were also performed on palladium foil of 0.25 mm thickness at three temperatures for 66.5 Pa.

Figures 5.6 and 5.7 show the phase lag and relative amplitude modulation ratio Λ for palladium at 450 K, notice that the high frequency extrapolate at zero frequency in figure 6 is $\pi/2$ and in figure 7 Λ at zero frequency is 1, which indicate purely surface limited permeation by dissociative chemisorption. There is insufficient data to make a reliable estimate of permeation parameters. Owing to the very high flux, the experiments could not be conducted at higher pressure. because the output gauge was not suitable. Higher pressures, in fact, were necassary to see that the permeation changes over from p^1 to $p^{1/2}$. Even so, the estimated diffusivities at three temperatures, using Cummings and Blackburn surface limited model, are very close to value quoted by Volk and Alefeld [4], at 560 K. The estimated diffusion coefficient is $2.45 \times 10^{-8} m^2 s^{-1}$ and k_1 is $7.8 \times 10^{-4} mol H_2 m^{-2} s^{-1} Pa^{-1/2}$. To obtain quantitative information, it would be necessary to perform experiments on palladium over a wide range of input pressure. This is not a major objective of this project and was not persued further.

5.2.3 Cold worked nickel

87% cold worked nickel was investigated to see if work hardening modifies the permeation parameters of nickel. In order to ensure that the cold worked foil did not anneal during the bake-out, the region around the foil was kept water-cooled. First set of permeation experiments commenced at 398 K and were performed for 8 temperatures up to 573 K. Then the specimen foil was annealed *in situ* at 650 K before repeating second set of permeation experiments. Part of the cold worked foil was cut into 14 pieces, then batch annealing runs carried out in vacuum subjected to identical regimes of temperature as the one used in permeation experiments. Annealed pieces were taken out from the vacuum furnace one by one, then studied under the optical

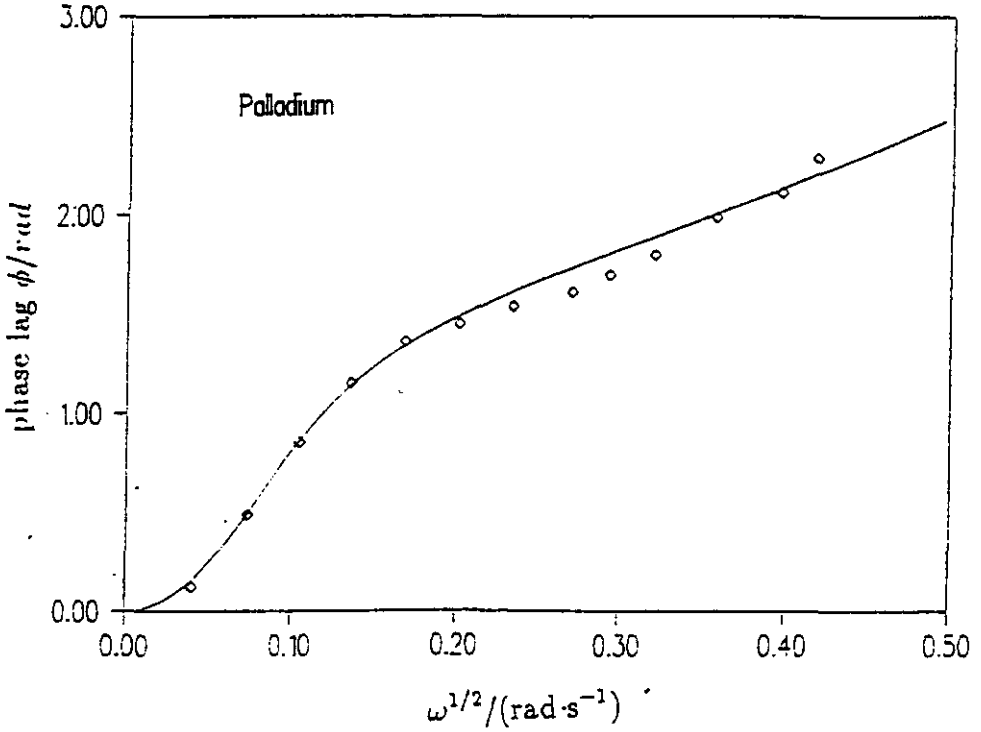

Figure 5.6 Measured variation of phase lag ϕ with root frequency $\omega^{1/2}$ for 0.25 mm Pd at 560 K, 800 Pa.

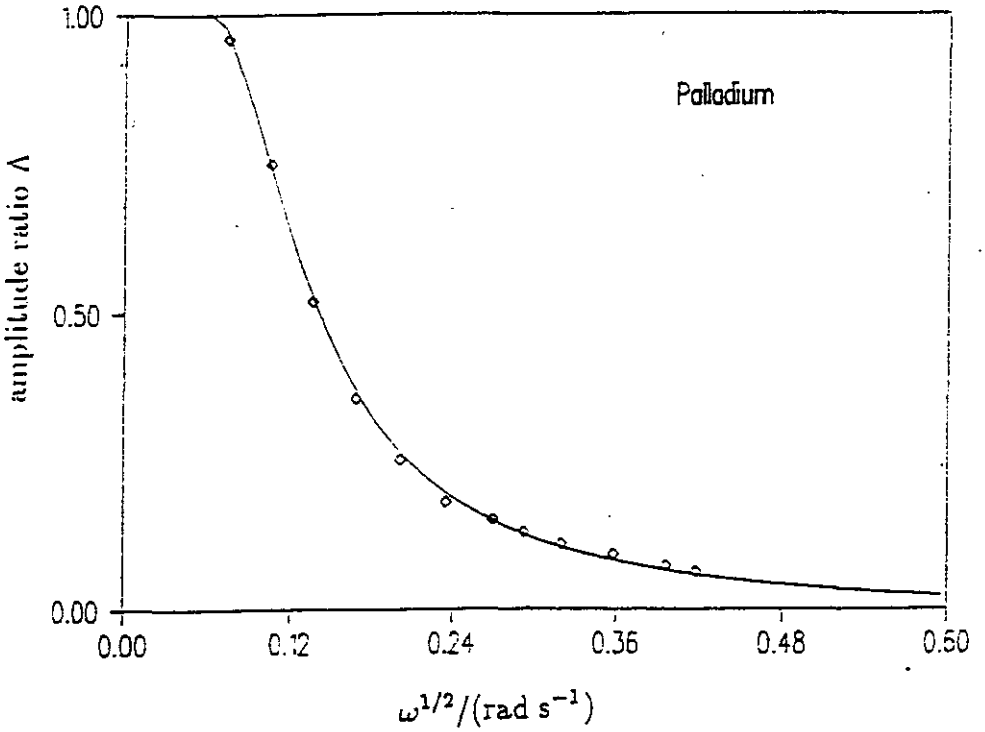

Figure 5.7 Measured variation of relative amplitude modulation ratio Λ with root frequency $\omega^{1/2}$ for 0.25 mm Pd at 560 K, 800 Pa

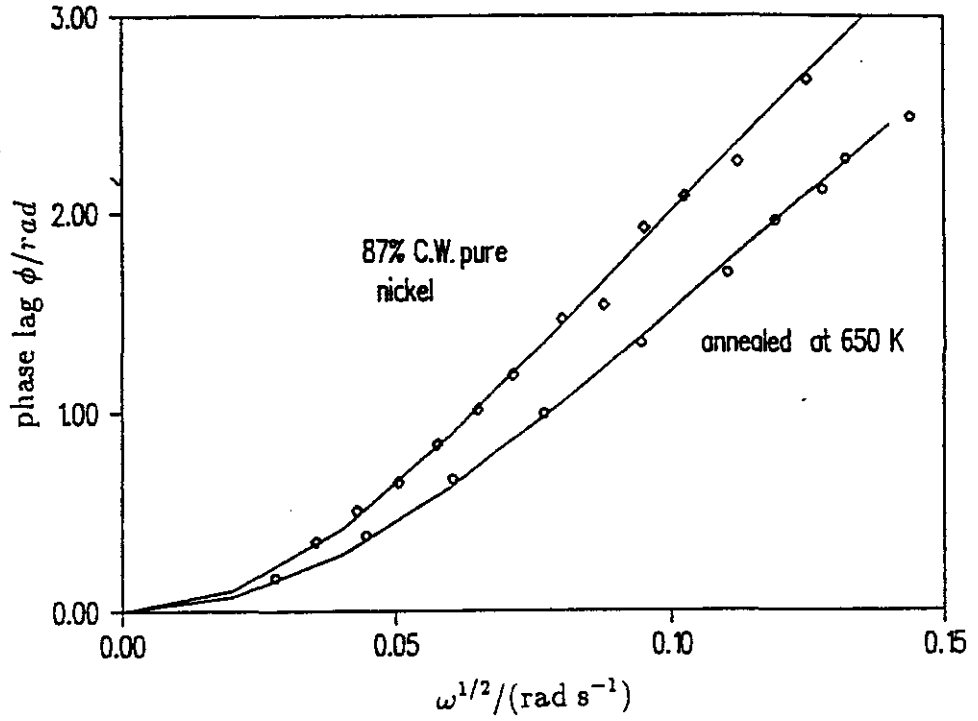

Figure 5.8 Measured variation of phase lag ϕ with root frequency $\omega^{1/2}$ for nickel at 423 K, mean pressure 8 kPa, ◇– 87% cold worked, o–after annealing at 650 K

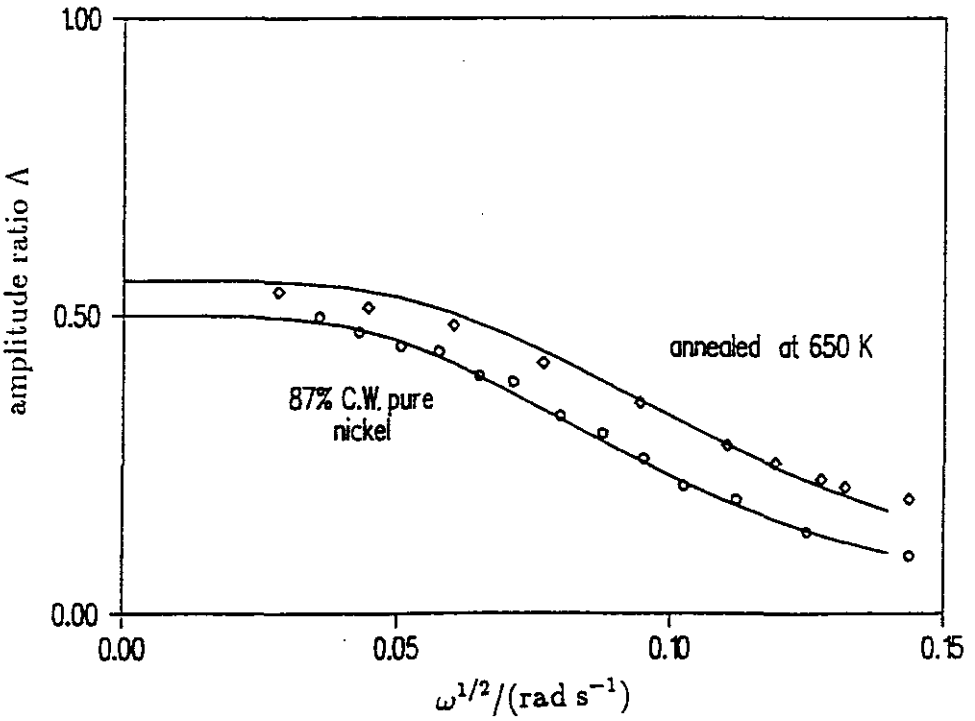

Figure 5.9 Measured variation of relative modulation amplitude ratio Λ with root frequency $\omega^{1/2}$ for nickel at 423 K, mean pressure 8 kPa, ◇– 87% cold worked, o–after annealing at 650 K

microscope and the electrical resistivity, microhardness were also measured. Figures 5.8 and 5.9 show the variation of phase lag ϕ and relative modulation amplitude ratio Λ with square root of frequency $\omega^{1/2}$ at an input pressure of 7 kPa. Data are shown before and after annealing *in situ* at 650 K. Similar results were obtained for experimental temperatures in the range 398 K-573 K. Above 523 K, the relative modulation amplitude ratio Λ and phase lag, ϕ, are identical for both annealed and cold worked nickel foil. In fact,the study of the optical microstructure together with the measurements of the microhardness and electrical resistivity at each step of experiment indicate substantial annealing was occurring as low as 523 K (figures 5.10-5.17).

The frequency response of the phase lag ϕ and relative modulation amplitude ratio, Λ in figures 5.8 and 5.9, show classical bulk diffusion limited flow. As noted in chapter 2, characteristics of diffusion limited flow are; the high frequency extrapolate of the phase lag ϕ, at zero frequency, $\pi/4$ and zero frequency value of relative modulation amplitude ratio, 0.5. At a given frequency annealing changes the the amount of phase lag ϕ as well as the amplitude ratio Λ in the direction of faster transport, but it preserves the characteristic features of bulk diffusion limited flow.

Figure 5.10 Optical microstructure of 87% cold worked nickel, no anneal, magnification: $\times 600$

Figure 5.11 Optical microstructure of cold worked nickel subjected to identical regimes of temperature as those used in permeation experiments, annealing time: 24 hrs at 398 K +24 hr at 423 K+ 16 hrs at 448 K, magnification: $\times 600$

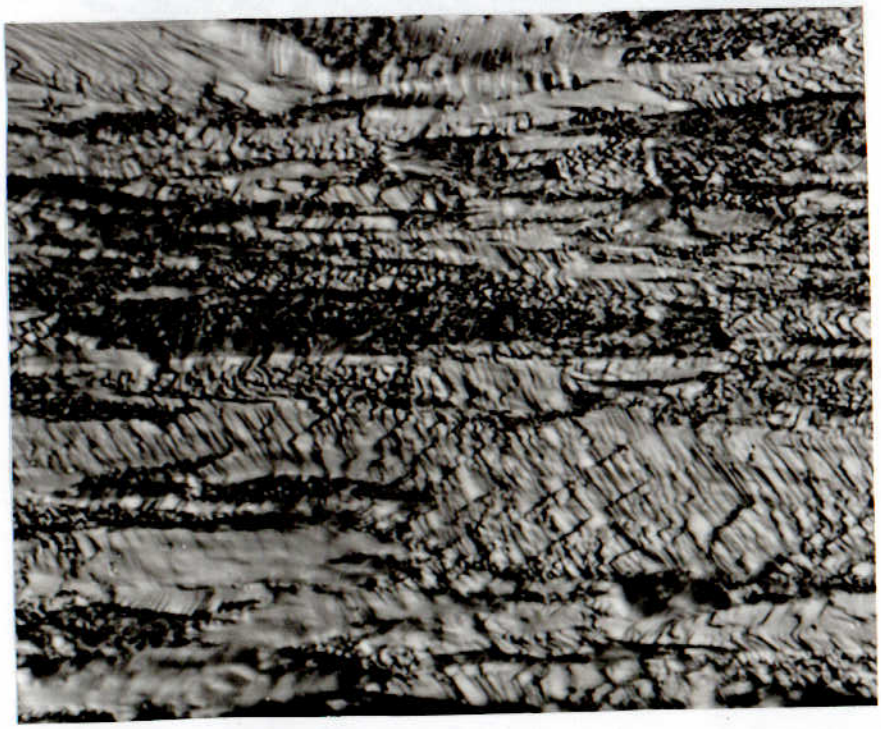

Figure 5.12 Optical microstructure of cold worked nickel subjected to identical regimes of temperature as those used in permeation experiments, annealing time: 24 hrs at 398 K +24 hr at 423 K+ 16 hrs at 448 K + 16 hrs at 473 K + 10 hrs 498 K, magnification: $\times 600$

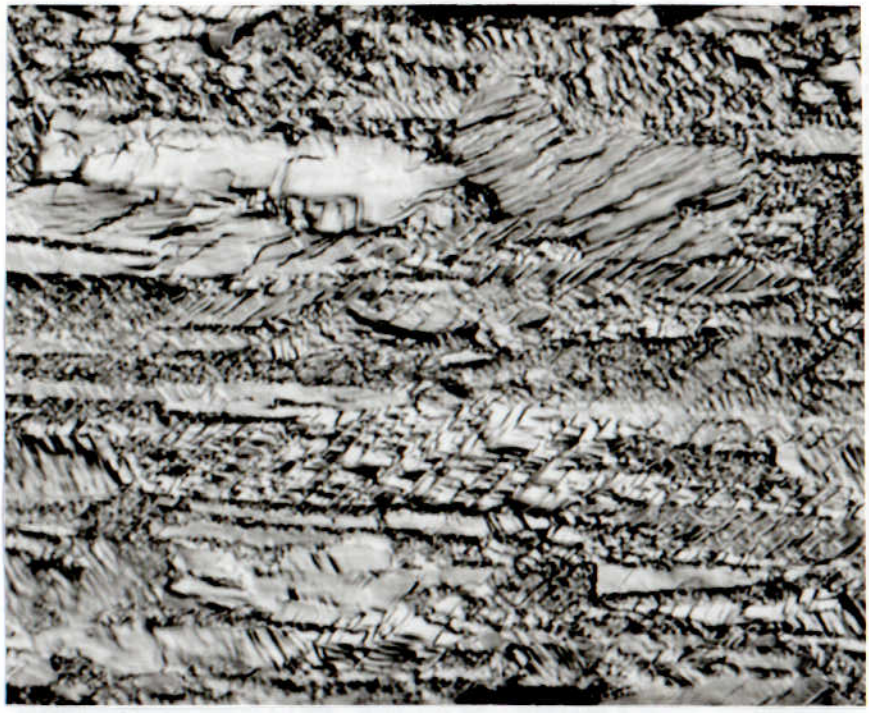

Figure 5.13 Optical microstructure of cold worked nickel subjected to identical regimes of temperature as those used in permeation experiments, annealing time: 24 hrs at 398 K +24 hr at 423 K+ 16 hrs at 448 K + 16 hrs at 473 K + 10 hrs 498 K + 10 hrs at 523 K, magnification: ×600

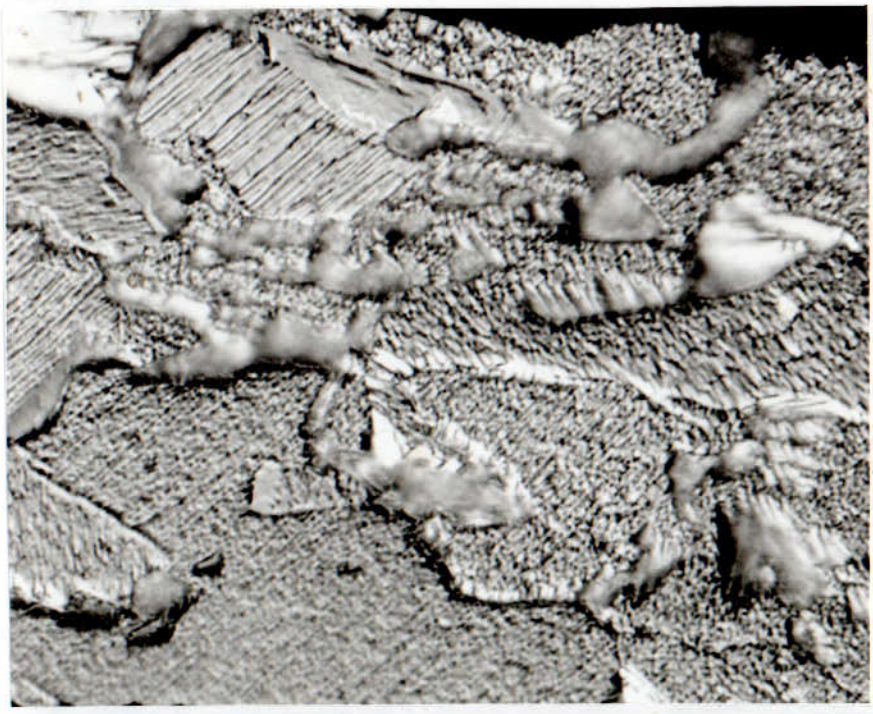

Figure 5.14 Optical microstructure of cold worked nickel subjected to identical regimes of temperature as those used in permeation experiments, annealing time: 24 hrs at 398 K +24 hr at 423 K+ 16 hrs at 448 K + 16 hrs at 473 K + 10 hrs 498 K + 10 hrs at 523 K + 8 hrs at 548 K, magnification: ×600

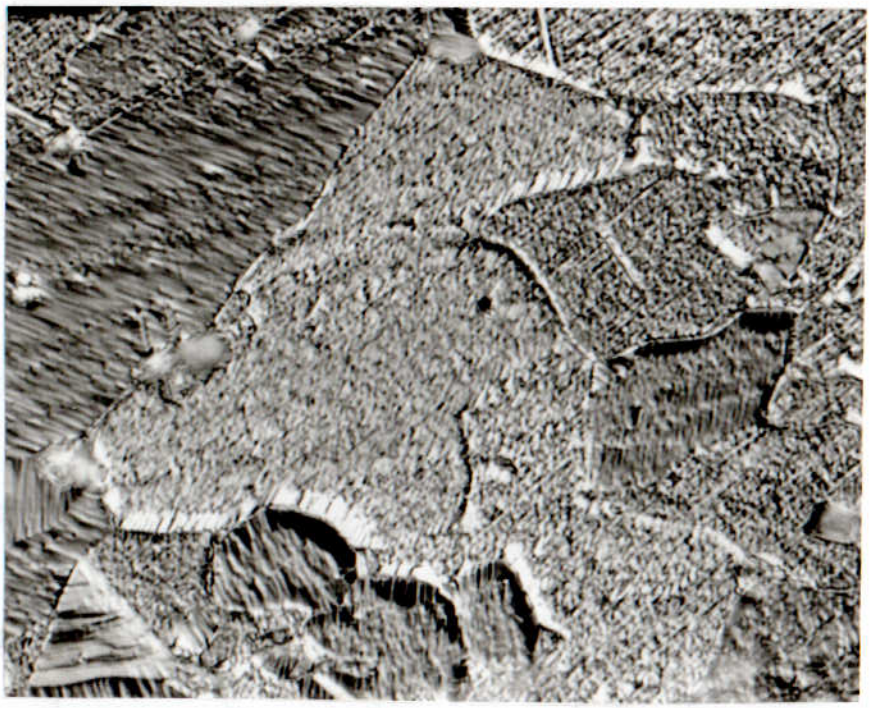

Figure 5.15 Optical microstructure of cold worked nickel subjected to identical regimes of temperature as those used in permeation experiments, annealing time: 24 hrs at 398 K +24 hr at 423 K+ 16 hrs at 448 K + 16 hrs at 473 K + 10 hrs 498 K + 10 hrs at 523 K + 8 hrs at 548 K + 8 hrs at 573 K, magnification: $\times 600$

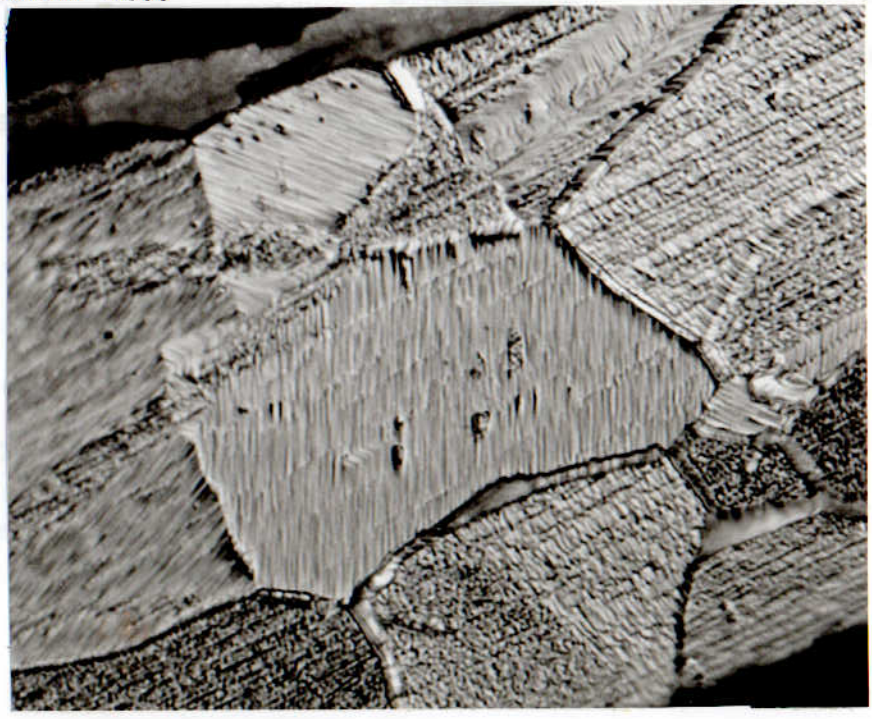

Figure 5.16 Optical microstructure of cold worked nickel subjected to identical regimes of temperature as those used in permeation experiments, annealing time: 24 hrs at 398 K +24 hr at 423 K+ 16 hrs at 448 K + 16 hrs at 473 K + 10 hrs 498 K + 10 hrs at 523 K + 8 hrs at 548 K + 8 hrs at 573 K + 2 hrs at 613 K, magnification: $\times 600$

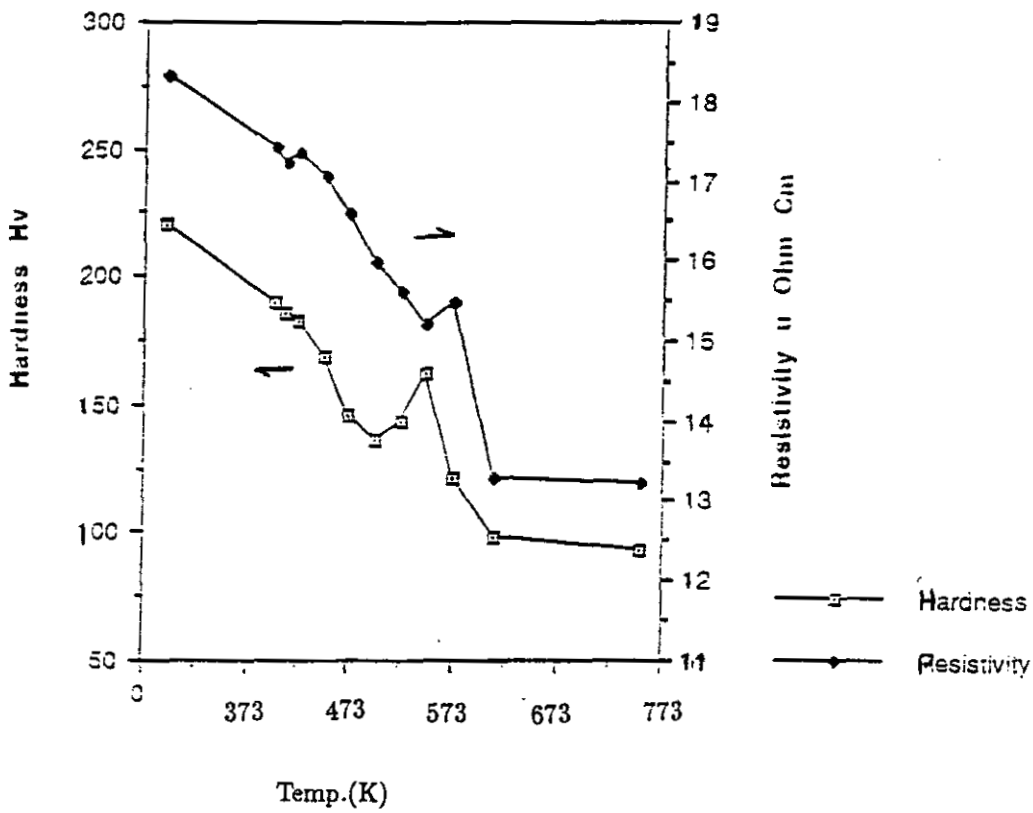

Figure 5.17 Measurement of microhardness and electirical ressistivity of cold worked nickel subjected to identical regimes of temperature as those in permeation experiments (batch processing)

Since there are no maxima/minima in the phase lag response and there is an increase in the phase lag for cold worked nickel, the trapping in cold worked nickel appears to be in dynamic equilibrium. In this case , as noted in chapter 2, it is not possible to obtain trapping and detrapping rates. The estimated diffusion coefficient using the diffusion limited flow is therefore an apparent diffusion coefficient D^{app}.

Figure 5.18 shows the variation of apparent diffusivity D^{app} deduced from the phase lag and amplitude data for cold worked and annealed nickel the apparent diffusivity in the cold worked nickel is lower than in the annealed metal.

Figure 5.19 shows that the variation of the permeability of cold worked nickel is identical with that of well annealed nickel. This suggest that hydrogen is trapped at sites introduced by cold rolling. Louthan et al observed a rise in permeability by a factor of 2.5 following cold rolling to 95% reduction in thickness, suggesting enhanced transport by dislocations [53]. Some workers have reported a trap binding energy of 8-25 kJ mol for dislocations and vacancies in cold worked nickel [66] [67].

Observations of microstructure and measurement of microhardness show that substantial annealing occurred during the experiment figures 5.10 and 5.17. The activation energy and number of traps cannot therefore be reliably extracted from the experimental data This could also be the case for previous work by others on cold worked nickel, most of whom did not detect trapping in nickel.

5.3 Nickel Thoria

The experiments performed on nickel thoria, also known as NITD, can be divided into two groups. The first presents the effect of cold work and annealing and the second presents the effect of pressure variation on phase lag ϕ and relative modulation amplitude ratio Λ.

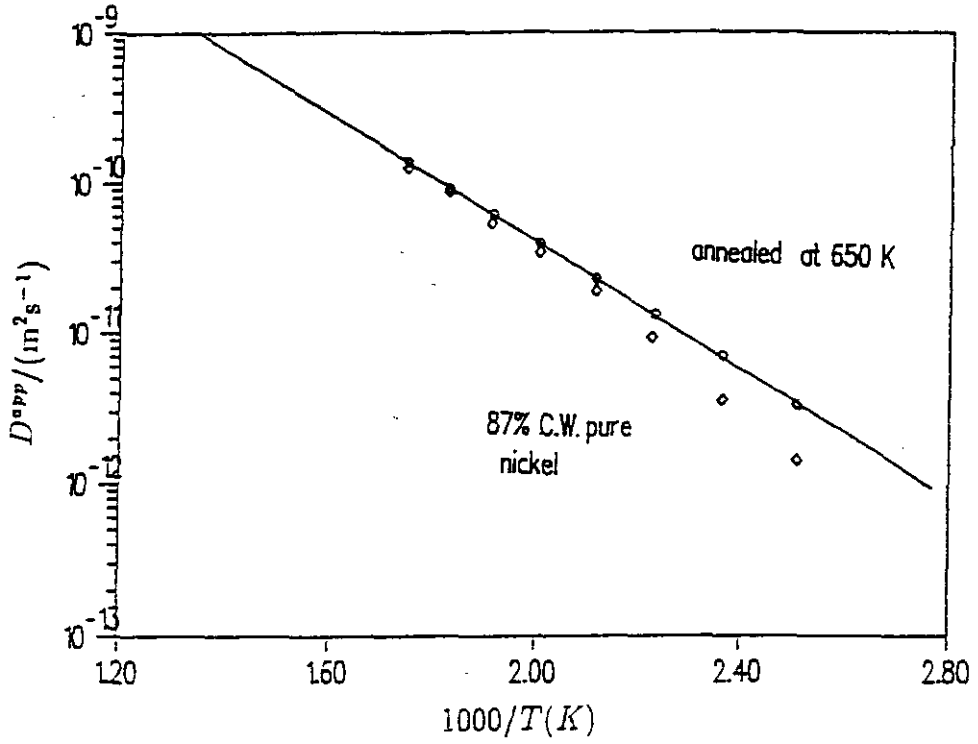

Figure 5.18 The Arrhenius plots of measured apparent diffusivities, D^{app} with $1000/T/K$ for nickel o–87 % cold worked , ◇–after annealing at 650 K, solid line is for 0.125 mm annealed nickel

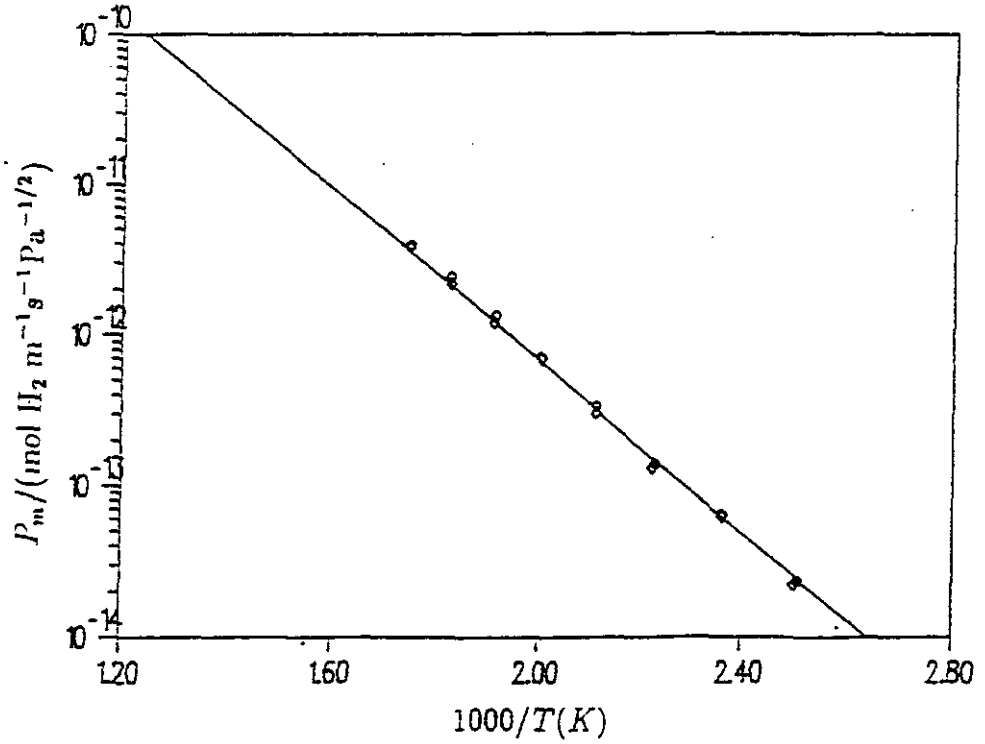

Figure 5.19 The Arrhenius plots of measured permeabilities, P_m for nickel o–87 % cold worked , ◇–after annealing at 650 K. solid line is for 0.125 mm annealed nickel

5.3.1 Effect of annealing

NITD contains insoluble dispersoids of thorium oxide, so analysis of well annealed nickel thoria should enable the interface effect to be seen. Cold work adds dislocation networks and voids which may affect the permeation characteristics. The microstructures of each specimen were studied by TEM to correlate the changes in permeation characteristic with the changes in microstructural features. Figure 5.20 shows the TEM picture of 87% cold worked nickel thoria. Notice that the voids formed around thoria particles. Figere 5.21 shows TEM pictures of 87% cold worked nickel thoria after annealing at 1423 K for 8 hours. Notice that cold worked structure did not fully annealed out. TEM study and measurements of microhardnes (table 5.1) of cold worked and annealed nickel thoria foils in this work are close to results from the study of Webster (1966). Four NITD foils were examined under the following cold worked conditions.
92% CW ($0.075mm$), 87% CW ($0.125mm$), 50% CW ($0.5mm$), 75% CW ($0.3mm$)
The experiments performed on each specimen were as follows;

- **92% cold worked**
  Mean pressure was 6.65 kPa for all runs
  Experiments were performed in the temperature range

- **87% cold worked**
  Mean pressure was 6.65 kPa
  Experiments were performed in the temperature range 473-623 K
  First experiments were performed for cold worked condition, then the foil were annealed in situ at 750 K for seven days and then the experiment repeated
  A third run was performed for the foil which is a part of same cold worked sheet after annealing in vacuum at 1425 K for 8 hours
  Last run performed for the foil which is also a part of same cold worked

% Cold Work	Thermal Treatment	Hardnes (HV)
Ni - as received		107 - 126
NITD as received		225 - 267
NITD 50%		244 - 308
NITD 75%		394 - 463
NITD 87%		502 - 569
NITD 92%		549 - 569
NITD 50%	annealed 8 hrs 1423 K	210 - 230
NITD 87%	annealed 8 hrs 1423 K	199 - 210

Table 5.1 Measurements of microhardness of nickel thoria foils for different annealing conditions

sheet after annealing in vacuum at 1625 K for 24 hours

- **50% cold worked**

  Mean pressure was 6.65 kPa

  Experiments were performed in the temperature range 573 -913 K

  First experiments were performed for cold worked condition

  Second run were performed for the foil which is a part of same cold-worked sheet after annealing in vacuum at 1425 K for 8 hours.

- **75% cold worked**

  Mean pressure was 65.5 kPa

  Experiments were performed in the temperature range 573-773 K for cold worked condition

Figure 5.22 and 5.23 show the variation of phase lag ϕ and relative modulation amplitude ratio A with $\omega^{1/2}$ for a 0.125 mm NITD foil for anneals of different durations at 523 K at an input pressure of 6.65 kPa.

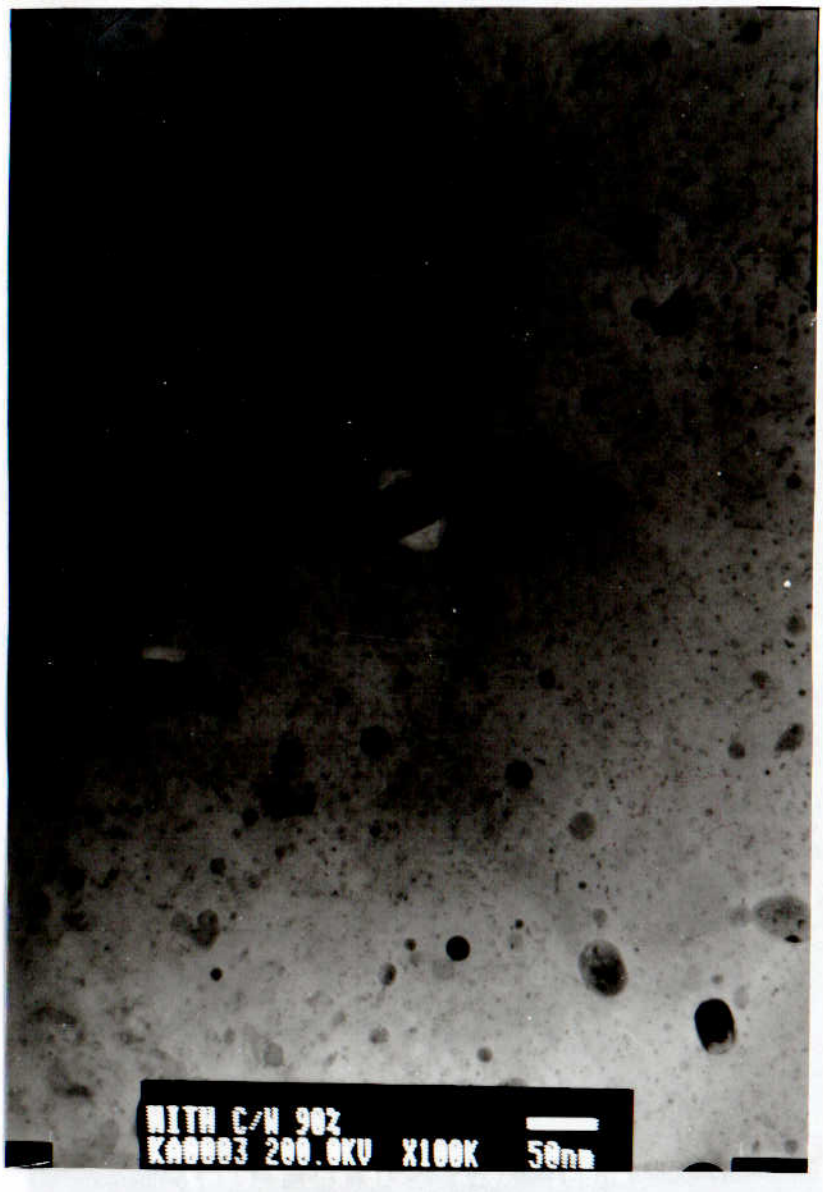

Figure 5.20 The TEM graphs of 92% cold worked nickel thoria

Figure 5.21 The TEM graphs of nickel thoria 92% cold worked and annealed at 1423 K for 8 hours

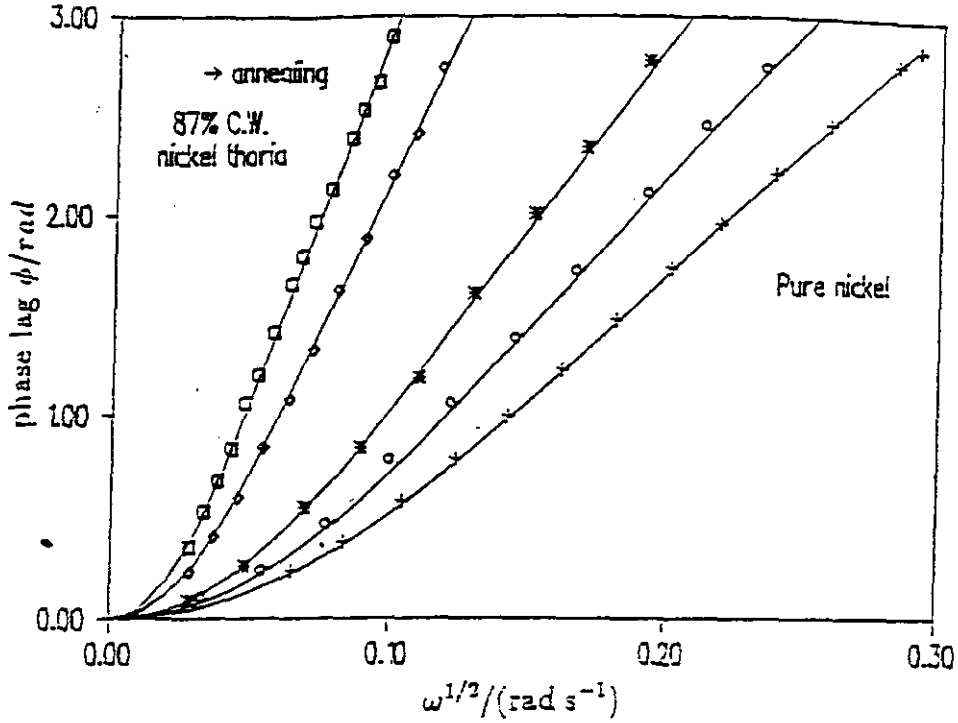

Figure 5.22 Measured variation of phase lag ϕ with root frequency $\omega^{1/2}$ for nickel thoria at 523 K, 6.65 kPa, □– 87% cold worked nickel thoria, ◇– annealed at 750 K for 7 days, ∗– annealed at 1425 K for 8 hours ○– annealed at 1625 for 24 hours; +– pure nickel

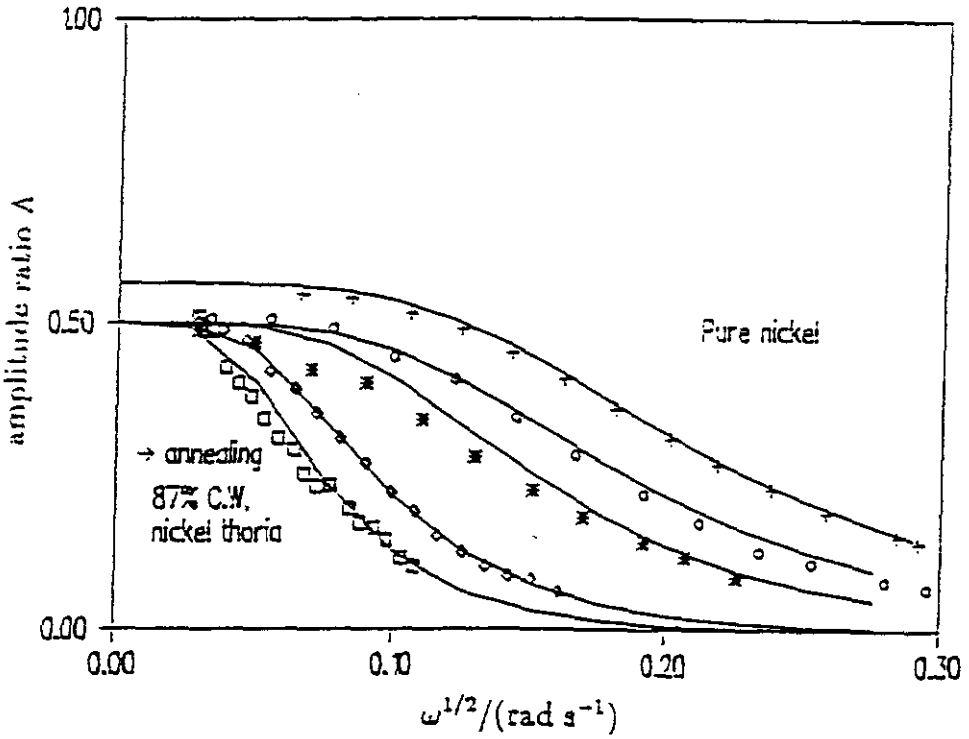

Figure 5.23 Measured variation of relative amplitude modulation ratio A with root frequency $\omega^{1/2}$ for nickel thoria at 523 K, 6.65 kPa, □– 87% cold worked nickel thoria, ◇– annealed at 750 K for 7 days, ∗– annealed at 1425 K for 8 hours ○– annealed at 1625 for 24 hours; +– pure nickel

Similar results were obtained at other temperatures. The variation of phase lag ϕ and the relative modulation amplitude ratio, Λ with square root of frequency $\omega^{1/2}$ are much the same in overall behaviour throughout the temperature range 398 K-918 K and show all the features of diffusion limited flow; $\Lambda = 0.5$ as $\omega \rightarrow 0$, high frequency extrapolate of ϕ at 0 frequency is $-\pi/4$. The diffusion limited features of these curves remain while annealing changes the phase lag, ϕ, and relative modulation amplitude ratio, Λ, in the direction of a faster transport rate.

These results suggest that the concentration of trapped hydrogen is in dynamic equilibrium with the concentration of hydrogen in normal lattice sites.

From these results it is only possible to find an apparent diffusivity, D^{app}. Figure 5.24 shows the measured apparent diffusivities, D^{app} for 87% cold worked nickel for anneals of different durations. A similar trend also was also found for 50% cold worked nickel thoria.

Figure 5.25 shows the measured apparent diffusivities for 50% cold worked and annealed nickel thoria. Notice that the diffusivities obtained for the cold worked foil have the same value with the pure nickel over 750 K. Above 750 K, the detrapping rate becomes faster than trapping rate so the system behaves as if there is no trapping at all.

Fig 5.26 shows the measured permeabilities with $1000/T(K)$. The permeabilities are not affected by cold work or subsequent annealing indicating that trapping does not affect the steady state permeation.

5.3.2 Pressure effect

The state of hydrogen in traps has yet to be understood. Most of the calculated values of trapping parameters depend on assumptions, not backed by experimental evidence, on whether hydrogen is trapped in gaseous form or is chemically adsorbed. The concentration dependence of the observed rate provides the possibility of investigating these alternatives simply by varying the input pressure. Varying the input pressure raises the possibility of establishing the nature of the traps and also helps to determine the quantity of such traps.

Experiments were performed on 0.075 mm NITD which was 92% cold worked

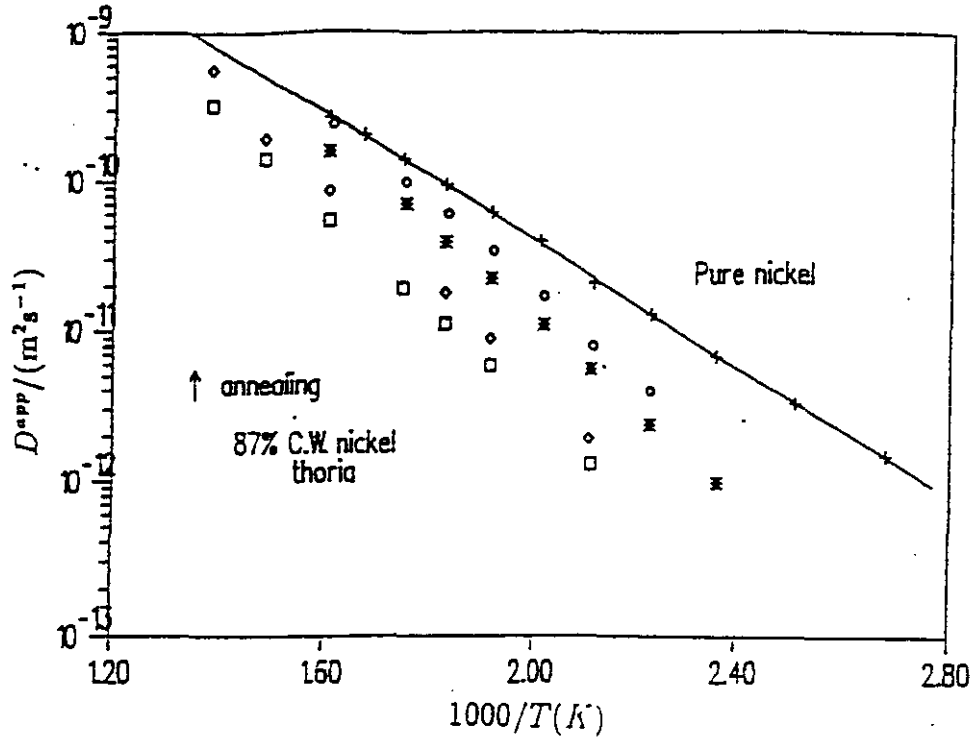

Figure 5.24 The Arrhenius plots of measured diffusivities, D^{app} for nickel thoria, □– 87% cold wored nickel thoria, ◇– annealed at 750 K for 7 days, ∗– annealed at 1425 K for 8 hours ○– annealed at 1625 for 24 hours; +– pure nickel

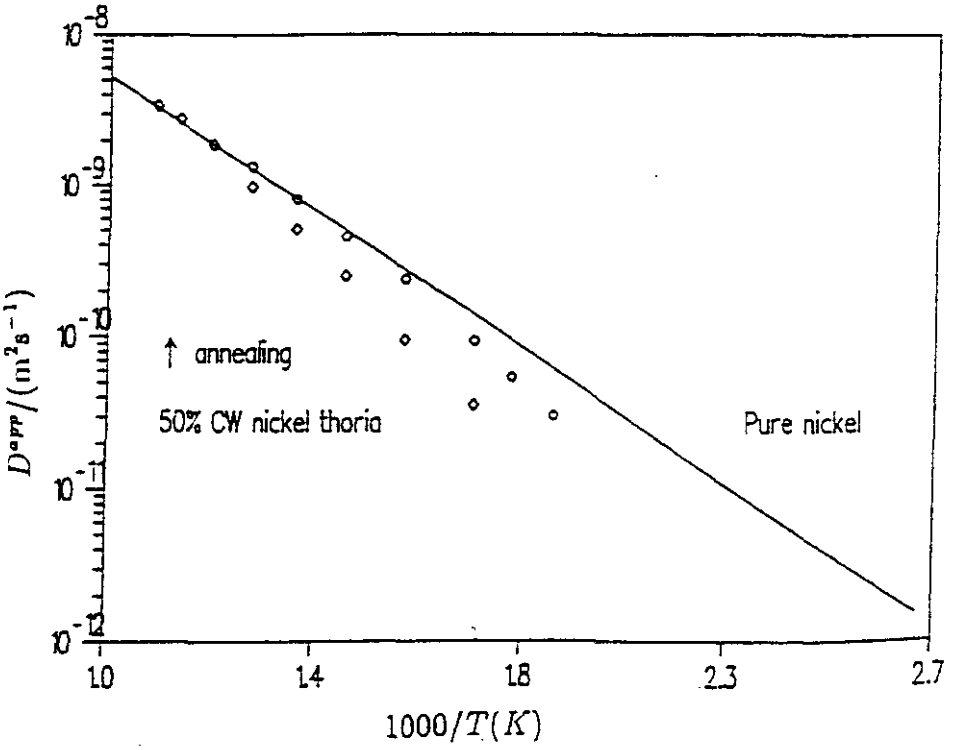

Figure 5.25 The Arrhenius plot of the measured diffusivities, D^{app} for 50% cold worked nickel thoria ◇–50% cold worked, ○–annealed at 1425 K for 8 hours, solid line pure nickel results

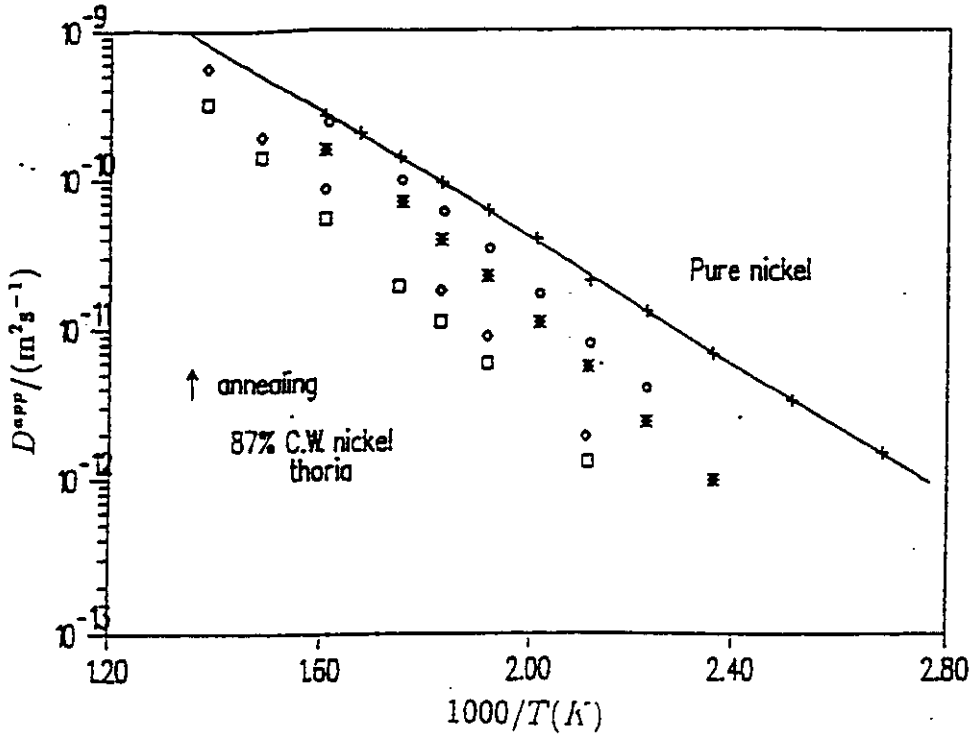

Figure 5.24 The Arrhenius plots of measured diffusivities, D^{app} for nickel thoria, □– 87% cold wored nickel thoria, ◇– annealed at 750 K for 7 days, ∗– annealed at 1425 K for 8 hours ○– annealed at 1625 for 24 hours; +– pure nickel

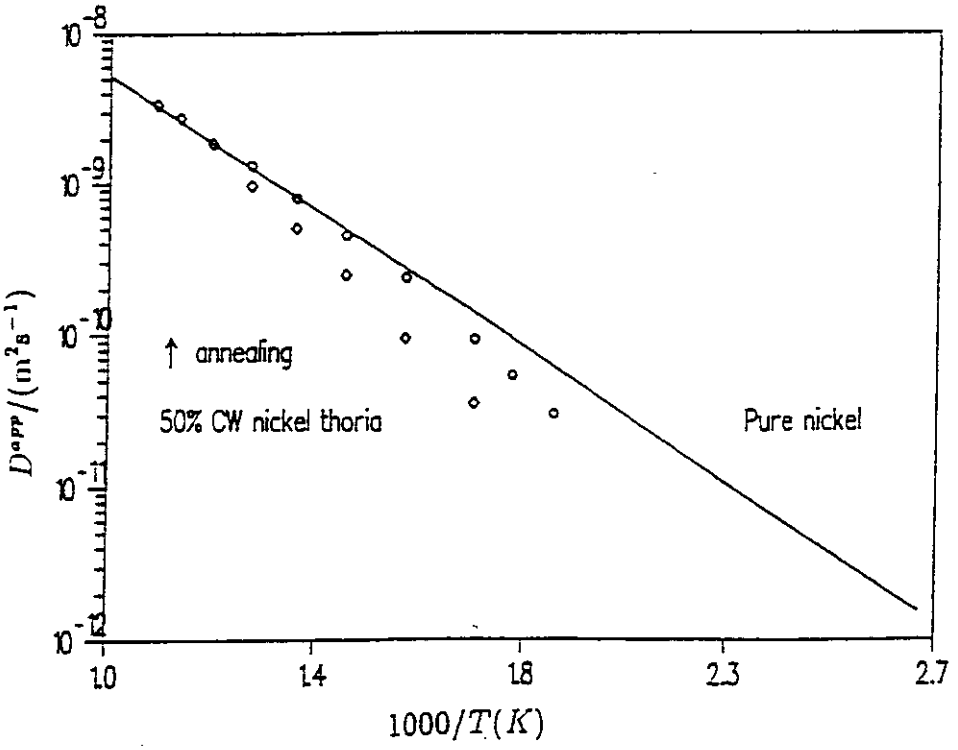

Figure 5.25 The Arrhenius plot of the measured diffusivities, D^{app} for 50% cold worked nickel thoria ◇–50% cold worked, ○–annealed at 1425 K for 8 hours, solid line pure nickel results

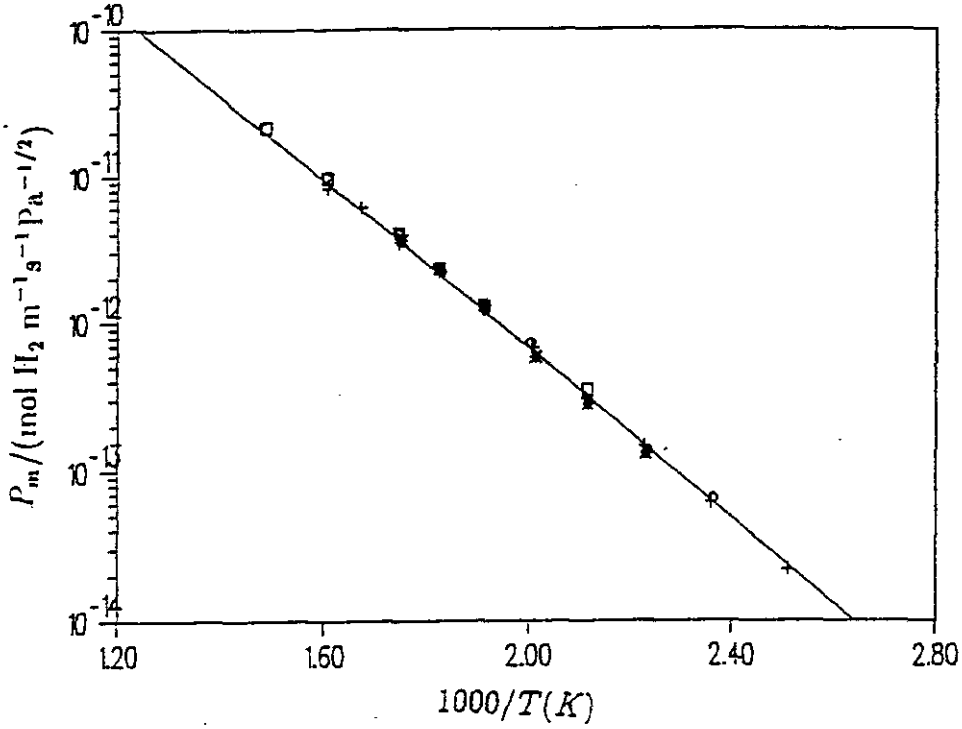

Figure 5.26 The Arrhenius plots of measured pemeabilities, P_m for nickel thoria, □– 87% cold worked nickel thoria, ◇– annealed at 750 K for 7 days, ∗– annealed at 1425 K for 8 hours o– annealed at 1625 for 24 hours; +– pure nickel

and then annealed at 1423 K for 8 hours at six different pressures in the range of 100 Pa -200 kPa and for temperatures between 298K and 623 K. Figures 5.27 and 5.28 typify the isothermal variation of phase lag ϕ and relative modulation amplitude ratio Λ with $\omega^{1/2}$ for 0.075 mm NITD foil for different input pressure at 498 K

Similar results were obtained at each temperature. These types of variations of phase lag ϕ,and amplitude ratio Λ with frequency do show all the features of diffusion limited flow as discussed above. The diffusion limited features of these curves remain even when the reduction of flux through the foil changes the amount of phase lag ϕ and relative modulation amplitude ratio Λ in the direction of a much slower bulk diffusion rate.

The reduction of the input pressure in this case does not reveal any surface inhibition ($\Lambda(\omega \to 0) = 1/2$ and high frequency extrapolate of ϕ back to zero, $\phi(\omega \to 0) = -\pi/4$), which indicates that pressure dependence of trapping is much more effective than the surface inhibition rate. These results are next used to estimate the apparent diffusivity, D^{app}, and the permeability P_m.

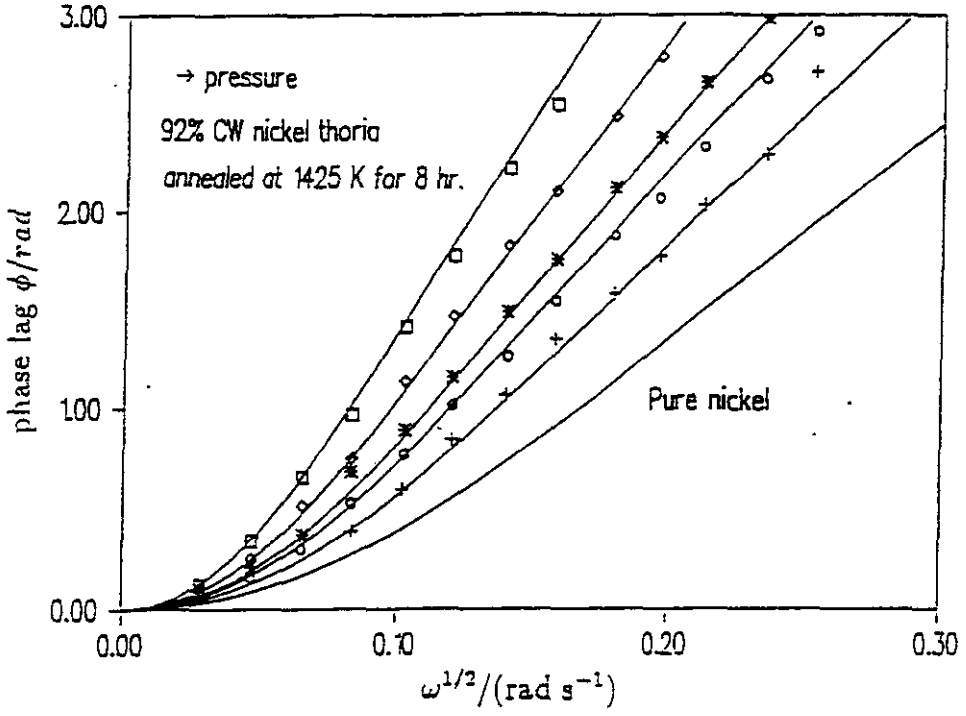

Figure 5.27 Measured variation of phase lag ϕ with root frequency $\omega^{1/2}$ for nickel thoria, annealed at 1425 K for 8 hours, at 498 K for different pressures, □– 930 Pa, ◇– 2.66 kPa ∗- 11.3 kPa o–33.25 kPa +– 101 kPa

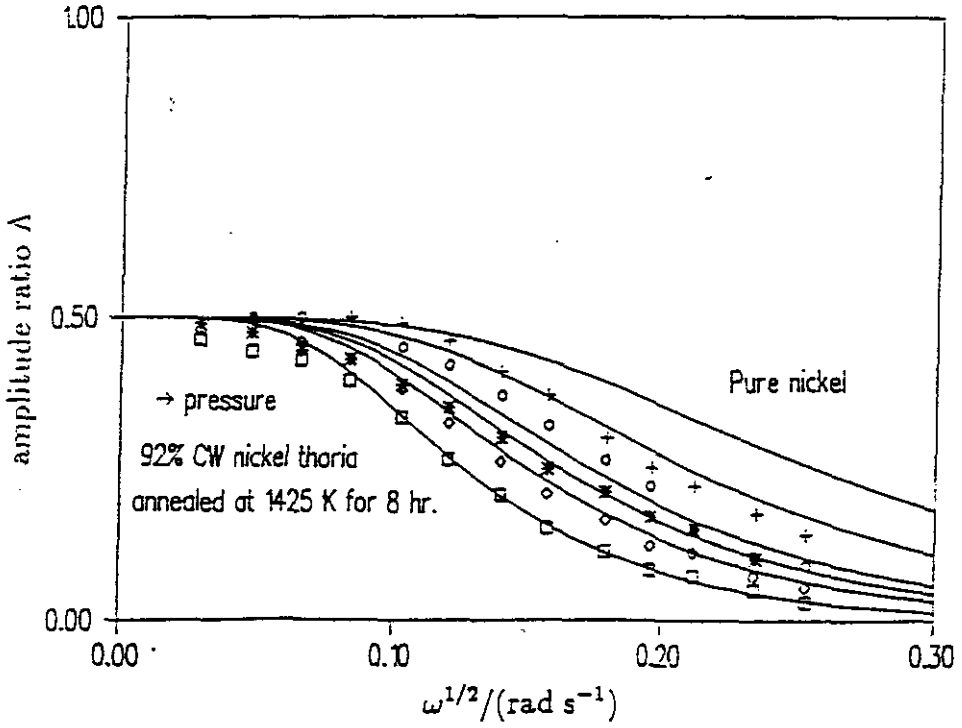

Figure 5.28 Measured variation of relative amplitude modulation ratio Λ with root frequency $\omega^{1/2}$ for nickel thoria annealed at1425 K for 8 hours, at 498 K for different pressures, □– 930 Pa, ◇– 2.66 kPa ∗- 11.3 kPa o–33.25 kPa +– 101 kPa

Figure 5.29 shows the Arrhenius plot of the measured apparent diffusivity. Comparing these results with figure 5.24 reveals the similar trend in the apparent diffusivities with reciprocal temperature. This indicates that active trapping sites have been introduced by cold work and varying the input pressure changes the concentration of these trapping sites. Again, measured permeabilities in figure 5.30 show that trapping does not affect the steady state permeabilities.

Since there are no maxima/minima in the phase lag, the system of thoria dispersed nickel appears to be in dynamic equilibrium.

The pressure effect also supports the view that the state of the hydrogen in the traps(active traps) is not diatomic. Kumnick and Johnson have found that the apparent diffusivity of cold-worked iron decreases with input pressure, indicating saturable, atomic trapping. Even the method they used (time-lag) is not capable of separating dynamic equilibrium, they based their calculations on the basis of dynamic equilibrium [69]. In the case of molecular trapping, or trapping in voids, one would expect a decrease in measured diffusion coefficient as the input pressure increases. If the active traps are the voids where hydrogen can be trapped in molecular form, the nature of the lattice/trap equilibrium (By Sievert's law) is that the trapped hydrogen should be an increasing fraction of the total hydrogen concentration as the lattice hydrogen concentration increases. This means that diffusion is even more impeded than it was before. This would require that the apparent diffusivity decrease with increasing lattice concentration or input pressure. The work by Ellerbrock *et al* details the void trapping model [34]

Both the annealing effect and the pressure effect suggest that there is only one type of active trap site and this has been introduced by cold rolling, because annealing drastically increases the apparent diffusivity towards the value in pure nickel for lattice diffusion.

Neither annealing nor pressure change the average activation energy.

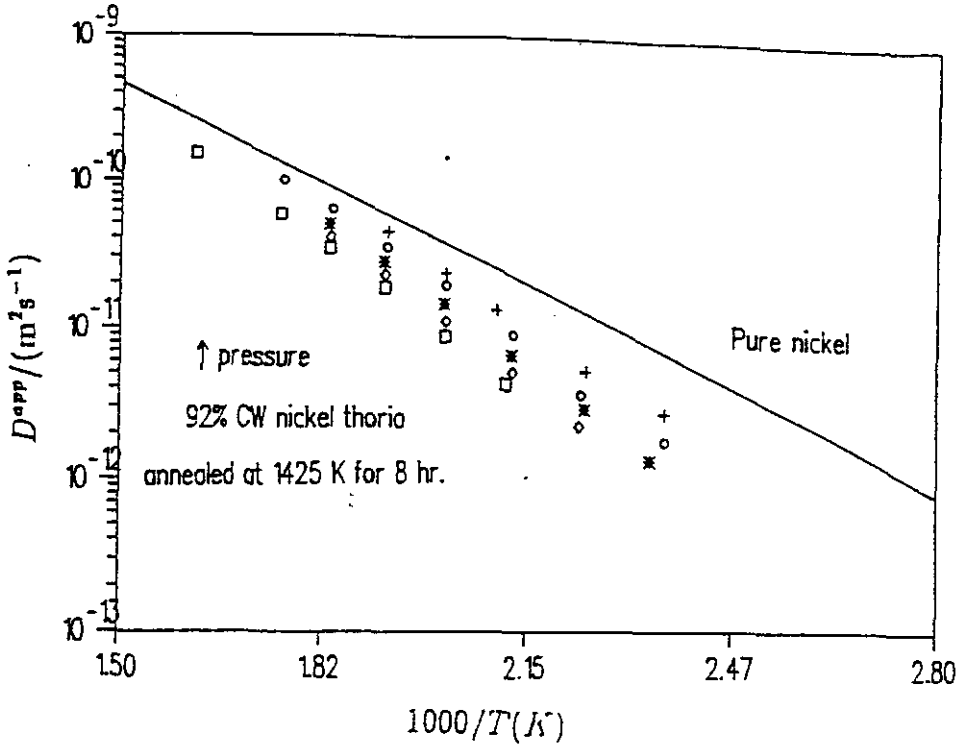

Figure 5.29 The Arrhenius plots of measured diffusivities, D^{app} for 87 % cold worked and annealed at 1425 for 8 hours nickel thoria, □– 930 Pa, ◇– 2.6 kPa, ∗–11.3 kPa o–33.2 kPa; +- 101 kPa

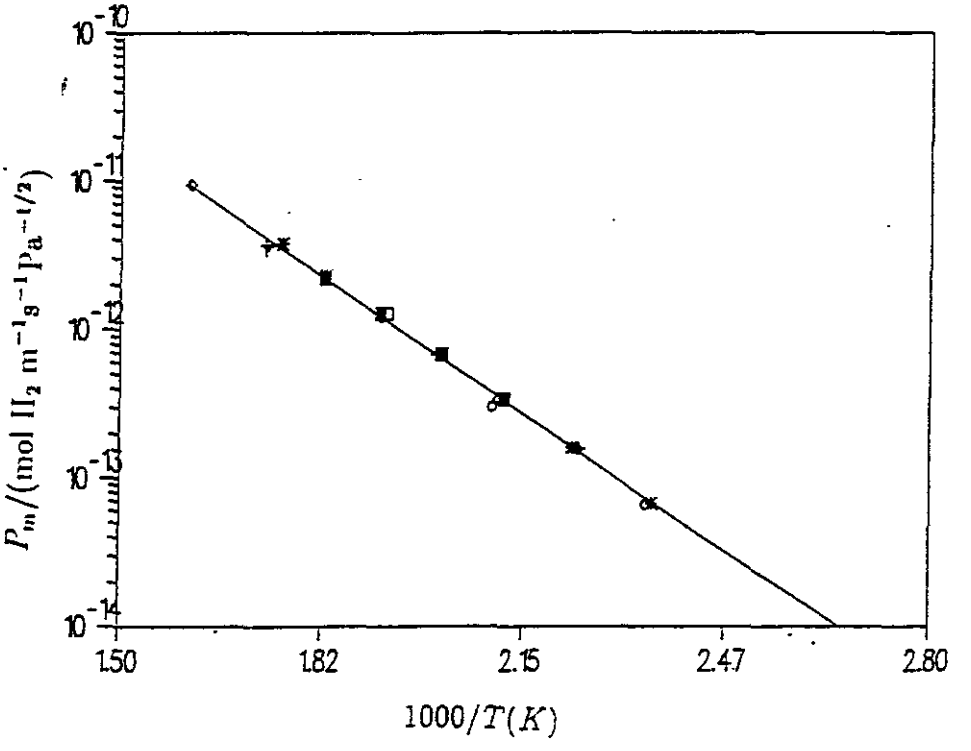

Figure 5.30 The Arrhenius plots of measured permeabilities, P_m for 87 % cold worked and annealed at 1425 for 8 hours nickel thoria, □– 930 Pa, ◇– 2.6 kPa, ∗–11.3 kPa o–33.2 kPa; +- 101 kPa

5.4 Estimation of trapping parameters

The experiments performed on nickel thoria foils strongly suggest that there is only one kind of active trapping site which slows down the transport rate through the foil. Both annealing runs and pressure runs indicate that the hydrogen trapping is in dynamic equilibrium. Pressure runs show that the system is not in a dilute regime such that one can neglect the non-linear term in the Mc Nabb and Foster model. In this case the Cummings and Blackburn solution for trapping cannot be used to find trapping parameters.
For the case of dynamic equilibrium, Oriani [33] has shown that the relation between the true and the apparent diffusivity D^{app} is,

$$D^{app} = D\left[1 + \frac{N_T N_L K}{(N_L + KC_L)^2}\right]^{-1} \tag{5.5}$$

where D is the true lattice diffusivity, N_L and N_T represents the number of normal(interstitial) and extraordinary(trap) sites per unit volume respectively. The term C_L is the hydrogen concentration in normal sites and K is the equilibrium constant for the trapping reaction, equal to $\exp(E_b/RT) = N_L k/\rho$, in which E_b ,k, ρ are trap binding energy, trapping rate and detrapping rate respectively. This equation also assumes that each extraordinary site can hold one hydrogen atom. For dilute occupation of traps this equation simplifies to,

$$D^{app} = D/(1 + KN_T/N_L) \tag{5.6}$$

A non-linear iterative least square analysis has been applied to equation (5.5) with known parameters, normal lattice site for hydrogen(octahedral site) in nickel, $N_L = 9.1 \times 10^{28} m^{-3}$ [62], D is the true lattice diffusivity found for pure nickel, with C_L is obtained from the relation $C_L = K_{sm} p^{1/2}$ where p is the input pressure.
The activation energy and number of traps, N_T are obtained for both annealing and pressure variations. Results are detailed in Table (5.2) for annealing runs and table (5.3) for pressure runs. Results obtained in this work do not actually allow one to estimate either the trapping rate or the detrapping rate. The trap depth obtained in this work along with the number of traps per

unit volume are in agreement with the result obtained by Robertson [32]. His results also suggest that the hydrogen was present as atoms in the traps as that the trapping changed with pressure implying that the dilute occupation assumption could not be used to find the trapping parameters. Robertson also suggested that full non-linear differential equation of the Mc Nabb and Foster model can describe the system of nickel thoria. He concluded that the result he obtained did not support the models which assume that equilibrium exists between the lattice hydrogen and trapped hydrogen for the system of thoria dispersed nickel. On the contrary this thesis strongly supports the view that the trapping in nickel thoria is in dynamic equilibrium. The difference in conclusion comes from the fact that the time lag technique used by Robertson does not provide a strong indication of the nature of the trapping on the pressure time curve. Conclusions made about parameters obtained through the fitting of data to relatively featureless curves have only limited value.

It is believed that the active trapping site for hydrogen is the stable dislocation network introduced by cold work around the thoria particles. Robertson suggested that the trapping was somehow related to the matrix particle interface but annealing runs performed here suggest that it is not the particles. He concluded on the basis of the results he obtained for the nickel thoria foil annealed at 1473 K for one hour, assuming that the cold worked structure annealed out. In this work, the analysis of microstructure under TEM (figures 5.20 and 5.21) show that neither the voids nor the dislocation network are completely annealed out.

It is important to note that the conclusion that the active trapping site for hydrogen is the dislocation networks around the particle/matrix interface does not exclude the fact that the particles may also trap the hydrogen. However, these trapping sites must be irreversible or have very high detrapping rate. Given the observation that traps are for atomic hydrogen, voids do not seem to play important role.

pre-treatment	temperature range/K	trap density, N_T/m^{-3}	trap energy, E_b / kJ mol^{-1}
92% CW, 1423K, 8h	423 - 523	2.0×10^{25}	37.7
87% CW	473 - 748	5.4×10^{25}	43.8
87% CW, 873K, 168h	473 - 748	9.2×10^{25}	43.2
87% CW, 1423K, 8h	473 - 748	2.1×10^{25}	40.5
87% CW, 1623K, 24h	473 - 748	1.7×10^{25}	39.3
50% CW	573 - 913	4.5×10^{25}	43.8
50% CW , 1423K, 8h	573 - 913	1.9×10^{25}	40.9

Table 5.2 Annealing results for 87% cold-worked nickel thoria, input pressure, 6.65 kPa

Pressure, Pa	n (495 K)	n (470 K)	n (446 K)	n (422 K)
101080	0.42	0.47	0.51	0.58
33250	0.299	0.34	0.38	0.44
11305	0.194	0.23	0.26	0.31
2660	0.107	0.127	0.14	0.181
1064	0.07	0.083	0.093	

temperature/K	trap energy, E_b / kJ mol^{-1}
523	40.1
498	36.4
473	36.4
448	37.3
423	37.7

Table 5.3 Pressure results for 92% cold-worked and annealed nickel thoria, 8 hrs at 1425 K

Chapter 6

Conclusion

The modulation technique has been shown to be capable of detecting deviations from diffusion limited flow, i.e, surface processes, internal trapping.
The extension of the operating range of the apparatus has enabled the observation of surface inhibition occurring on nickel and palladium.
The extension of modelling of surface processes to six rate constants suggests that the modulation experiment has the capability to resolve further the surface processes occurring during the permeation experiment. This also enables one to obtain quantitative data on the surface reaction rate which limits the permeation of hydrogen through the foil. This extension of the modelling also justifies the assumptions used to calculate the dominant surface reaction rate.
Comparison of the experimental data for nickel with the six-rate surface model has enabled the identification of the dominant surface process as being dissociative chemisorption. It is possibly that the same is true for the palladium results for which it has been shown that the permeation of hydrogen could be solely limited by surface reaction rate.
The experiments conducted on cold-worked nickel have revealed that hydrogen is trapped within the bulk during the permeation. It is proposed that the dislocation networks introduced by cold work are responsible for trapping of hydrogen. Measurements of micro-hardness and observation of the microstructure show that substantial annealing occurred under the experimental conditions. The activation energy and the number of traps can not

therefore be reliably extracted from the experimental data, but comparison of the data with the model suggests that the trapping process was in dynamic equilibrium.

A series of experiments on nickel+2% thoria has also revealed that the hydrogen is trapped within the bulk during the permeation.
Observation of microstructures has revealed that the cold working introduced voids and dislocation networks around hard thoria particles.
Investigation of permeation characteristics on cold-worked nickel+2% thoria has shown that the effect of trapping diminishes as the degree of annealing increases, suggesting that the trapping sites were introduced by cold working. This eliminates the thoria particles from being the active trapping sites.
Investigation of permeation characteristics over a wide input pressure range suggests that hydrogen is trapped as atomic species rather than in molecular form. This eliminates the voids formed around thoria particles from being the active trapping sites. It also suggests that occupation of trapping sites is not dilute, upon increasing the input pressure they tend to saturate.

Analysing all the nickel+2% thoria data and comparing them with the model strongly suggests that the hydrogen trapping is in dynamic equilibrium.
All experimental results on nickel+2% thoria suggest that there is only one type of active trapping site. It is believed that the active trapping sites for hydrogen are the stable dislocation networks.

It has been shown that the modulation technique is sensitive to the nature of the trapping. This has enabled the adoption of realistic assumptions to obtain more reliable estimates of the parameters involved in trapping processes. The activation energy of trapping has been extracted for cold- worked nickel thoria. The number of trapping sites has also been estimated for each foil.

Future developments

The experiments should next be extended to even lower temperatures, i.e down to 350 K, over a wide range of pressure for cold worked nickel in order to obtain reliable trap activation energies. Unfortunately the existing experimental apparatus is not appropriate for such purposes. It would substantiate the evidence obtained for trapping sites in nickel thoria as dislocation networks, if a similar trend is observed with nickel thoria.

The solution of Mc.Nabb's and Foster's full non-linear differential equation for modulated flow through thin metal foils will show the frequency response of the nonlinear internal trapping. This in turn will enable one to obtain quantitative information on internal trapping especially when trapping occurs under non-dynamic equilibrium conditions. An immediate application would be to determine the hydration and de-hydration rates in hydrogen- metal hyride systems where such kinetic information would allow one to design more sophisticated hydrogen based energy systems.

Further experimentation on materials having dispersed hard particles, i.e. nickel thoria, but with a much greater matrix diffusion coefficient at very low pressures (in order to have dilute occupation of traps) may test further the Cummings and Blackburn trapping model.

It is also possible to extend further the modelling of modulated gas flow to multi-layer foils. This would enable the measurements of permation parameters of very low diffusivity/solubility materials, if they can be coated on to a suitable substrate material. For example, there are not really any reliable data on carbon when deployed as an impermeable coating material(such as on the first wall future fusion reactors).
It is also possible to extend the modelling to infiltrated materials(a porous metal matrix infiltrated by second metal), which would enable the investigation of the permeation characteristics of some composite materials.

Both the modelling of multi-layer foils and infiltrated foils would allow the investigation of the effects of interfaces.

Both the modelling of multi-layer foils and infiltrated foils would allow the investigation of the effects of interfaces.

Chapter 7

References

[1] Y. Fukai and H. Sugimoto, Advances in Physics, 34 (1985) 263.

[2] K. Kiuchi and R.B. McLellan, Acta Metall., 31 (1983) 961.

[3] A.D. LeClaire, Diffusion and Defect Data, 34 (1983) 1.

[4] J. Völkl and G. Alefeld, Diffusion of Hydrogen in Metals, G. Alefeld and J. Völkl, eds., Hydrogen in Metals I. Basic Properties, Springer-Verlag, New York, (1978) 321.

[5] R.M. Cotts, Ber. Bunsen-Gesellschaft. 76 (1972) 760.

[6] H. Lütgemeier, R.R. Arons and H.G. Bohn, J. Mag. Resonance, 8 (1972) 74.

[7] R.E. Norberg, Physical Rev., 86 (1952) 745.

[8] D. Zamir and R.M. Cotts, Physical Rev., 134 (1964) A666.

[9] T. Springer, Springer Tracts in Modern Physics, Vol.64, Quasielastic Neutron Scattering for the Investigation of Diffusive Motions in Solids and Liquids, Springer-Verlag, Berlin Heidelberg New York (1972).

[10] J.L. Snoek, Physica, 8 (1941) 711.

[11] P. Raj and A. Sathyamoorthy, Hyperfine Interactions, 35 (1987) 845.

[12] H. Wipf and A. Heidemann, J. Phys. C: Solid State Phys., 13 (1980) 5757.

[13] J.H. Austin and T.S. Elleman, J. Nucl. Mater., 43 (1972) 119.

[14] H. Wipf. J. Less-Common Metals, 49 (1976) 291.

[15] J. Völkl. Ber. Bunsen-Gesellschaft, 76 (1972) 797.

[16] A. Zeilinger and W.A. Pochman. J. Appl. Phys., 47 (1976) 5478.

[17] D.G. Westlake, S.T. Ockers and D.W. Regan. J. Less-Common Metals, 49 (1976) 341.

[18] O.W Richardson, Phil. Mag, 7 (1904) 266.

[19] C.J. Smithells and C.E. Ransley, Proc. Royal Soc., A150 (1935) 172.

[20] J. Wang, Proc. Cam. Phil. Soc., 32 (1935) 657.

[21] N. Boes and H. Züchner, J. Less-Common Metals. 49 (1976) 223.

[22] P. Børgesen, B.M.U. Scherzer and W. Möller, Nucl. Instr. and Methods in Phys. Res., B7/8 (1985) 67.

[23] R.A. Kerst and W.A. Swansiger, J. Nucl. Mater., 122 & 123 (1984) 1499.

[24] T. Tanabe, Y. Furuyama and S. Imoto, J. Nucl. Mater., 145-147 (1987) 305.

[25] R.M. Barrer, Phil. Mag., 28 (1939) 148.

[26] H.A. Daynes, Proc. Royal Soc., A97 (1920) 286.

[27] R. Kirchheim and R.B. McLellan, J. Electrochem. Soc.: Solid-State Sci. Technol., 127 (1980) 2419.

[28] J.R. Phillips and B.F. Dodge, A.I.Ch.E. Journal, 14 (1968) 392.

[29] K.K. Shah, H.G. Nelson, D.L. Johnson and F.M. Hamaker, Metall. Trans. A, 6A (1975) 373.

[30] R. Wagner and R. Sizmann, Z. Angew. Phys., 18 (1964) 193.

[31] A. McNabb and Foster, Acta. Met. Soc. AIME, 227 (1963) 618.

[32] Wayne M. Robertson, Met. Trans. A, 10A (1979) 489.

[33] R.A. Oriani, Acta. Met. 18 (1970) 147.

[34] H.G Ellerbrock, G. Vibrans and H.P. Stuwe, Acta. Met 20 (1972) 53.

[35] W.J. Kass, Scr. Met. 8 (1974) 170.

[36] C.M. Allen-Booth and J. Hewitt, 6 (1972) 689.

[37] Y. Hayashi, M. Nagano and N. Ohtani, Trans. Japan Inst. Metals (suppl.), 21 (1980) 201.

[38] P. Kedzierzawski, K.M. Benczek and A. Sadkowski, Bull. Acad. Pol. Sci. Ser. Sci. Chem., 24 (1976) 595.

[39] H.M. Morrison, D.A. Blackburn and K.M. Chui, J. Nucl. Mater., 69 & 70 (1978) 578.

[40] W.M. Robertson, Proc. 2^{nd} Int. Conf., Environmental Degradation of Engineering Materials in Hydrogen, Blacksburg, VA, (1981), M.R. Louthan, R.P. McNeil and R.D. Sisson, eds.

[41] D.L. Cummings, R.L. Reuben and D.A. Blackburn, Metall. Trans. A, 15A (1984) 639.

[42] D.L. Cummings and D.A. Blackburn, Metall. Trans. A, 16A (1985) 1013.

[43] D.L. Cummings and D.A. Blackburn, J. Nucl. Mater., 144 (1987) 81.

[44] D.M. Grant, D.L. Cummings and D.A. Blackburn, J. Nucl. Mater., 149 (1987) 180.

[45] D.M. Grant, D.L. Cummings and D.A. Blackburn, J. Nucl. Mater., 152 (1988) 139.

[46] D.M. Grant, D.L. Cummings and D.A. Blackburn, Z. Phys. Chem. Neue Folge, 164 (1989) 1585.

[47] A. Sieverts, Z. Phys. Chem., 77 (1911) 591.

[48] K. Sawada, T. Tanabe and S. Imoto. Technol. Reports Osaka Univ., 34 (1984) 211.

[49] W.J. Kass and W.J. Andrzejewski, A.E.C. Report, SC-DR/72/0136 (1972).

[50] V.A. Kurakin, A.A. Kurdyumov, V.N. Lyasnikov and M.I. Potapov, Sov. Phys. Solid State, 21 (1979) 616.

[51] A. Tahara and Y. Hayashi, J. Japan Inst. Metals, 47 (1983) 180.

[52] S.-M. Lee and J.-Y. Lee, Metall. Trans. A,17A (1986) 181.

[53] M.R. Louthan, J.A. Donovan and G.R. Caskey, Acta Met, 23 (1975) 745.

[54] M.R. Louthan, Jr., J.A. Donovan and G.R. Caskey. Jr., Nucl. Technol., 26 (1975) 192.

[55] R.L. Reuben, PhD thesis, Oxford, 1981.

[56] J.J. Sullivan, J. Vac. Sci. Technol., A3 (1985) 1721.

[57] Dennis and Heppel, Vacuum System Design.

[58] R.T. Bayard and D. Alpert, Rev. Sci. Instrum., (1950) 571.

[59] P.A. Silberg and C.H. Bachman, J. Chem. Phys. 29 (1958) 777.

[60] M.I. Baskes, J. Nucl. Mater., 92 (1980) 318.

[61] R.A. Causey and M.I. Baskes, J. Nucl. Mater., 145-147 (1987) 284.

[62] B.L. Doyle and D.K. Brice, Radiation Effects, 89 (1985) 21.

[63] M.A. Pick and K. Sonnenberg, J. Nucl. Mater., 131 (1985) 208.

[64] W.M. Robertson, Z. Metallkde, 64 (1973) 436.

[65] A.D. Le Claire, UKAEA Rep. AERE-R-10846, 1982.

[66] J.A. Donovan, Met. Trans. A, 7 (1976) 1677.

[67] P. Borgesen, B.M.U. Scherzer and W. Moller, J.Appl. Phys. 57 (1985) 2733.

[68] D. Webster, Trans. Met Soc. AIME, 242 (1968) 640.

[69] A.J. Kumnick and H.H. Johnson, Acta Met, 28 (1980) 33.